THESIS

A THERMOPLASTIC MATRIX CONTINUOUS FIBER REINFORCED COMPOSITE IMPREGNATION METHOD BY DIRECT POLYMER EXTRUSION

Submitted by

Kevin M. Hedin

Department of Mechanical Engineering

In partial fulfillment of the requirements

For the Degree of Master of Science

Colorado State University

Fort Collins, Colorado

Summer 2018

Master's Committee:

Advisor: Donald W. Radford

Kaka Ma
Paul Heyliger

ABSTRACT

A THERMOPLASTIC MATRIX CONTINUOUS FIBER REINFORCED COMPOSITE IMPREGNATION METHOD BY DIRECT POLYMER EXTRUSION

During component design, continuous fiber reinforced composite material systems are often chosen largely based on their structural efficiency. Their mechanical properties, such as specific strength and specific stiffness, are often cited as significant advantages over the use of other materials. However, composite component production often lacks the capability to provide the local variation necessary to ensure that 1) the reinforcing fibers are best aligned with anticipated loads, and 2) the ideal matrix composition and fiber volume fraction are found throughout the composite part. In practice, these limitations result in composite components that do not demonstrate the maximum possible efficiencies inherent to the fiber-reinforced composite material system.

To further increase the flexibility of polymer matrix continuous fiber reinforced composites manufacturing methods, a new thermoplastic impregnation method was developed. This proposed method adds a thermoplastic matrix, which has previously been proven to allow significant variation of local fiber orientation, to the reinforcing fiber just prior to the consolidation of the composite. The increased independence of matrix and fiber addition should allow the local variation of volume and composition of the added matrix, while using less and simpler hardware than previous, similar efforts.

In this work, the quality of material deposited from the proposed process is evaluated. The maximum possible quality of the proposed method and also that of a similar process that uses a commercially available material system were determined, primarily using short beam shear (SBS) testing. The material system of both methods consisted of E-glass continuous fiber reinforcement with a PETG matrix. It was found that both manufacturing processes are capable of producing samples with an SBS strength of approximately 53 MPa, and it was concluded that the proposed process has the capability to deposit material of comparable quality to that produced by the baseline method. Subsequent thermal analysis, fiber volume fraction/void content measurement, and metallographic imaging were conducted to investigate the effects of using two different PETG compositions on the SBS strength of composite material produced by the proposed process. It was found that, while using the proposed process, the PETG matrix with a lower glass transition temperature allowed better consolidation of the resulting composite part, ultimately increasing SBS strength. Each process parameter used in the proposed process was evaluated for the practical significance of its effects on SBS strength, which facilitated 1) an understanding of the underlying mechanisms of the process, and 2) a tenable simplification of the process that should reduce operating costs and also demonstrates its robustness via insensitivity to many of the possible process variations. Finally, it was established that the material inputs to the proposed process are relatively inexpensive: Using PETG and continuous E-glass fiber in the proposed process reduces material input cost by at least 52% compared to using commingled PETG and E-glass fibers in the baseline process, on a $/kg basis.

ACKNOWLEDGEMENTS

The research contained herein would not have been possible without the support of my family as well as the friends and instructors I've met while a student at Colorado State University. I would like to thank Dr. Paul Heyliger and Dr. Kaka Ma for generously contributing their time and advice as my committee members. I would also like to extend my gratitude to my advisor, Dr. Donald Radford, who has consistently shared both his vast expertise of and also countless opportunities to learn about composite materials, as well as pretty much anything else I was curious about. Lastly, I must acknowledge the extensive patience of my wife, Esther, and my daughter, Lilly, for her enthusiastic confidence in my abilities, no matter how misplaced it may occasionally be.

TABLE OF CONTENTS

LIST OF TABLES

LIST OF FIGURES

1. INTRODUCTION

1.1. Fiber Reinforced Composite Manufacturing and Increased Efficiency via Fiber Path Control

Continuous fiber reinforced polymer matrix composites (FRPs) are attractive material systems largely based on their high modulus and strength to weight ratios. These specific properties contribute to FRPs' reputation as structurally efficient material systems. Often, FRPs are used in designs that require high strength and high stiffness. However, what distinguishes FRPs as being more efficient than other materials, such as steel and aluminum, is their relatively low mass. This results in part from the use of low density polymers as a matrix in the composite material. The fiber reinforcement, often carbon or glass fiber, is denser than the FRP matrix, and so the final mass of the composite is a function of the relative proportion of the fibers to the polymer, known as the fiber volume fraction (V_f).

Other significant contributors to the efficiency of FRP material systems include their anisotropic material properties. Their high specific stiffness and specific strength are commonly lauded, but other material properties such as CTE, electrical conductivity, and thermal conductivity are also anisotropic. Most often, increased material properties are seen along the fiber direction, while the FRP composite shows significantly reduced properties in other directions [1, 2], as seen in Figure 1. Consequently, the most efficient use of the material system in FRP part design is to place the fiber reinforcement in the position and orientation that will produce the best response to 1) the component's anticipated loads, and 2) the predicted physical and environmental changes to which the part will be subjected. Even small deviations from the optimized fiber orientation can significantly reduce the ultimate efficiency of the FRP component.

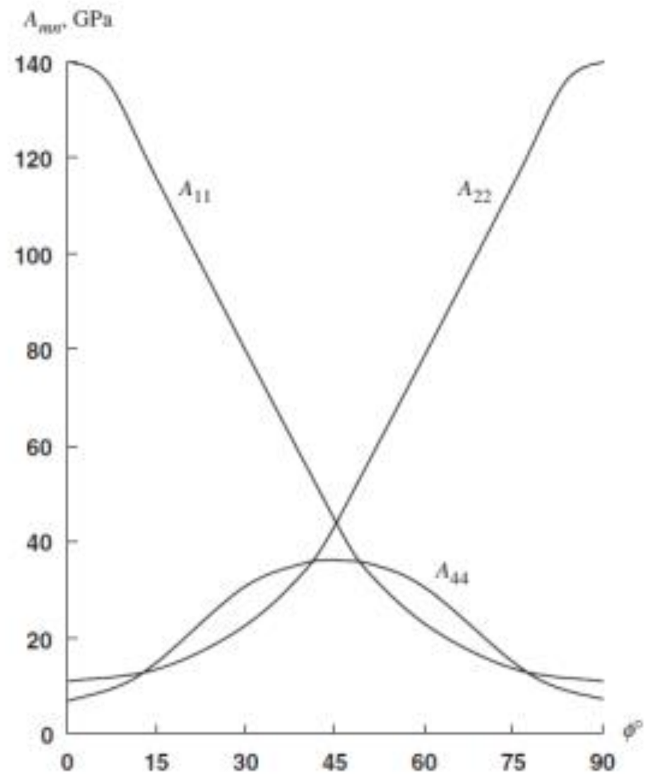

Figure 1: Relationship between stiffness and orientation of a unidirectional carbon FRP. A11 and A22 are tensile values of stiffness in orthogonal directions. A44 is in-plane shear stiffness [3].

Most often, FRP parts are made into a necessary size and shape by layering plies of FRP material into laminates. The plies are composed of fiber reinforcement placed in one direction (unidirectional tape), or two directions (woven fiber), which are consistent throughout the ply. These fiber directions are usually intended to be within the plane of the ply. An FRP component is often comprised of a single, consistent laminate throughout the entire part. However, if the part requires local variation, this is created using subsequent processes such as 1) machining to remove material, or 2) the bonding of smaller, additional plies to provide local reinforcement.

Most commonly, V_f is ideally kept constant throughout each ply and also through the thickness of the laminate, although exterior coatings are sometimes added after part manufacture. One way that the matrix is incorporated into the FRP is by using fiber reinforcement that is fully-impregnated with the resin before the component fabrication. Another method of adding the matrix to the reinforcement is to place the entire fiber laminate and then infuse it with resin. In practice, unwanted V_f variations are sometimes found in FRP laminates: As seen in Figure 2, resin rich areas develop between plies. Also, V_f variations over the area of an FRP component are common. Variations of consolidation pressure, impediments to matrix flow, uneven temperatures as well as other factors can cause V_f variation during the manufacture of the FRP part. This unintended material heterogeneity is avoided, rather than encouraged, as it can create discrepancies between the designed part and the manufactured part, resulting in unpredictable properties and performance.

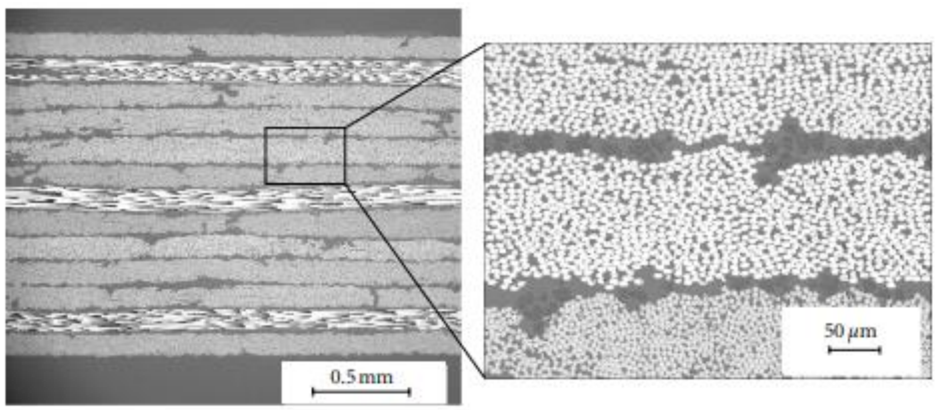

Figure 2: A typical FRP microstructure showing resin rich areas between plies in the laminate [4].

Other opportunities to increase FRP efficiency result from designing with the FRP material system in mind, rather than designing for an isotropic material and then creating a laminate construction that fits the now specified geometry. FRP manufacturing processes are generally similar to those of their polymer matrix and FRP parts can be cast to approximately net shape and size. This manufacturing strategy can reduce wasted material compared to common subtractive processes. Also, part count can be reduced, and necessary features can be integrated by making larger parts that can incorporate complex curvature and local features. This approach can reduce assemblies to individual parts, as illustrated in Figure 3, which uses as an example the assembly of an aircraft. For example, mechanical joints, previously requiring additional hardware and machining, can be eliminated, mitigating associated issues with lower strength and stiffness, as well as the increased effort to design and manufacture the joint.

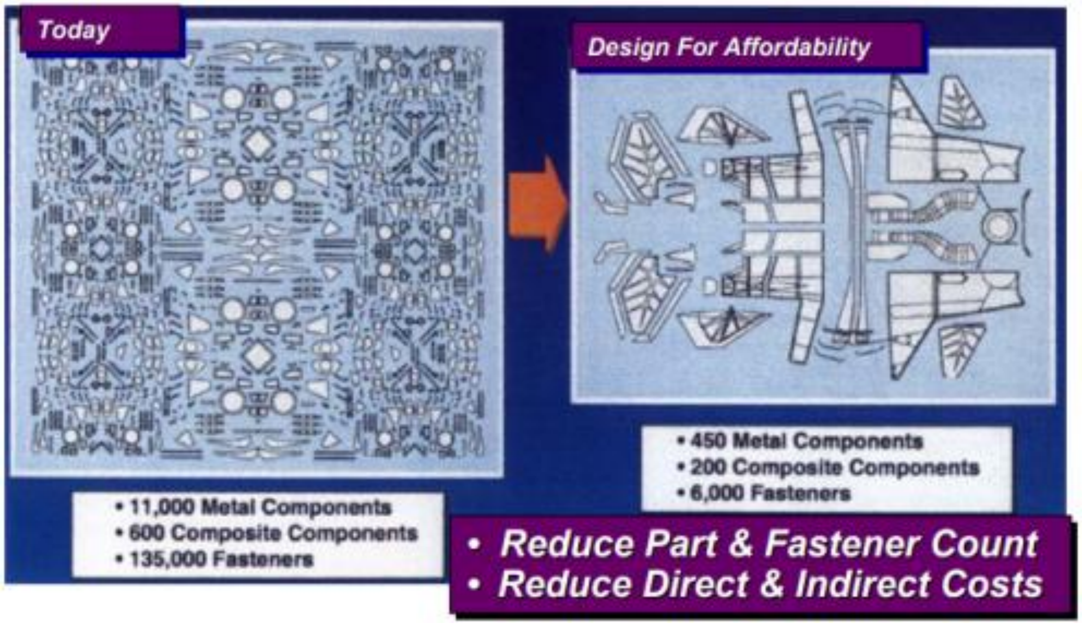

Figure 3: Some of the advantages that designing structures for the FRP material system can offer [5].

Larger FRP parts that contain integrated features such as 1) holes and 2) joints that provide a connection to other components increase the opportunity for varying loads to occur throughout a part. A common example is a fuselage that will be pressurized while also being loaded as a part of the aircraft's structure which still needs to provide openings for windows, doors for entrance and egress, and access for plumbing and electrical routing, while also supporting the wings. Perhaps a structural feature that leaves the surface of the part is needed in an FRP component, analogous to the tree branch's orientation with respect to the tree trunk. The loadings on these out-of-plane features are likely to cause locally varying stress states in the primary structure into which the feature is incorporated. Complicated stress states may be anticipated in certain areas which may be completely different than the stress states in another area. In these locations, altered load paths, possibly in out-of-plane directions, or with increased or decreased stiffness in various directions may be desired.

Because of the clear way fiber orientation determines the relationship between load and response within an FRP part, local variation of loading implies the need for local variation of fiber orientation. However, because laminates are composed of plies of constant fiber angle, and because those angles are in-plane within the ply surfaces, it is unlikely that both the integrated features and the structure as a whole will contain reinforcing fibers in the best orientation to respond to the varying load vectors. Using this approach with globally constant fiber angles and locally varying loads, significant compromises need to be made. This compromise diminishes the efficiency of the composite component. One common approach to addressing these inconsistencies is to create a laminate that contains plies that can adequately respond to the globally-applied loads, and then add material in areas of abruptly changing localized loads, to stiffen and strengthen those areas in the appropriate directions. Areas that are cut away from the FRP create discontinuous reinforcing fiber, which weakens the component beyond what the mere subtraction of material accomplishes, increasing the need for reinforcement. In response to the challenges of FRP parts of complicated shape, with localized variations in loading and potential areas of removed material, one often simply adds more material in the weakest and most compliant areas to prevent failure or excessive deformation. However, abrupt changes in thickness usually need to be made more gradual, and so complexity and mass is increased even further by adding tapers and ply drops to prevent premature failure. Out-of-plane structures that need to be added to the primary structure are typically joined with additional hardware. However, this approach leads to redundant structural material and excess mass, limiting the advantages of a material system valued for its high specific properties.

The ultimate control of fiber orientation necessary to realize the maximum efficiency of the FRP material system requires the ability to place fiber along any path in three dimensional space. However, the combination of placing fiber while tensioned, a common method to consolidate the composite, but also allowing the freedom of the fibers to move in radial directions with respect to the fiber results in the fiber following the shortest distance between any two fixed points. This is true regardless of whether the fibers are unencumbered by other objects, resulting in a straight line between the two points, or when fibers are placed along a supporting surface, possibly producing a fiber path of curvilinear shape along a mold, for example. When fibers are placed so that they are in contact with a curved surface, they tend to orient along this shortest path allowed by the surface. This path is referred to as the geodesic path. Although placing fibers along the geodesic path provides a stable orientation and position of the tensioned fibers, it also functions as a severe limitation to achieving the best performance from FRP material by strictly dictating the available orientation of those fibers. For example, the Clairaut relationship describes the inverse correlation between a mandrel diameter and the fiber angle of the reinforcement placed along the geodesic path on the mandrel surface. The fiber angle must increase as the mandrel diameter decreases, for example. As seen in Figure 4, this design constraint causes fiber laid along the geodesic path to be unable to traverse the entire length of the mandrel once the fiber angle (Θ) increases to 90°. However, the non-geodesic paths (1-3) than can span the length of the part, shown in Figure 4, are inherently unstable. And so, this model helps to predict the location and orientation of a fiber following the geodesic path. However, rigidly coupling the fiber angle to the geometry of a produced part is a significant limitation when it prevents reinforcement from being placed to most efficiently respond to loads. This geodesic limitation essentially prevents effective, local fiber path variation.

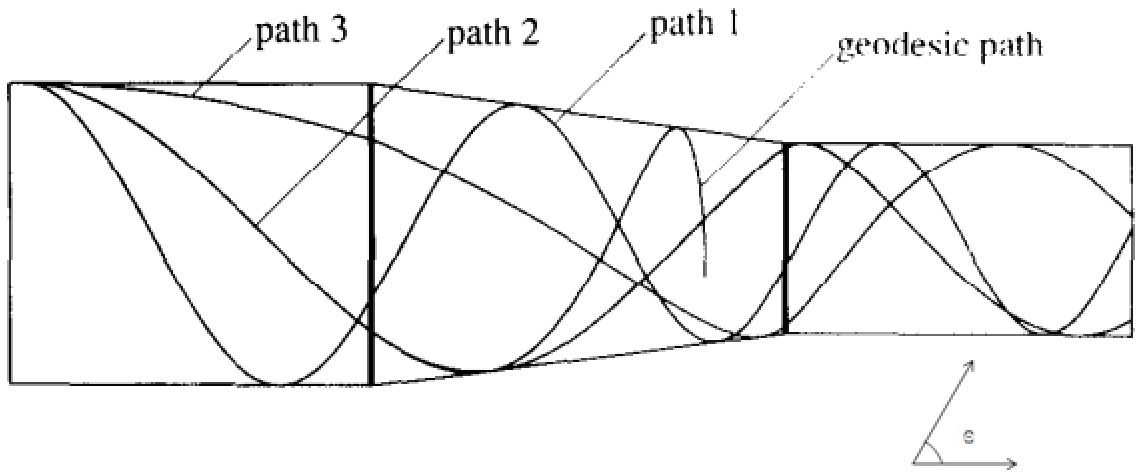

Figure 4: The geodesic path shown here abides by the Clairaut relationship and is unable to span the length of the mandrel. Paths 1-3 are alternatives to the geodesic path [6].

1.2. Previous Efforts to Increase Efficiency via Local Fiber Variation

The recognition of the need for increased control over manufactured fiber paths in FRP parts has driven the research conducted using many of the main FRP manufacturing approaches, as discussed in the following sections.

1.2.1. Efforts Using Filament Winding

Practitioners of the filament winding technique have been interested in both characterizing and following the maximum allowable deviation from geodesic paths for some time [6, 7, 8]. Essentially, filament winding involves the wrapping of reinforcing fibers, often in the form of roving, around a mandrel to create a laminated composite shell. The shape of that shell is primarily determined by the mandrel, while a fiber-dispensing eye runs back and forth along the length of the emerging part to generate plies of a specified fiber angle. As with most FRP parts, filament wound parts are made from thermoset resins due to their low viscosity during manufacturing, which facilitates rapid wetout of the reinforcement. Because of filament winding's inherent advantages of 1) relatively simple automated kinematics, 2) potentially high deposition rates, and 3) accurate fiber placement; parts that deviate from the simplest consistent axisymmetric shapes have also been attempted using the filament winding process. But, as seen in Figure 4, maintaining a constant fiber angle along a cylinder with a changing diameter requires a non-geodesic fiber path, for example. Even producing a simple FRP cylinder of constant cross-section requires non-geodesic fiber angles at each end to anchor the reinforcing fiber for the next pass along the length of the part if a special, pinned mandrel is not used.

Researchers of filament winding have created predictive models that can restrain part design to the confines of realistic deviations from the geodesic path. This deviation is usually accomplished using a combination of resin tack and reinforcement undulation that inhibits the sliding of non-geodesic roving along the deposition surface back towards the geodesic path [7, 9, 10]. The resin tack can be generated by the matrix of a towpreg or from the addition of resin to the fiber immediately prior to contact with the mandrel (wet winding). Experimental techniques have been developed to quantify the inputs to the predictive model as well [7, 9, 10]. As seen in Figure 5, in spite of these accomplishments, the actual deviation of fiber angle from that allowed by the geodesic limitation has been quite modest. In this diagram, the slippage coefficient, λ, represents the force that is applied to the roving to move it off of its intended path: A larger allowable slippage coefficient value, λ_{max}, indicates that larger deviations from the geodesic path are possible [6, 11]. With additional fixtures, fiber paths that leave an axisymmetric surface can be produced, as when winding a pipe T-fitting, for example, but the reinforcement paths commonly remain geodesic and the increased kinematic complication and necessary hardware is significant [12, 13].

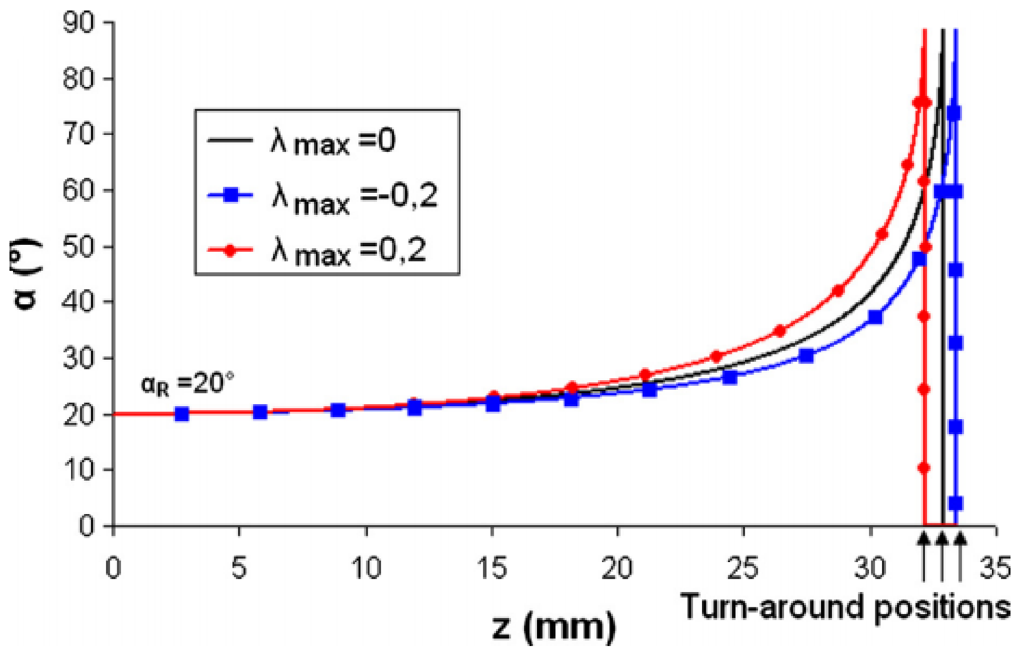

Figure 5: An example of the variation in fiber angle (α) produced as roving travels from the base of a filament wound dome to its turn around point using non-geodesic paths[11].

Recently, progress has been made at CSU's CMMS lab to demonstrate the possibility of extremely non-geodesic and out-of-plane fiber paths using thermoplastic polymer as a matrix, shown in Figure 6, but there are few additional efforts such as this in the literature.

Figure 6: Extremely non-geodesic fiber paths (left) and out-of-plane fiber paths (right) produced using a thermoplastic matrix [14].

1.2.2. Efforts Using Automated Tape Laying and Automated Fiber Placement

Processes like automated tape laying (ATL) and automated fiber placement (AFP) use a roller to consolidate laminates made from wide prepreg tapes or relatively narrow widths of prepreg, respectively, against a surface that is relatively flat compared to parts made from filament winding. Most often, the ATL or AFP deposition head has access to one side of an open mold, in contrast to the deposition on all sides of a rotating mandrel typically used in filament winding. However, the mold surface can contain complex curvature including concave surfaces [15] that are typically avoided in filament winding, which can cause defects such as fiber bridging.

Since the deposition surface of an ATL or AFP process is relatively flat, most deviations from a straight line will be non-geodesic. In response to the need to create non-geodesic reinforcement, these two processes have made significant progress in the endeavor to exert significant control over FRP fiber paths, as shown in Figure 7. Partially due to the use of high-quality prepreg, current efforts are focused on improving the quality of the laminates and interfaces between bands and tows within plies while fibers are placed along extremely non-geodesic paths along open molds seen in Figure 7.

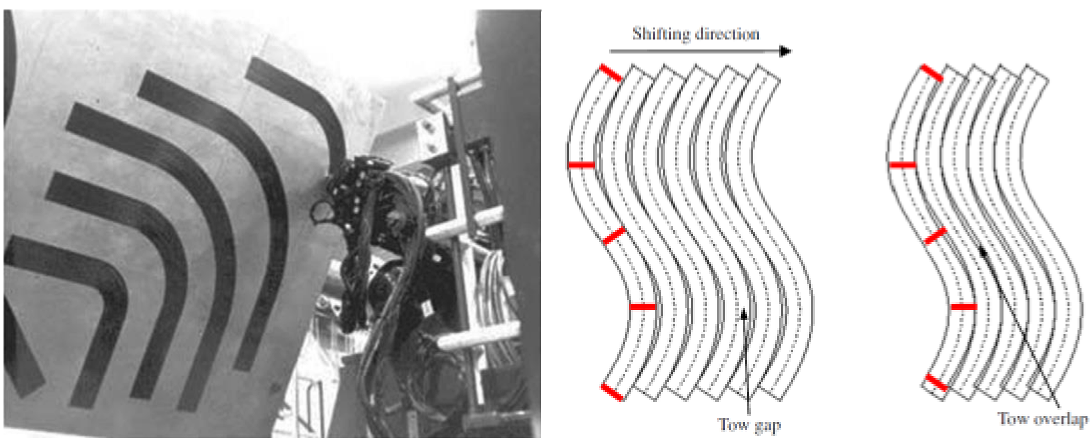

Figure 7: Left: An AFP head demonstrating non-geodesic tape paths [16]. Right: Current quality issues such as gaps and overlap between the non-geodesic prepreg tape [17].

Quality within the deposited prepreg bands, defined in this work as low void content, sufficient fiber dispersion, minimal defects, high V_f, and straight reinforcing fibers has already proven to be fairly high for extremely non-geodesic fiber paths [16, 17, 18]. Research is focused on avoiding gaps and overlaps between these tows and bands and on creating uninterrupted, smooth transitions of changing fiber angles across each ply [16, 17, 18]. As seen in Figure 8, practical, experimental demonstrations show the benefit of this control over the fiber path when designing and fabricating a part containing a defect of approximately the same size and shape of a window-sized hole that would be placed in an airplane fuselage, for example. The work illustrated in Figure 8 is intended to increase the buckling strength of the panel when it is loaded with in-plane compression from the top and bottom edges. Although there has been some work intended to crate fiber paths that deviate from the primarily flat, open mold surface [20], evidence that ATL and AFP can maintain their current level of high quality as FRP material leaves the mold surface is not readily available. The capital costs for ATL and AFP machines are high relative to other FRP production processes mentioned here.

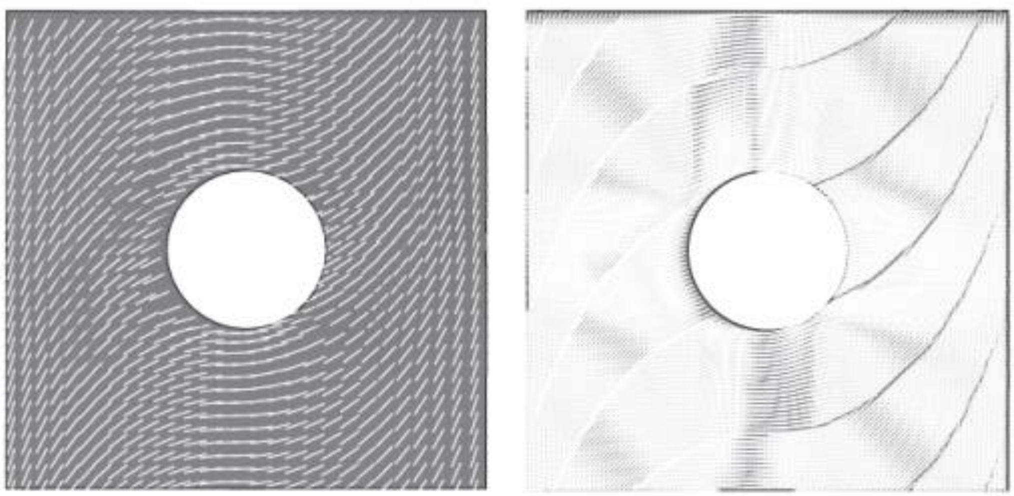

Figure 8: Panel with compliant region incorporated into an idealization of the fiber angles (left) and the predicted as-built panel (right)[19].

1.2.3. Efforts Using Variations on 3D Printing Processes

The most recent developments in the production of FRP components with non-geodesic fiber paths have combined 3D printing hardware with composite manufacturing techniques [21-25]. There are commercially available fused deposition modeling (FDM) machines that incorporate continuous fiber reinforcement into thermoplastic polymers that are extruded onto a print bed, similarly to how FDM methods would be used to create unreinforced polymer parts [26]. Many of these efforts have demonstrated the ability to create significantly non-geodesic fiber paths along the print bed surface, as seen in Figure 9. Most often, thermoplastic matrices are used so that the matrix can begin to be cooled and solidified immediately after the FRP is dispensed in order to anchor previously deposited material [21-23, 25].

Figure 9: Significantly non-geodesic parts made with FDM [24].

More recently, high quality FRP parts that demonstrate out-of-plane fiber paths without using a supporting surface have also been demonstrated using FDM [28] and modified FDM [27] hardware to create parts that extend into three dimensional space and follow non-geodesic paths [27, 28]. The latter parts made from modified FDM hardware are of high quality. However, this process has only been shown to make, essentially, pultruded FRP rods of limited length. The rods are not designed to adhere to one another and so plies and laminations cannot be made, limiting the size and shape of parts that could be made using this method without performing significant secondary operations, as shown in Figure 10.

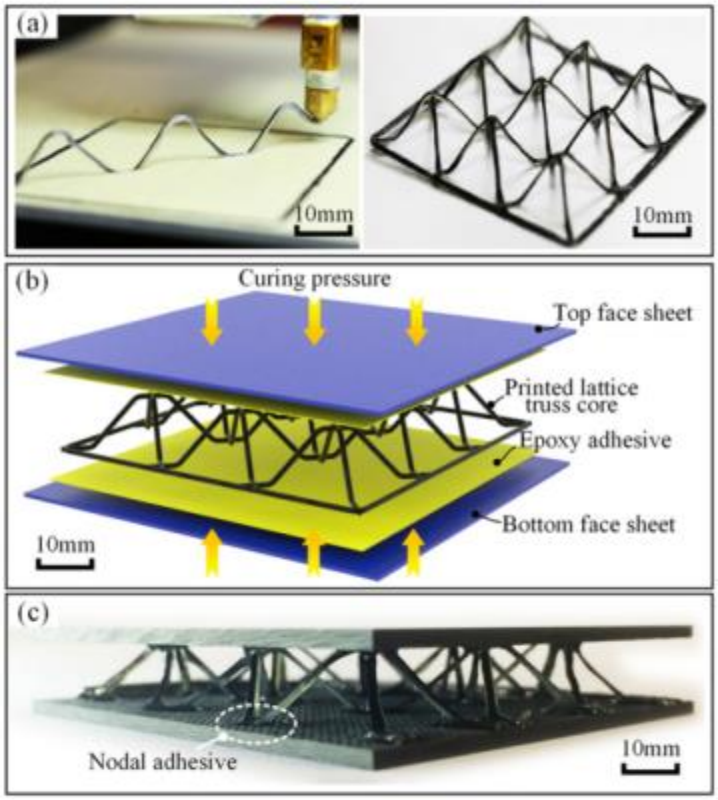

Figure 10: A complete part manufacturing process including significant secondary operations after the initial automated fabrication of the truss core, shown in the top image [28].

1.2.4. Review of Efforts to Vary Fiber Paths

The use of filament winding, ATL and AFP, and FDM to locally vary fiber paths all have associated merits and drawbacks. None of them have demonstrated that they can produce laminated FRP parts of high quality, composed of continuous fiber reinforcement that can follow significantly non-geodesic, out-of-plane paths. Consequently, the efficiency of the FRP material system can still be improved for large, complex parts that can most benefit from increased control of fiber orientation during manufacture, due to large variation of local loads. In many cases, the FRP system is already sufficiently efficient to outperform those made from other materials systems. But, research into the accurate placement of reinforcing fibers continues. To date, a review of these processes shows that out-of-plane, non-geodesic fiber orientations can most likely be achieved using a resin that can stiffen immediately after deposition to resist any movement away from its intended position and orientation. Any quickly curing resin could be a candidate to be used in this way. However, thermoplastic resins are a common choice in the current research in this area, as they 1) soften with heat, 2) only need ambient temperature air to stiffen, and 3) can also subsequently bond after cooling with another application of heat.

1.3. Increasing Efficiency via Matrix Variation

The ability to locally position and orient reinforcing fiber in strict accordance with an optimized design is one way to increase the efficiency of the FRP parts. However, instead of focusing solely on the reinforcing material in composite parts, there are other ways of increasing efficiency, such as developing the flexibility of the matrix composition of the FRP material system, and increasing its independence from the fiber deposition. To ensure adequate wetout, many FRP material systems begin with a product that contains the matrix and fiber combined and distributed into one another. Prepreg tapes and commingled roving are common examples. Naturally, the amount and type of matrix added to the reinforcement is predetermined when forming these products, and so the variability of the matrix within the final FRP part will also be limited.

However, locally varying the relative quantity of matrix (V_f) and matrix composition would also give the capacity to provide the minimum amount of reinforcing material and the desired matrix qualities in each location within a part. Since reinforcing fibers in an FRP system are almost always more dense that the polymer matrix, reducing the amount of reinforcement to the minimum necessary would increase the specific properties of the composite part by reducing mass. And so, a process that could create local variations of fiber orientation to optimize local mechanical response of the reinforcement, while at the same time, minimizing the mass in that area by decreasing the V_f, would maximize the specific properties in that area. This might be particularly attractive in regions of thickness transition, for instance. Decreasing the V_f, instead of simply subtracting existing composite material would impart additional design flexibility, such as allowing the geometry and size of a design to be preserved without one being required to add more mass than is necessary. Designing with the ability to locally change the matrix composition would give one the ability to locally tailor the FRP's properties such as stiffness and toughness, for example. FRP component properties are a function of the reinforcement and matrix properties, and polymers display a wide range of values of mechanical performance and physical attributes, as seen in Table 1.

TABLE 1: Some common polymers and their widely varying mechanical properties [34].

Material	Specific Gravity	Tensile Modulus [GPa (ksi)]	Tensile Strength [MPa (ksi)]	Yield Strength [MPa (ksi)]	Elongation at Break (%)
Polyethylene (low density)	0.917–0.932	0.17–0.28 (25–41)	8.3–31.4 (1.2–4.55)	9.0–14.5 (1.3–2.1)	100–650
Polyethylene (high density)	0.952–0.965	1.06–1.09 (155–158)	22.1–31.0 (3.2–4.5)	26.2–33.1 (3.8–4.8)	10–1200 40–80
Poly(vinyl chloride)	1.30–1.58	2.4–4.1 (350–600)	40.7–51.7 (5.9–7.5)	40.7–14.8 (5.9–6.5)	
Polytetrafluoroethylene	2.14–2.20	0.40–0.55 (58–80)	20.7–34.5 (3.0–5.0)	–	200–400
Polypropylene	0.90–0.91	1.14–1.55 (165–225)	31–41.4 (4.5–6.0)	31.0–37.2 (4.5–5.4)	100–600
Polystyrene	1.04–1.05	2.28–3.28 (330–475)	35.9–51.7 (5.2–7.5)	–	1.2–2.5
Poly(methyl methacrylate)	1.17–1.20	2.24–3.24 (325–470)	48.3–72.4 (7.0–10.5)	53.8–73.1 (7.8–10.6)	2.0–5.5
Phenol-formaldehyde	1.24–1.32	2.76–4.83 (400–700)	34.5–62.1 (5.0–9.0)	–	1.5–2.0
Nylon 6,6	1.13–1.15	1.58–3.80 (230–550)	75.9–94.5 (11.0–13.7)	44.8–82.8 (6.5–12)	15–300
Polyester (PET)	1.29–1.40	2.8–4.1 (400–600)	48.3–72.4 (7.0–10.5)	59.3 (8.6)	30–300
Polycarbonate	1.20	2.38 (345)	62.8–72.4 (9.1–10.5)	62.1 (9.0)	110–150

1.4. Previous Efforts to Increase Efficiency via Matrix Variation

Documented attempts to develop manufacturing processes to increase the independent control of the matrix component, either through the local variation of V_f, or by locally varying matrix composition, are uncommon. It is less common to find work to create methods to achieve this independence that are consistent with those techniques that have been shown to be able to create local variation of fiber orientation. Most often, when developing FRP material systems and manufacturing methods, considerations regarding the matrix are instead primarily focused more on preserving the quality of the matrix, ensuring adequate wetout, and meeting the targeted V_f value. Improving the quality of the composite is the primary consideration.

1.4.1. Efforts Using Variants of the Fused Deposition Modeling Process

The designers of hardware used to make FRP parts using the FDM process occasionally claim to be able to control V_f [23, 28, 29]. Sometimes V_f is modified by adding neat polymer alongside the reinforced material so that the V_f is varied only by averaging over the total cross-sectional area of the part [23]. Other attempts to make composite parts with FDM include mixing the continuous fiber and the matrix in the FDM hot end [28], as shown in Figure 11. In this case, V_f can be varied by changing the volumetric flow rate of the matrix while fiber deposition rate is held constant, increasing the V_f. These efforts demonstrate very limited control of the V_f [23], are not experimentally confirmed [29], or generate FDM parts with lower quality than is generally expected from a useful FRP part [28]. Either the bonding between roads of material is low [28], a defect commonly seen in FDM parts, or the FRP part contains significant voids [23, 28], poor interfacial strength [23, 28], wavy fiber reinforcement [23], or low V_f [23]. Rather than modifying V_f, the ability to place a variety of matrices during the manufacture of an FRP part using FDM seems more likely as it is common-place for FDM to be able to switch between matrices, although using this approach to make FRP parts is not apparent in the academic literature.

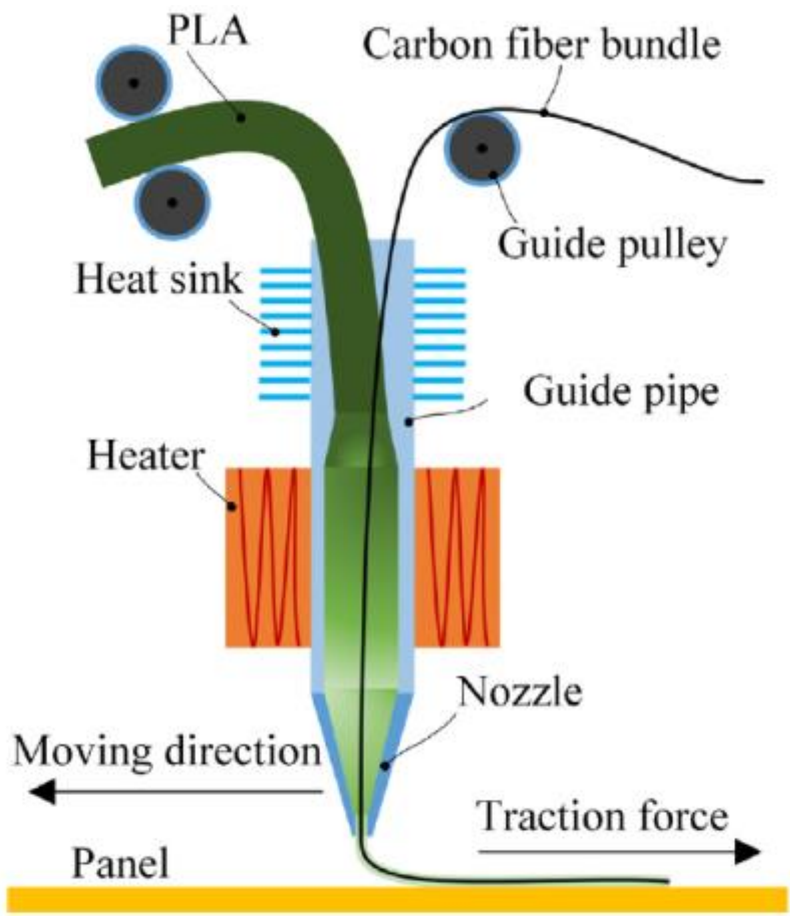

Figure 11: Mixing continuous carbon fiber and a PLA matrix in an FDM hot end [22].

1.4.2. Efforts Using In-Line Fiber Impregnation Processes

Researchers have made a few attempts to separate the fiber addition from the matrix addition by developing processes to impregnate fiber reinforcement just before deposition onto a supporting surface. Most efforts involve a melt-impregnation process combined with thermoplastic winding: First, the softened thermoplastic impregnates the reinforcement, and then tubes are wound on the mandrel [31, 32, 33]. At least one effort has instead incorporated a powder impregnation scheme into the same approach [30]. These efforts have produced FRP parts of fairly good quality with varying V_f [31, 33], they have lowered cost by reducing the use of value-added materials such as prepreg [32], and they have demonstrated relatively high deposition rates with higher speeds usually limited by the high tension developed in the reinforcing fiber due to being pulled through small dies during the impregnation process [32-34]. In all of these cases, the impregnation processes always require a significant amount of additional hardware compared to that needed for conventional thermoplastic filament winding with towpreg or commingled tow, while also requiring the concurrent control of an independent impregnation process during the FRP part manufacture, as shown in Figure 12. One research group attempted to vary the V_f through the thickness of a filament wound tube, but the variation through the thickness was not confirmed [33]. These investigations with in-line impregnation did not explore the idea of varying the matrix material throughout FRP parts.

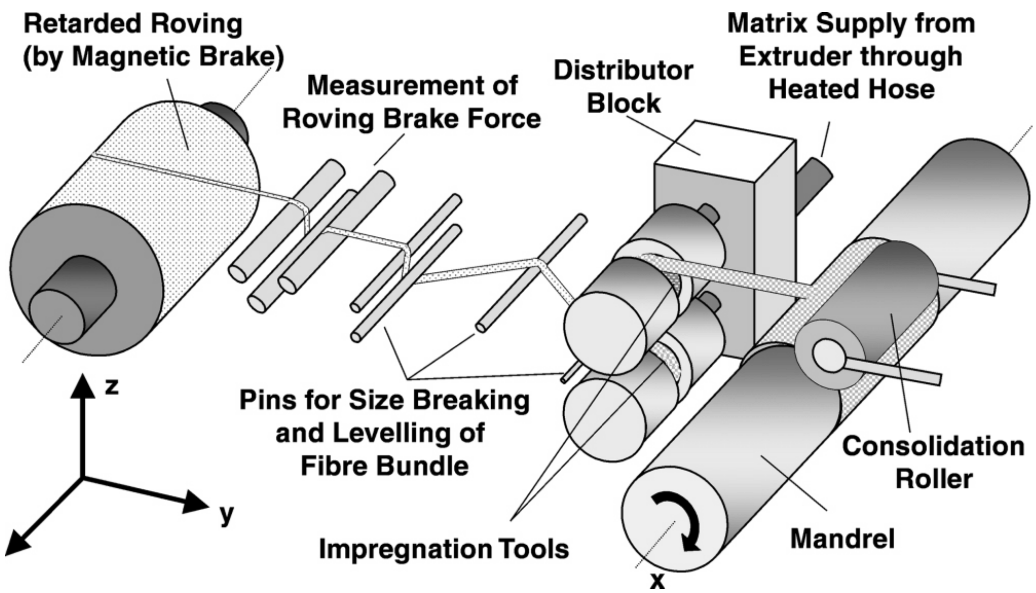

Figure 12: Hardware used in the in-line roving impregnation and winding process. Not shown are the nip point heating and temperature control hardware, as well as the device that controls the impregnation environmental temperature [33].

1.5. Experimental Motivation and Objectives

A polymer matrix continuous fiber reinforced composite (FRP) manufacturing method that could address the inefficiencies in the FRP material system stemming from both misplaced reinforcement and inflexible application of the matrix could significantly increase the specific properties of FRP components. A fiber reinforced composite material system that contains 1) fibers that are misoriented to the load vector and 2) a matrix that cannot vary to change local V_f and matrix composition limits the performance of a resulting part. In this work, a process will be investigated that is consistent with the techniques that have been developed to locally vary fiber orientation. However, by separating the matrix and the fiber addition, this new process could also improve the localized variation of V_f and matrix composition within a single FRP part. The proposed process uses 1) automated fiber placement and 2) a thermoplastic matrix which will quickly stiffen upon cooling, that have both been shown to be able to produce locally-varying, out-of-plane, non-geodesic fiber paths that can form laminated components. The proposed process is also likely to be able to locally vary the amount and type of the deposited matrix by separating fiber placement from the matrix deposition. Since the proposed process impregnates and consolidates in the same area at the same time, it reduces reliance on additional impregnation hardware while increasing the independence of the added matrix volume and composition. Because the process uses separate matrix and reinforcement materials, it should also be less expensive to perform, compared to processes that use a previously integrated matrix and fiber material system. The process investigated here adds a thermoplastic matrix to reinforcing glass fiber just prior to the beginning of the consolidation of the FRP material by a heated pressure foot. Due to the delayed addition of the matrix, the automated process could be described as a 'just in time, automated' (JITA) composite manufacturing process. And so, the addition of the matrix, the impregnation of the fibers, and the consolidation of the composite all begin concurrently. In the JITA process, PETG is extruded from a fused deposition modeling print head in advance of a heated pressure foot that impregnates continuous E-glass fibers and consolidates the composite against a heated mandrel. To direct this research effort, the scope of the investigation will be delimited by the following hypothesis: *Through the combination of extruded thermoplastic matrix material and dry fiber at the point of contact with the tooling surface, a composite material of a comparable quality to that of more conventionally produced continuous fiber reinforced thermoplastic matrix composites can be achieved.*

To make process comparisons based on a quantitative measurement of quality, the short beam shear (SBS) strength of FRP beams, produced with the JITA process, will be maximized using a statistics-based optimization study. The JITA beam optimum strength will be subsequently compared to the maximized SBS strength of optimized beams produced by similar hardware, but a different initial material system consisting of commercially available, commingled PETG/E-glass instead of separate dry roving and PETG polymer. Further comparisons of beams from each process, using additional results of the optimization studies, microscopy, physical testing, and thermal analysis techniques, will be made.

2. PRELIMINARY RESEARCH EXPERIMENTAL

2.1. Process Description and Machine Raison D'être

The proposed process (JITA) was developed with the intent to remain consistent with those processes that have shown to have additional control over the reinforcement fiber paths in polymer matrix continuous fiber reinforced composites (FRP). Consequently, it uses automated fiber placement with a thermoplastic matrix. Additionally, one of the primary goals of the process is to increase the independence of the matrix addition from the fiber addition. This last feature should allow for matrix volume and composition to be varied locally within an FRP part. In order to create this independence, the material inputs to the process are separate neat polymer and dry roving. The thermoplastic matrix is added separately at the same deposition surface location that the fiber is added in order to maintain the independence. Impregnation is accomplished concurrently with consolidation, requiring no additional hardware for impregnation except for an extruder to heat and then add the matrix.

The ultimate effect of allowing local fiber and matrix variation would be to increase the specific properties of the resulting FRP components, and so to increase the FRP material system efficiency. Since, in the JITA process, 1) there would be a minimal addition of hardware beyond that needed by the commercial baseline system, and 2) the JITA material inputs would be less expensive, the JITA process should be cost competitive with the commercial system. If the proposed process is cost competitive, the demonstration that the JITA and commercial systems make parts of comparable quality would further justify continued development effort of the JITA system. This work will describe the development of the JITA process, establish that it does make FRP parts of comparable quality compared to a more conventional process, and confirm that the JITA system's costs-competitiveness on the basis of material inputs to the process.

2.2. Manufacturing Requirements and Machine Development

2.2.1. The JITA Process Development

Like all FRP manufacturing processes, the JITA process requires 1) the accurate placement of the continuous fiber reinforcement, 2) complete wetout of the fiber by the matrix, 3) the removal of voids during the wetout process, and 4) consolidation of the composite. In addition to these common requirements, the JITA process needs to accommodate the use of a quickly and easily solidifying polymer as its matrix and needs to use automated hardware to place the continuous fiber reinforcement. A process that is very similar to a thermoplastic filament winding process can fulfill these needs with relatively simple hardware and was the manufacturing approach upon which the JITA system was based. This approach includes 1) the precise, automated placement of continuous reinforcing fiber onto a rotating mandrel, 2) the extrusion of heated thermoplastic matrix onto the mandrel just before fiber is placed down on the mandrel, and 3) both the impregnation of the fiber by the matrix and also the consolidation of the matrix and the fiber as they pass between a pressure foot and the mandrel.

2.2.2. Process Parameters of Interest and Required Hardware

The process variables that were most likely to have an impact on JITA part quality and that were chosen as variables in this study are 1) the temperature of the mandrel, 2) the temperature of the extruder, 3) the temperature of the consolidation foot, 4) the force from the consolidation foot, 5) the roving tension, and 6) the process speed. The FRP parts made by the conventional process would be affected by the same parameters, except there would be no extrusion of the matrix as the commingled material system does not require any matrix to be added. The hardware used in this research effort must allow the variation and control of the FRP manufacturing parameters necessary to optimize the quality of the FRP parts resulting from both the JITA process and from the baseline conventional process. The establishment of these process variables led to the need for the following hardware components, seen in Figure 13: a) a heated, cantilevered mandrel, b) a heated foot with variable consolidating pressure, c) a heated matrix extruder (hot end), and d) a fiber payout device (brake spool) that created variable fiber tensioning (not shown).

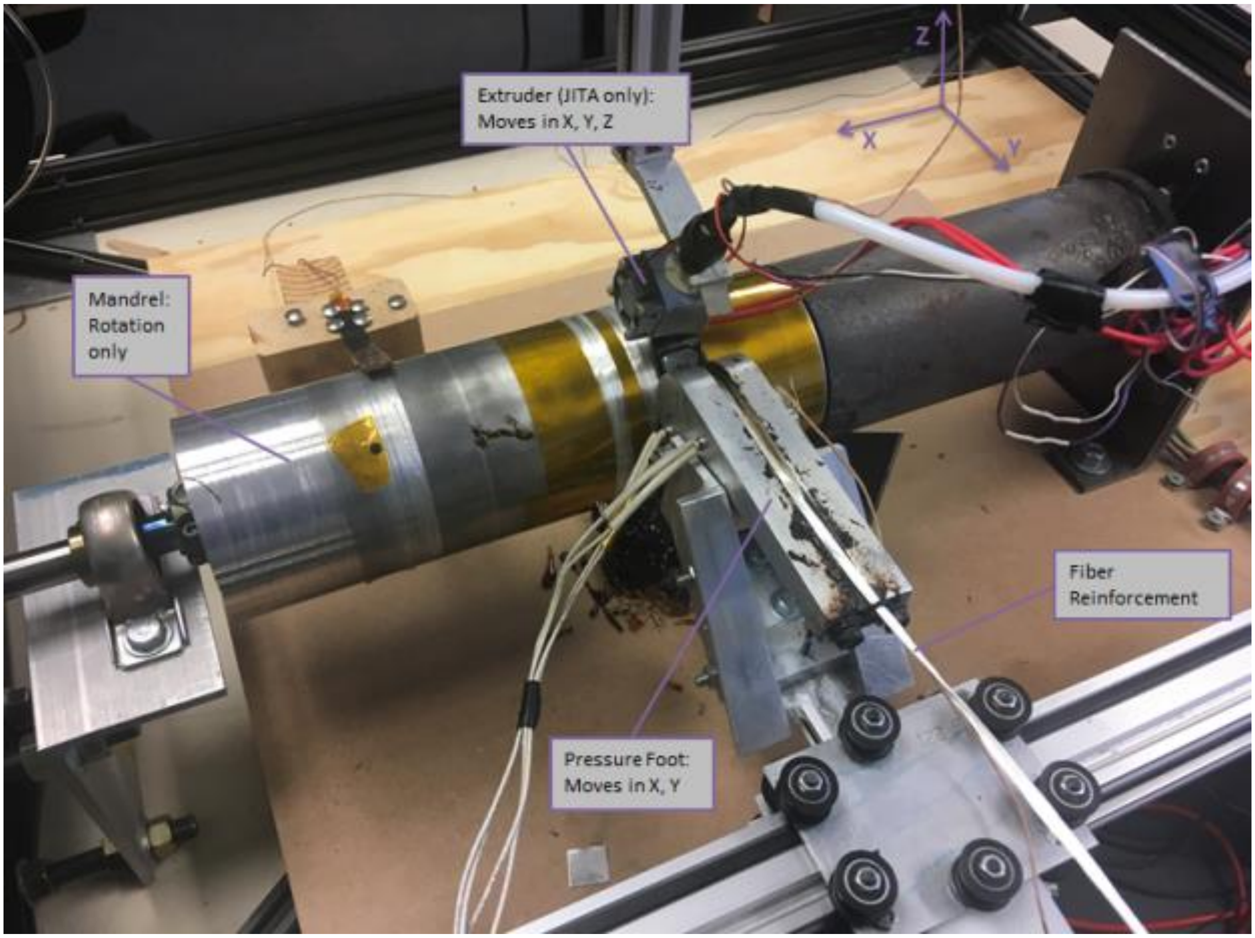

Figure 13: Machine components and the directions in which each component can move.

2.2.3. Previous Work

The motion control hardware of the machine was developed by colleagues in previous efforts and is essentially a Cartesian coordinate gantry system with an additional component to control the rotation of a mandrel. All motion is generated with stepper motors that can produce both the specified speed and position of the hardware. A stepper motor also drives the FDM-style polymer filament through a commercial FDM extruder head during the JITA process.

2.2.4. Hardware Design, Development, and Manufacture

Modifications made during the course of this work to the existing hardware included 1) the stiffening of the frame to resist the movement of the cantilevered mandrel under the consolidation force loading, 2) the reinforcement of the cantilevered arm that position the pressure foot, 3) alterations to the FDM hot end nozzle to allow for higher extrusion rates and to spread the matrix immediately after extrusion onto the mandrel, and 4) modifications to the hot end so that higher temperatures can be reliably reached. Additionally, new functionality was added by the design and fabrication of a heated mandrel, and a heated consolidation foot. The final configuration of hardware shown in Figure 13 allowed the necessary control of the process variables identified as necessary for investigation.

2.3. The JITA and Commercial Manufacturing Processes

One significant difference between the JITA process and the comparable commercial process used here is the material input; the former process requires the addition of a matrix to the dry roving, and the latter uses commingled roving, which already contains both the reinforcement and the matrix, each in fiber form. Therefore, the JITA process requires an extruder (hot end) to add a thermoplastic matrix, while the commercial winding method does not.

The process to create the FRP tubes consists of the following sequential steps:

a) Kapton film is placed around the mandrel to serve as a release film to facilitate the removal of the tube from the mandrel.

b) Either dry roving or commingled roving is wound onto the brake spool. The brake creates the tension in the roving when making JITA or commingled tubes, respectively.

c) The roving is anchored on the mandrel and the roving tensile force is set by adjusting the brake while the mandrel is moving at the specified rotational speed for the production of the current tube.

d) The pressure foot is then adjusted to create the desired consolidation force by adjusting the length of a spring that ultimately presses the foot against the mandrel

e) If the hot end is to be used, it is positioned in the same location before each part is made.

f) The mandrel and the consolidation foot are set to their specified temperature. When using the JITA process, the hot end is brought up to its specified temperature at this time.

g) The G-code program that controls the stepper motors is run through the motion control hardware to produce the desired FRP part.

h) Fiber Placement: During part fabrication, as the dry or commingled roving is pulled from the fiber brake, it follows a groove that is machined along the top of the pressure foot. It then proceeds down the face of the pressure foot and is wound around the mandrel. The pressure foot travels back and forth along the length of the mandrel to place the roving and applies consolidation pressure to make the FRP tube, as is shown in Figure 14.

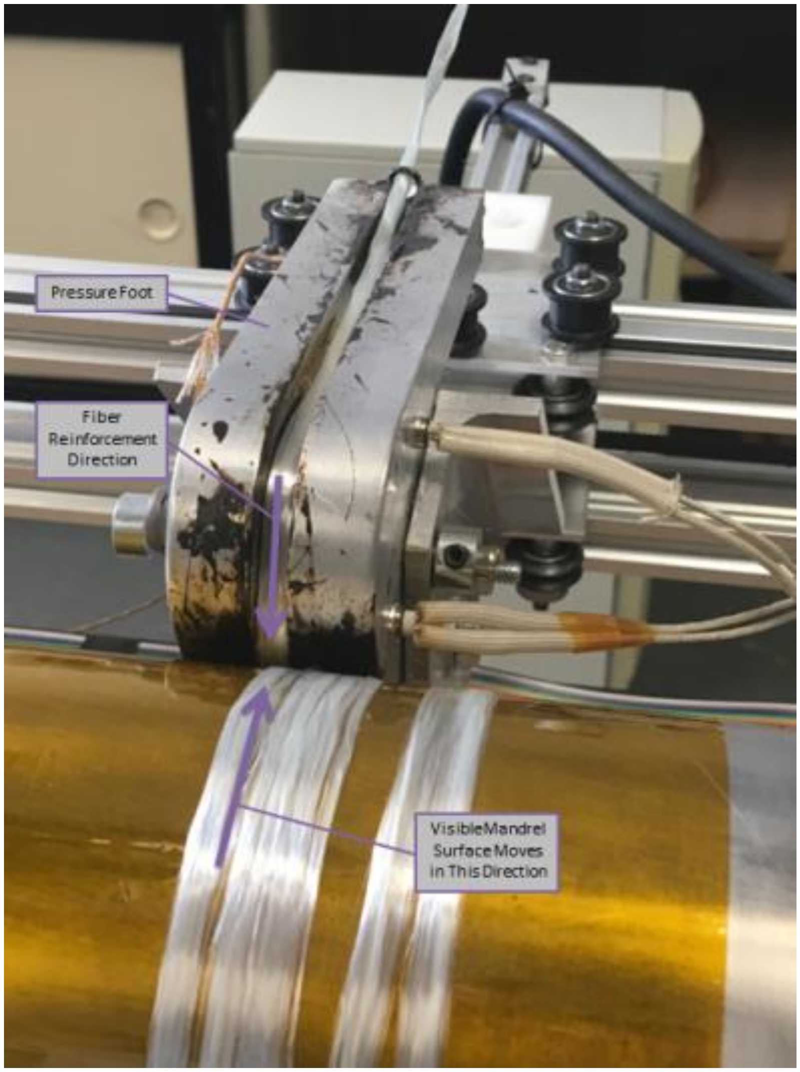

Figure 14: Fiber reinforcement path as it is deposited onto mandrel.

i) Matrix Placement: During the JITA process, the FDM hot end moves along the length of the mandrel concurrently with the pressure foot, as shown in Figure 15, as the hot end extrudes thermoplastic onto the mandrel just prior to fiber deposition. The extruded matrix is placed on what will be the center of the path of the roving. During impregnation and consolidation, it is the rotation of the mandrel that moves both the fiber and matrix between it and the consolidation foot.

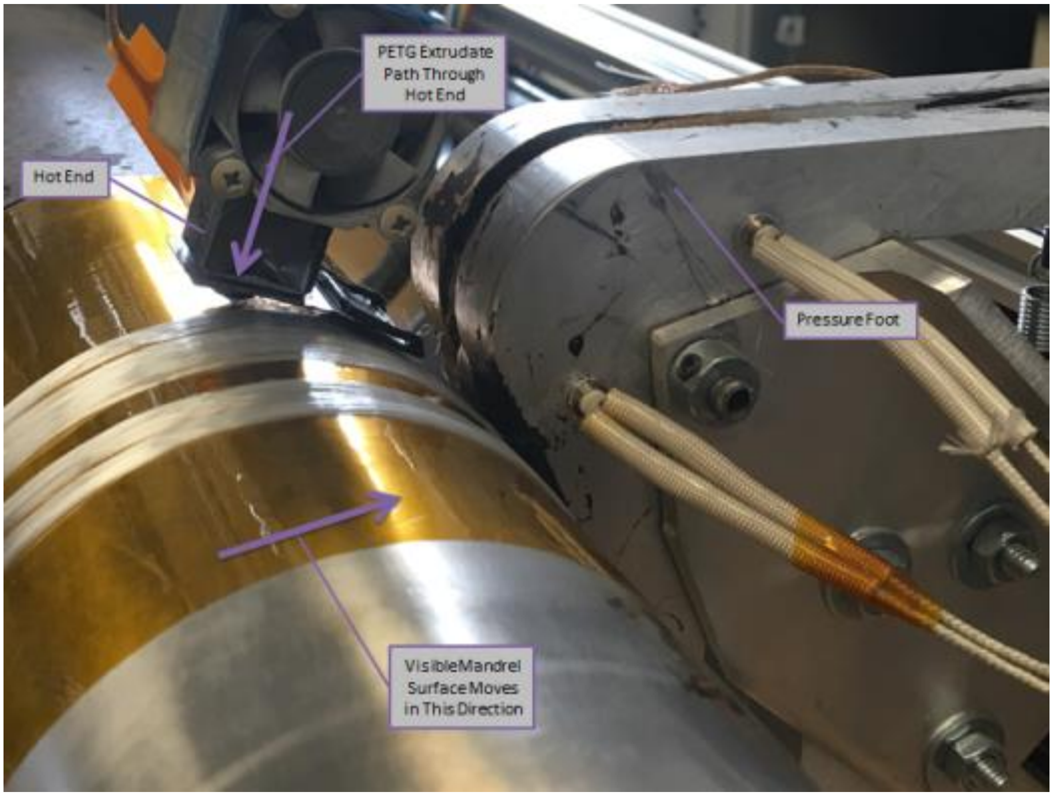

Figure 15: Image of matrix deposition during JITA process, which uses hot end to extrude PETG onto mandrel.

j) After the FRP tube has been made, all heated equipment is turned off and the part is allowed to cool. The roving tension is not released until the part has cooled.

k) Once the tube has reached room temperature, it is removed from the free end of the mandrel.

The JITA process hardware kinematics include the rotational movement of the mandrel and the linear movement of the pressure foot and the hot end. In accordance with the coordinate system shown in Figure 13, the hot end can move in both directions along the x, y, and z-axes at variable speed. The mandrel can rotate in either direction at variable speed. The heated pressure foot can move along the x and y-axes in both directions at a specified speed. All of the machine components can be moved concurrently. A G-code program was developed to make the desired FRP parts for each manufacturing process. The JITA process requires the coordinated motion of the hot end, mandrel, pressure foot, and matrix filament extruder, while the commercial process does not need hot end or extrusion control.

2.4. Test Specimens

Simple parts were made during this study in order to establish the highest quality tubes that both the JITA and the commercial processes could make by reducing the effects of complicated geometries and multiple fiber paths. The geometric requirements for the filament wound tubes were that they produce enough material for evaluation, and that the radius of curvature be large enough that the short beam shear testing could be performed. And so, tubes with 25.4 mm of testable width, a 102 mm ID, and 3.43 mm thickness were produced using both the JITA method and the commercial method. All tubes were wound so that their fiber angles were in the XZ plane as shown in Figure 13 (hoop wound). Figure 16 depicts tube features that illustrate the manufacturing process used for all tubes, which was as follows: 1) an anchor, composed of one mandrel revolution of fiber deposition is wrapped around the mandrel, 2) the roving deposition is moved 15 mm away from the anchor while the mandrel is turned one more revolution, 3) the pressure foot deposits a 25.4 mm width of material onto the turning mandrel, 4) a 0.5 revolution dwell is wound around the mandrel, and, finally, 5) additional 25.4 mm wide layers are deposited, with a 0.5 mandrel revolution dwell at each end before creating a new layer. The final, total width of each tube will vary as the consolidating forces and hardware temperatures were different during the production of each sample. However, the tubes were all constructed to the 3.43 mm thickness before terminating the manufacturing process. The fiber angle in the testable, ‘hoop-wound’ area was deposited at 88 degrees in all samples, relative to the x-axis in Figure 13.

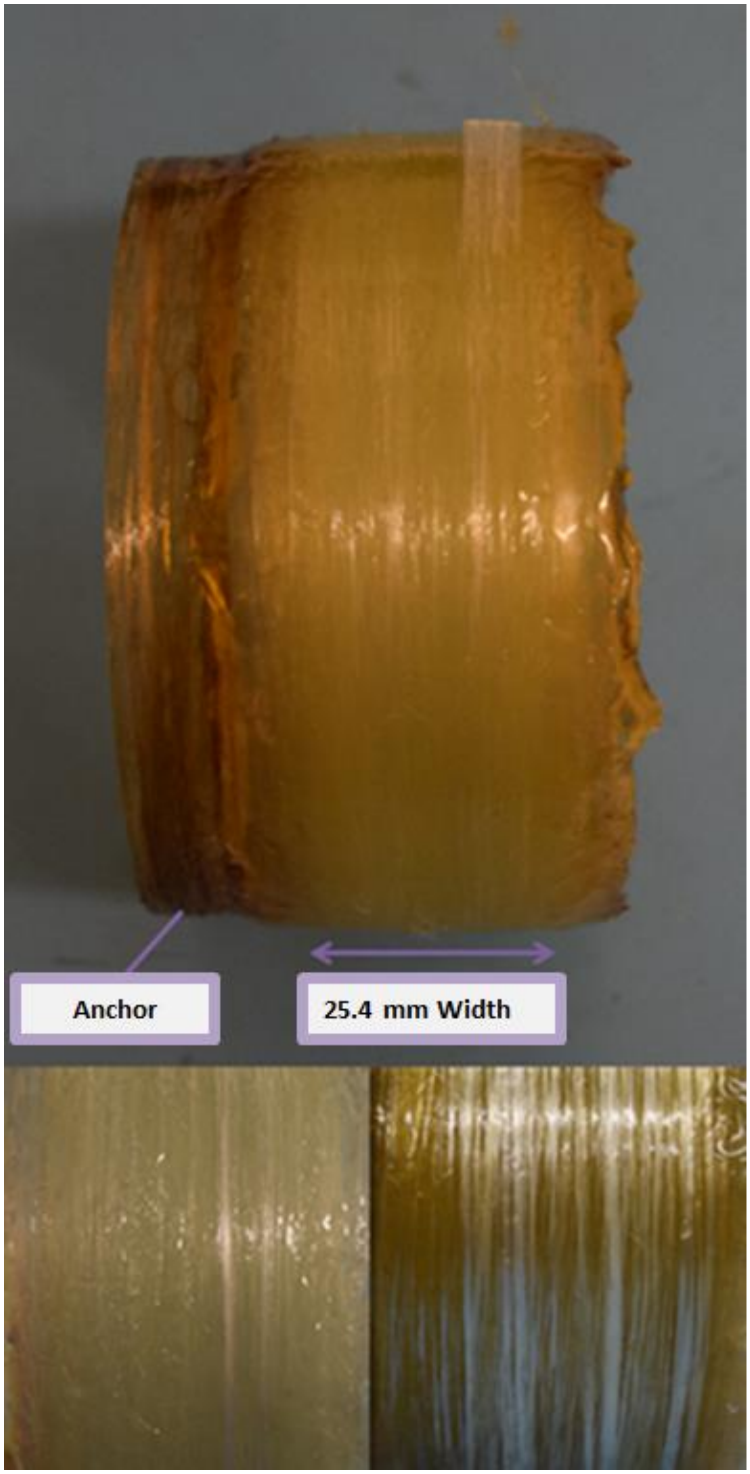

Figure 16: A typical FRP tube is shown in the top image. The image in the bottom left shows the typical outer surface of a commingled tube. In the bottom right is the typical outer surface of a JITA sample.

2.5. Material Systems

The tubes made in this study all contained continuous E-glass fibers with a thermoplastic PETG matrix. The material system used as the commercial baseline was FGI Twintex commingled E-glass and PETG, 2690 tex. This commingled roving consists of intermixed continuous glass fibers and PETG fibrils of roughly the same diameter, of 20 microns. The dry E-glass roving used in the JITA process was PPG Tufrov 4588, 2200 tex, which is sized for thermoplastic polymers. The Tufrov fiber diameter is approximately 12 microns. During the preliminary research, the JITA matrix consisted of 3.0 mm Form Futura PETG FDM filament, while the JITA matrix used for the main study was 3.00 mm PETG FDM filament from Maker Series. Kapton film, 0.025 mm thick, was used as the release film for all samples.

2.6. Test Methods and Evaluation Techniques

2.6.1. Short Beam Shear Testing

Due to their fabrication via lamination, FRP parts of poor quality can often trace the cause of low performance to their interlaminar region [35, 36]. Consequently, tests that evaluate the interlaminar shear strength (ILSS) of a composite are often used as indicators of component quality and as verification of acceptable processing parameters [35, 37, 38, 39]. Testing methods that load FRP parts with normal stresses along the fiber direction are less sensitive to defects in the interlaminar region and are also less sensitive to the variation of manufacturing parameters [40]. For example, split-ring testing (ASTM D2290) is often used to test filament wound FRP components, but this test loads hoop-wound FRP samples in the fiber direction and, as a result, has shown this aforementioned insensitivity to weak interlaminar regions and process variability, compared to the results of ILSS testing [33].

As the main purpose in the mechanical testing of FRP parts produced during this study was to compare measures of quality, ILSS testing was needed, but there are few available tests of ILSS that can accommodate curved components [36, 39]. A more recent solution to this need is the compression shear test (CST), which requires little material, needs only a small amount of sample preparation, and produces relatively consistent shear stress through the sample, allowing it to be used to produce accurate shear properties for FRP design [35, 36, 39]. However, the test requires a unique test fixture solely for the purpose of ILSS testing. A more common test method of ILSS is the short beam shear (SBS) test (ASTM 2344) [36-39, 41-45]. The CST fixture and the short beam shear test fixture are depicted in Figure 17. Similarly to the CST test, the SBS fixture can also be used to evaluate curved components and also requires only small amounts of material for analysis. However, it instead uses a simple and common 3-point bend fixture. Although SBS tests load the sample in bending, the span of the support pins is reduced to exaggerate accompanying shear stress in the tested beam relative to flexural stresses to the degree that interlaminar shear failures are often produced.

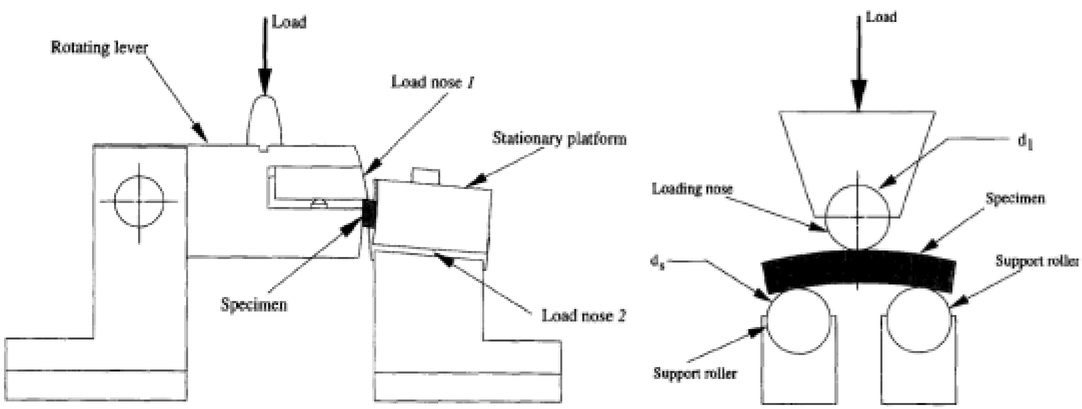

Figure 17: On the left is the device used to create uniform shear through the specimen using CST. An SBS test fixture is shown on the right [35].

However, the three contact points are too close together to appropriately apply Saint-Venant's principle, and an unanticipated shear distribution around the central loading nose, illustrated in Figure 18, is created, which can cause unintended failure modes [35-39, 46]. Also, high compression stresses can be found under the loading nose during SBS testing [35, 36, 38, 46]. Lastly, the shear stress is produced by a bending load, and, as a consequence of these complicating factors, a complex stress state results [35-37, 46]. Therefore, it is recommended that SBS not be used to generate quantified shear properties [35, 37, 38, 39].

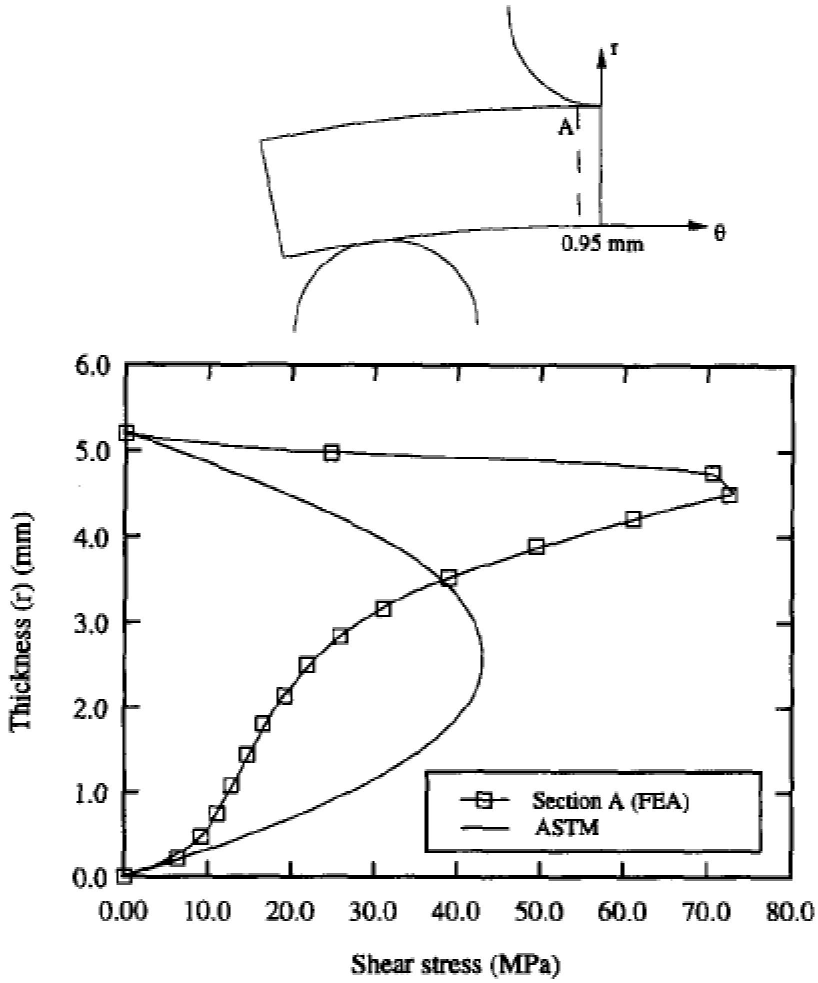

Figure 18: Shear stress variation through the thickness of a beam near the loading nose during SBS testing. Not shown are the significant compression stresses near the contact points [35].

In this study, mechanical testing is not intended to quantify the interlaminar shear strength and modulus of the FRP parts. It is instead meant to evaluate the relative quality of the samples. So, although SBS is not the ideal test for generating numerical measurements of shear properties, it is used here in both the preliminary and the main studies as a commonly-accepted quick and efficient measure of quality [35, 37, 38]. Additionally, SBS testing will be used here to *compare* the quality of multiple samples instead of using the absolute measurements of SBS strength; this use further alleviates concern that SBS would be an inadequate test, as long as the testing procedure remains consistent.

The performance of an FRP part during mechanical testing generally relies on 1) the reinforcing fiber properties, 2) the matrix properties, 3) the character of the bond between the fiber and matrix, and 4) the microstructure of the resulting FRP material. As the SBS test is intended to cause failure in the interlaminar region, the fiber properties are likely to be less significant than those of the polymer matrix during testing. The reinforcing fibers in this study were sized for a thermoplastic matrix, and so it will be assumed in this work that the interfacial bond is sufficiently strong to not be the primarily determinant of the SBS testing results. Additionally, the fiber angles in all samples should be the same, and so the FRP fiber orientation and dispersion will be assumed to by similar in the samples unless the metallographic analysis proves otherwise. The degree of wetout and consolidation of the FRP material are likely to vary as processing conditions are changed. Consequently, variation of the matrix properties are likely to have the largest unintended effect on the SBS testing results.

Glycol-modified polyethylene terephthalate (PETG) is the matrix component in the FRP material system used in this work, and is a random copolymer of PET and glycol-modified PCT [64]. In contrast to PET, the PETG polymer resists the development of crystallinity to remain a glassy thermoplastic both during and after processing [64]. As an amorphous polymer, there are no complications from a varying amount or changing morphology of crystallinity in predicting the effect of polymer properties on the strength of the polymer [65]. The property of a specified glassy thermoplastic polymer most likely to produce a change in strength is molecular weight [65-67]. Up to the critical molecular weight (MW_C), strength increases rapidly as molecular weight increases due to increasing molecular entanglement [65-67], which decreases the ease of relative motion between neighboring polymer chains. Molecular weights larger than MW_C are more likely to allow enough generated stress in the chain that failure is produced by chain scission [67]. However, the lack of crosslinking and crystallinity in PETG, and the emphasis on deviatoric stress produced during SBS testing is more likely to produce polymer failure from relative motion of the polymer chains in the creation of shear bands than to cause failure by chain scission during an alternative failure mode such as crazing, for example [65]. Consequently, assuming equal amounts and morphology of defects within the matrix, variations of the strength of the matrix during SBS testing is more likely to rely on the average MW within the PETG polymer than on the strength of the atomic bonds within the polymer chain backbone.

The results from SBS testing will be reported as SBS strength, not as shear strength since the quantitative shear properties are not of interest in this work. This testing was conducted in inch-pound units, but is reported here in SI units. Each sample tube created by JITA or the commercial process produced five SBS test specimens, removed from random locations within testable width of the sample. Each of these five curved beams were 5.72 mm wide, by 2.84 mm thick, with a chord length of 17.1 mm, and their inner radius of curvature was 51 mm. An example of a typical SBS specimen is shown in Figure 19.

Figure 19: An example of an SBS beam used in this study. The continuous glass fibers are approximately horizontal in this image.

2.6.2. Additional Evaluation Techniques

Additional techniques were also used to evaluate the samples resulting from the JITA process and the comparable commercial process. Light microscopy gave an indication of the microstructure and the location and size of voids. Archimedes testing (ASTM D792) and burnout testing (ASTM 3171) were used to measure the V_f and the void content percentage of FRP samples. Statistical analysis revealed 1) the predicted maximum possible part quality from each process, 2) which process parameters or combinations of parameters made significant contributions to the FRP quality, and 3), as a result, which simplifications to the processes could be made by reducing the unnecessary control of process parameters. Finally, thermal analysis techniques, such as thermogravimetric analysis (TGA) and differential scanning calorimetry (DSC) were used to characterize and compare the three different PETG matrices that were used in this work.

3. PRELIMINARY STUDY

3.1. Motivation and Background

To evaluate the potential of the proposed (JITA) process, a brief, initial comparison of the JITA method to the commercial baseline process was conducted. This evaluation was made on the basis of resulting part quality. Indications that the JITA process could make polymer matrix continuous fiber reinforced composite (FRP) parts of comparable quality would justify further investigation into the maximum quality parts that both processes could produce. Establishing that the JITA process can make parts of comparable would validate the feasibility of a process that could allow for the local variation of fiber and matrix within an FRP part. The ability to locally vary the material characteristics of FRP components would create added design potential, ultimately leading to a more efficient and therefore more attractive material system.

The JITA manufacturing process and the commercial baseline process use similar hardware to produce FRP test specimens. Both processes utilize the following components: 1) a heated mandrel, 2) a heated consolidation foot that can apply varying amounts of force, 3) a fiber brake to both dispense and create tension in the roving, 4) a motion control system to coordinate the movements of the mandrel and the foot, and 5) temperature control to independently regulate the temperature of the mandrel and the foot. As shown in Figure 20, a heat gun was used to regulate the mandrel temperature during the preliminary study. Later, an oven element was instead inserted into the end of the mandrel to more reliably reach higher temperatures. Simple, hoop wound tubes made from continuous E-glass fiber with a PETG matrix were fabricated as test specimens using both processes in order to maintain the focus of the study on part quality, rather than on part complexity.

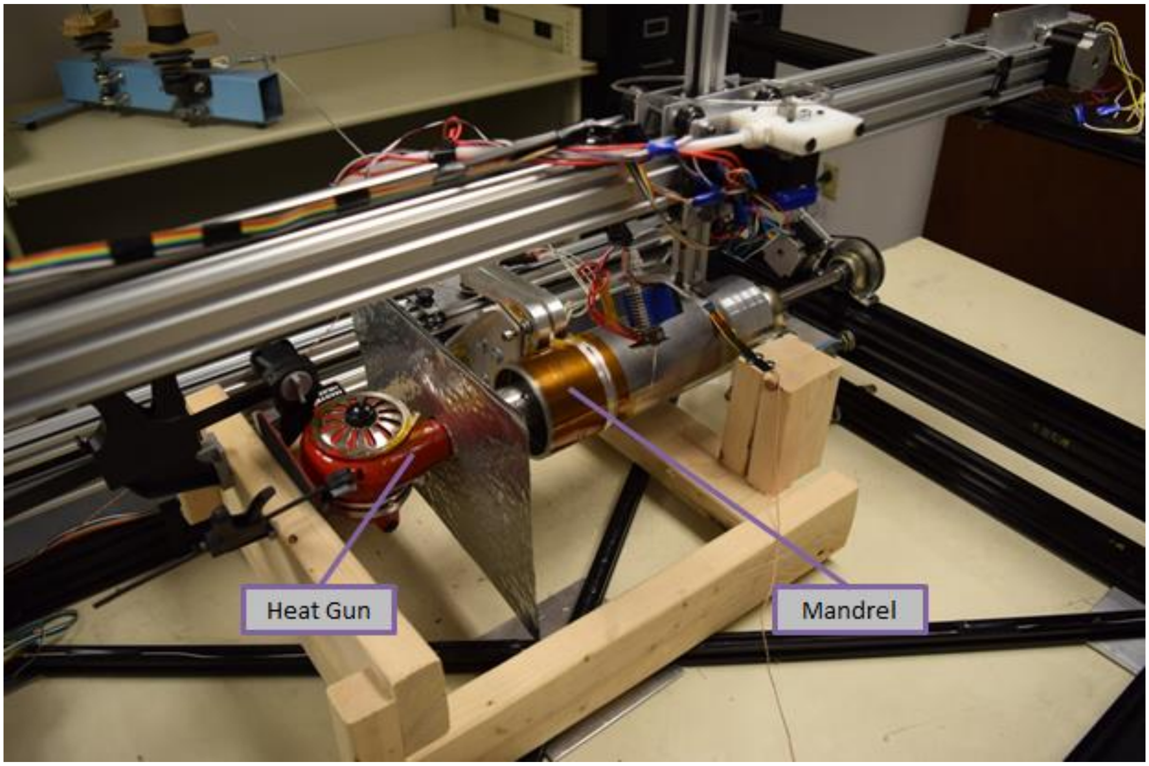

Figure 20: The hardware configuration for the preliminary study. The heat gun shown in this image was later replaced by a different heating element to be used in the main study.

There are a few significant differences in the hardware and manufacturing methods of the two processes, which are partially the result of fundamentally different material inputs. The JITA process requires a thermoplastic extruder (‘hardware requires precise motion control and temperature regulation, as well as control of the PETG delivery to the extruder. Since the commercial baseline process uses commingled roving to make the FRP tubes, it does not need additional matrix material, nor does it need the additional associated hardware. Samples made with the commercial baseline process are fabricated by 1) threading the commingled roving through the groove at the top of the consolidation foot, 2) anchoring the roving to the mandrel, 3) setting all desired hardware temperatures and positions, as well as the desired roving tension and foot pressure, 4) winding the roving around the mandrel to anchor the material, and 5) starting the automated motion control, which moves material deposition away from the anchor and subsequently creates the test sample. The machine is then turned off and the part is cooled and removed. After the specimen has cooled, the Kapton release film is peeled from the inner surface of the tube, if still attached, before testing and analysis.

In comparison, the JITA process is similar in that the fiber deposition proceeds in much the same way, except the reinforcing fiber is not mixed with the matrix in the as-received state, as it is when using commingled material. Consequently, the PETG needs to be added to the fiber, which occurs via the extruder. The extruder leads the pressure foot as they both travel along the length of the mandrel, and deposits matrix along the center of the anticipated fiber path. The matrix and fiber are mixed and ultimately consolidated as the FRP components pass between the heated mandrel and the heated pressure foot.

The material systems used in the preliminary research were 1) commingled roving used for the baseline technique and 2) dry roving and PETG 3D printing filament, used in the JITA process. The commingled roving was FGI Twintex commingled E-glass and PETG, 2690 tex, with a 54% V_f as-received. The JITA process used PPG Tufrov 4588, 2200 tex as the E-glass reinforcement and 3.0 mm Form Futura PETG FDM filament as the matrix. This PETG matrix used for the JITA process in the preliminary study was a different brand and, it was discovered later, a different composition compared to the PETG matrix used in the main study. This difference in composition appears to have had a significant impact on the quality of the resulting FRP samples. Consequently, the matrix used in the preliminary study and, when necessary, the associated preliminary process and its resulting samples will distinguished from those in the main study by referring to the former as 'JITA-P' and the latter as 'JITA-M'. However, the commingled material used in the preliminary work was the same as that used in the main study.

3.2. Design of Experiment

In the preliminary study, only hardware temperature was varied during the comparison of the JITA-P and the commercial processes. All hardware was set to the same temperature as each tube was made. Based on prior fabrication experience, two temperatures that were likely to produce parts of high quality were chosen at which to evaluate the samples from each process, 190 °C and 220 °C. And so, for example, during the JITA-P process either 1) all of the hardware was set to 190 °C, or 2) all hardware was set to 220 °C. Tubes made with the baseline process using commingled material used the same combinations of process parameters, except a hot end was not included in the process. The parameters combinations used in the study can be found in Table 2. The other process variables remained consistent for all samples made at the levels that, based on prior experience, were most likely to create quality parts: the winding speed was low, the consolidation force from the foot was high, and the roving tension was high. Four sample tubes were made in total, one for each combination of manufacturing process and temperature. The test specimens had an inner diameter of 102 mm, a thickness of 3.43 mm, and a 25.4 mm wide strip of consistent FRP material, suitable for testing and evaluation.

3.3. Results

3.3.1. Visual Results

At the higher temperature setting, the PETG appears somewhat discolored, as shown in Figure 21. This relationship between processing temperatures and discoloration of the matrix continued throughout this work, but, as seen here, did not seem to be the sole factor that determined SBS strength or the other quality indicators. The discoloration of the PETG at elevated temperatures and its apparent lack of correlation to strength were similar in the baseline and JITA-P samples.

Figure 21: The color differences in the matrix of the commingled sample produced at 190 °C on the left compared to the commingled sample on the right, produced at 220 °C.

Figure 22 shows that the outer surface of the JITA-P samples looks drier than their inner surface, indicating incomplete wetout on the outer surface of the JITA-P tubes. Material deposited on the mandrel surface has more time for the matrix to impregnate the fiber and also to consolidate the FRP as the tube thickness in increased. This material also experiences the highest number of passes of the consolidation foot. However, in both JITA-P and commingled tube processes, the hardware is immediately shut down upon reaching the desired sample thickness, and so fibers on the outer layer of a sample have had both the least amount of impregnation time and also the least time of exposure to the consolidation force. The appearance of inconsistent wetout through the thickness of JITA-P samples is significantly reduced as the SBS specimens are fabricated and SBS beam thickness is reduced from 3.43 mm to 2.87 mm.

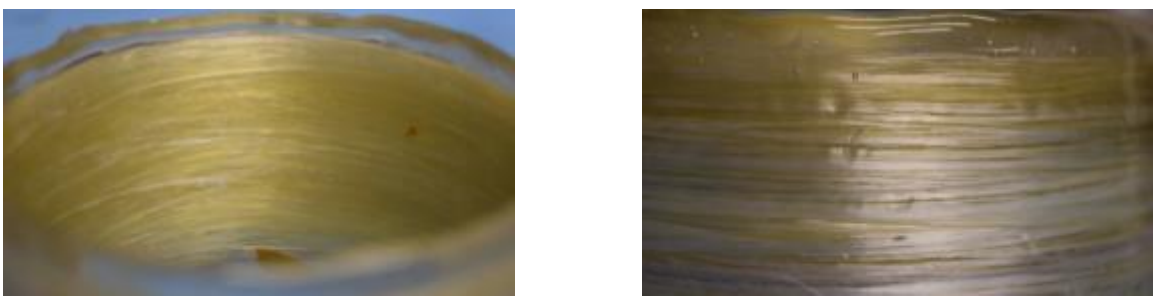

Figure 22: A JITA-P sample at 190 °C and the variation of wetout seen in the inner and outer surfaces.

The appearance of inconsistent wetout through the thickness is more evident in the JITA-P samples, compared to the commingled samples, which are shown in Figure 23. The as-received commingled material has the PETG matrix fibrils intermixed with the glass reinforcement, and has a shorter distance to flow to any dry areas between fibers. As a result, all other things being equal, wetout is likely to occur more quickly in the commingled samples than in the JITA-P samples, once the FRP material has increased in temperature and consolidation pressure has been applied. Therefore, it is unsurprising to find that wetout in the last layers to be deposited in a commingled sample is more consistent with wetout of the first-deposited material, when compared to a JITA-P sample.

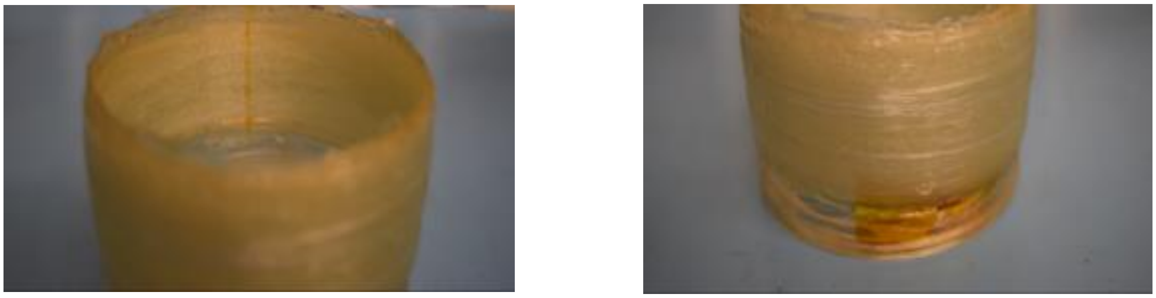

Figure 23: A commingled sample produced at 190 °C and the wetout seen on the inner and outer surfaces.

3.3.2. Metallographic Results

Micrographs from the cross-section of each of the four tubes are shown below in Figure 24. Fiber reinforcement in all sample cross-sections is evenly dispersed and closely packed, indicating sufficient consolidation. Cross-sectional profiles of the glass fibers appear to be round, rather than the elliptical shape that would be seen if the fibers were significantly misaligned from the intended hoop wound fiber angle. The average fiber diameters in the commingled samples are larger than those in the JITA samples, which were measured at 20 microns and 16 microns, respectively.

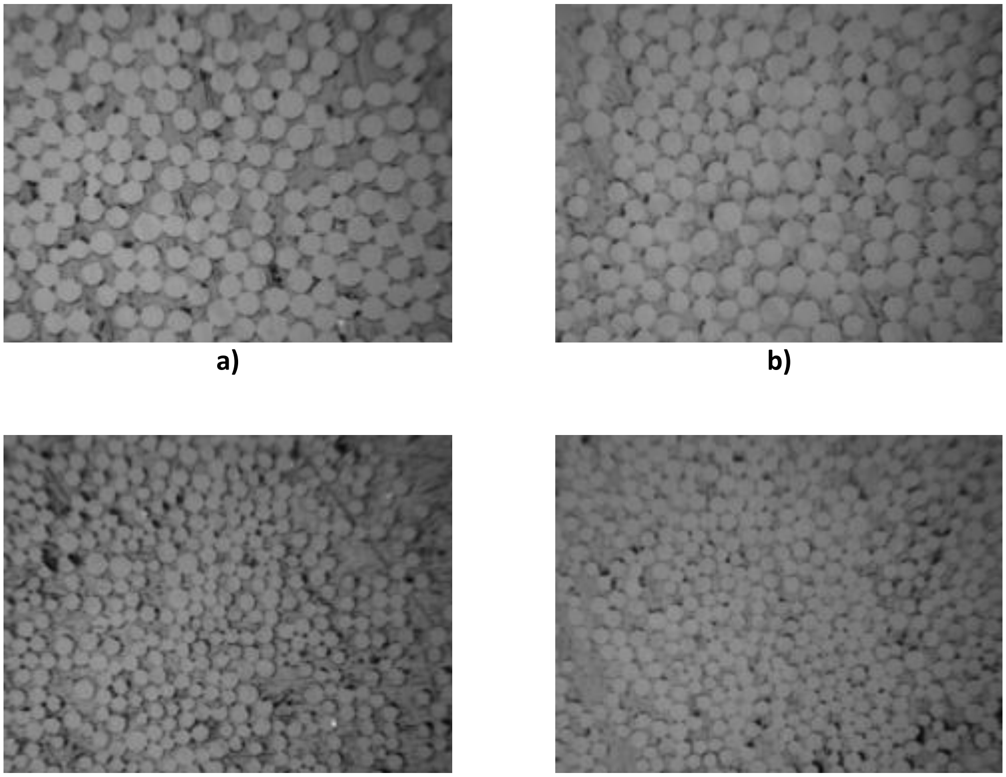

a) b)

c) d)

Figure 24: Micrographs of the following processed materials: a) commingled at 190 °C, b) commingled at 220 °C, c) JITA-P at 190 °C, and d) JITA-P at 220 °C. All four images are at 200X magnification.

3.3.3. Mechanical and Physical Evaluation

The results from the SBS testing of five test samples from each of the four FRP tubes produced in the preliminary study are presented in Table 2. All specimens failed in the inelastic failure mode described in the ASTM D2344 standard, and the reported SBS strength value is based on peak strength. The SBS strengths of the JITA-P samples are significantly higher than the SBS strengths of the commingled specimens. The strength and V_f standard deviation (SD) presented is the result of repeated measurement, not replicated measurement, as a total of four samples were produced during the preliminary study, one for each variable combination as shown in Table 2. The SD represents the variation of both strength and V_f within each sample tube.

TABLE 2: Strengths, fiber volume fractions, and their standard deviations for commingled and JITA-P samples at 190 °C and 220 °C.

Sample	SBS strength (MPa) and SD	V_f (%) and SD
Commingled at 190 °C	38.2 ± 1.0	62.8 ± 5.2
Commingled at 220 °C	34.9 ± 1.1	59.2 ± 3.6
JITA-P at 190 °C	51.3 ± 0.8	64.1 ± 8.2
JITA-P at 220 °C	55.3 ± 1.4	59.2 ± 2.1

Fiber volume fractions of all samples were roughly consistent, indicating that the higher SBS strengths of the JITA-P samples were most likely not solely a function of V_f. It is noteworthy that increasing temperatures appears to produce a slightly lower V_f, which is unexpected since the matrix is a thermoplastic polymer. All other things being equal, higher temperatures usually reduce viscosity, allowing higher degrees of consolidation and reducing void content. However, void content was not measured and so the higher V_f of the samples produced at lower temperatures may have had a larger percentage of unmeasured voids, artificially inflating the associated V_f numbers. Also of note is that the commingled samples had a higher V_f than the as-received commingled roving, implying that significant consolidation occurred. This idea is further corroborated by the presence of neat polymer that has appeared on either side of the commingled samples during processing, as seen in Figures 21 and 23, as well as the micrographs showing tightly-packed glass fibers in the FRP tubes, shown in Figure 24.

3.4. Summary and Conclusions

Both the JITA-P process and the commingled process produced samples with a high fiber volume fraction, relative to other processes intended to make non-geodesic FRP parts using comparable material systems [21-23, 25, 47, 48]. Based on the SBS testing of similar materials [49, 50], the SBS strengths of the FRP composite made using both processes were reasonably high, given the cursory nature of the study's design, suggesting that both the hardware and processes used in the preliminary study would be adequate to make FRP components of high quality. SBS strengths of the JITA-P process were certainly competitive with the commercial baseline commingled process giving confirmation that the JITA manufacturing process was sufficiently developed, as well. Micrographs show a tightly-packed, relatively even distribution of glass fiber reinforcement in the cross-section of the samples, with few voids. Consequently, the hardware and manufacturing processes appeared sufficiently developed, and the JITA process was deemed worthy of further investigation.

4. MAIN COMPARATIVE STUDY

4.1. Motivation and Background

After the preliminary study was conducted, it was known that further investigation was both justified and necessary. This initial study demonstrated that the proposed process in its preliminary form (JITA-P) and its associated hardware had been sufficiently developed to produce samples of reasonably high quality. These JITA-P samples showed a high fiber volume fraction (V_f), a desirable microstructure, and short beam shear (SBS) strengths comparable to similar materials. The commingled samples produced in the preliminary study showed similar properties, with the exception that their SBS strengths were significantly lower than those of the JITA-P samples. The quality of the JITA-P samples appeared to be competitive with the baseline quality and encouraged further investigation of the JITA process. Although there was a discrepancy in SBS strengths, given the close likeness of JITA-P hardware and the baseline hardware, it would be unlikely that the hardware was sufficiently developed for an unproven and most likely more difficult process, the JITA-P system, while being inadequately developed for the use of the commercial baseline process.

The competitiveness of the JITA-P results indicated that the manufacturing processes and hardware employed in the preliminary study should be preserved in the main study. However, the size of the discrepancy in SBS results was surprising since 1) the manufacturing techniques of the two processes were similar, and 2) the baseline process uses a material system that has been developed for commercial use. The preliminary experimental design was both rudimentary and brief, and so the lower performance of the commercial baseline process could very well have been the result of inadequate sample size and selection. This inadequacy could be addressed with a rigorously designed optimization study, which was subsequently conducted, and is the subject of this chapter.

4.2. Methods of Manufacturing Process Evaluation

The JITA process is likely to be able to ultimately produce polymer matrix continuous fiber reinforced composite (FRP) components with local fiber and matrix variation, which could increase the utility of the FRP material system. And, the limited preliminary results suggest, but do not confirm the feasibility of the JITA process. Therefore, thorough evaluation of the JITA method is necessary. However, there are multiple ways in which a manufacturing technique can be evaluated in order to be deemed worthy of use or further development.

4.2.1. Demonstration Parts

One possible method for assessing the JITA system would be to evaluate the success of making specific FRP parts. This approach has the advantage that, if successful, it demonstrates a specific instance of utility of the process. However, while making more complicated components, the quality of the material deposited by the process may have been significantly limited by the design inputs used to make the part. And these influential design inputs vary, depending on which component is made. In contrast, using a process to create very simple parts that are approaching general material deposition allows a more direct measure of manufacturing technique’s maximum potential, defined in this work by the quality of the deposition material. By increasing the generality of the results, this approach increases the likelihood of successfully extending the knowledge gained by this study to a wider variety of components and alternative material systems.

4.2.2. Efficiency

Another way to evaluate a manufacturing process is to assess the efficiency of using the process, which can be generally conceived of as being the ratio of productivity to the associated required resources. And these ratios of productivity to inputs could be assessed for competing processes and used to justify an assertion that one is more efficient than the other. The productivity of a FRP manufacturing process could be assessed in terms of part count [32], or by material deposition rates, although quality is often considered to be an important component. The general concept of cost used here includes measurements of the quantity of a resource used during the deposition of material. Costs that could be considered are money, energy, time, labor, and environmental resources.

4.2.3. Quality

Yet another way to assess the worth of a manufacturing process is to measure the quality of the material it produces. Potential metrics of quality could be the individual matrix and fiber material properties after processing, the interfacial strength, or evidence of contamination or general manufacturing errors. However, the quality of an FRP part can also be evaluated using mechanical testing and by assessments of the void content, the microstructure, and the fiber volume fraction, which are employed in this work.

One reason for using quality to evaluate a processing method is that quality is likely to be one of the primary concerns of anyone who is considering using the process. FRP components are expected to be reliable, and, after proper design and material selection has been conducted, the most common way to avoid unanticipated part failure is by meeting high standards of quality.

Another reason to assess a manufacturing process using quality indicators is that measurements of quality can reduce the total testing needed to build confidence in the future performance of an FRP material system or component. For example, instead of performing excessive mechanical testing simulating every aspect of a part's performance, quality is evaluated, and, if the quality is deemed sufficient, acceptable performance is assumed. However, there are multiple methods used to evaluate quality, such as measurements of T_g, nondestructive inspection (NDI) tests, and microstructure composition characterization. Additionally, properly selected mechanical tests can be used to assess overall quality, especially if they are directed towards anticipated areas of low quality. This use of mechanical testing can reduce and simplify testing even further. Instead of conducting mechanical testing to simulate anticipated loads, these tests can function as a measure of the specific mechanical performance that is most likely to give an indication of the adequacy of the manufacturing process. As an example, SBS testing emphasizes the measurement of the interlaminar shear strength (ILSS), which can be of particular concern when manufacturing thermoplastic composites as interlaminar adhesion can be difficult when using a high viscosity matrix. Consequently, judicious mechanical testing can be an efficient evaluation tool of FRP quality, which can reduce the need for 1) both the extensive mechanical testing needed to completely characterize expected performance and 2) multiple, generalized physical evaluations of an FRP material system.

4.2.3.1. Statistical Control and Process Variation

The evaluation of quality can take different forms depending on which aspect of quality is specifically under consideration. A process that is considered capable of making high quality parts is assumed to be able to not only make a good part, but 1) to also make the intended part, and 2) make the intended part consistently. And successfully satisfying these requirements is more likely if the results of the process are under the influence of the varying process parameters. The issues of manufacturing process repeatability and control over the resulting parts are addressed by techniques such as process capability analysis (PCA) and the Taguchi method of quality improvement [53, 54, 55].

4.2.3.2. Maximum Quality

Another approach to using quality measurements for the evaluation of a manufacturing method is to assess the maximum quality that could result from the process. Although this method results in a single value to represent each process, it is a more generalized evaluation technique compared to other strategies. The evaluation results in a combination of optimum process parameters that can be immune to misleading influences based on 1) preconceived notions of the best method to make specific parts, 2) past experience with the process under investigation, and 3) the knowledge of process parameter levels that work well for other similar processes. Determining maximum quality evaluates processes in a quantitative way in which they can be compared fairly, while also allowing for possible discrepancies in process parameter levels necessary for each method to produce the best parts. Also, an estimation of maximum quality is more likely to address initial concerns about the utility of a new process if the specific, desired FRP part has not been selected. Therefore, the experimental work conducted after preliminary research was directed towards the evaluation of the JITA and baseline processes via maximized SBS strengths.

4.2.4. Evaluating the JITA Process

An exhaustive evaluation of a manufacturing process would include all of the approaches previously mentioned. However, achieving this level of completeness is beyond the scope of this work. And, many of these evaluation techniques rely on information about the implementation of the JITA process which has not been established, such as the desired production volume and the specific parts to be made along with their associated tolerances. However, what is certain is that there will be an interest in the quality of parts that can be made with the JITA process, both the maximum possible quality as well as the quality variation inherent to the manufacturing process.

The primary method of evaluation in the main study was to utilize optimization techniques to determine and compare the maximum quality for each process. This comparison allows the maximum possible quality from the JITA system to be placed in context to make a useful evaluation of its significance. In addition, a statistical confidence in that maximum value was developed, which necessarily involved measuring the variation in quality inherent to each process. Conducting a rigorously designed study also provided an opportunity to evaluate the efficacy of each included process parameter, measured by evaluating its effect on SBS strength. Conclusions regarding which process parameters were indeed influential would 1) support the development of an understanding of the relationship between process parameters and material behavior, and 2) justify decisions of how best to refine the current JITA manifestation, possibly reducing the amount of control over those parameters.

Reduced control over process parameters would have significant effects on the efficiency and efficacy of the JITA system. The discovery that any part of the process is unnecessary could eliminate the associated hardware, its motion control, and any affiliated temperature control system. This would reduce the costs associated with FRP part production and may improve the reliability and robustness of the process. However, even the discovery that the quality of JITA parts is merely insensitive to changes in a process parameter, while still requiring some level of control, could produce some of these positive effects. Process robustness would increase and required labor may decrease as the precise control of a parameter becomes unnecessary to make parts of high quality. Given the hardware and processing similarities of the two processes evaluated here, they are likely to incur similar capital costs, require comparable quantities of labor to fabricate parts, and have similar environmental impact. However, if the optimum quality of each process requires significantly different processing speeds or temperatures, the energy cost and time required for each part could be significantly different. These discrepancies could affect the relative overall efficiency of each system. Demonstrating the feasibility of the JITA process in its current form, which uses a significantly different material system compared to the baselines process, would confirm any significant discrepancies in material input costs, possibly increasing the attractiveness of the JITA process, especially when used at high production volumes. Consequently, the relative cost of the material systems used here was evaluated as well. Lastly, additional analytical techniques were used to explain discrepancies in SBS strength by investigating the microstructure and composition of the composite and its components.

4.3. Main Study Design of Experiment

The experimental designs of the main studies used to optimize the quality of both the JITA process and the baseline process were response surface methodology (RSM) studies in the central composite design (CCD) style. The RSM experimental approach is a statistical method commonly used in industry for the improvement and optimization of products involving multiple input variables and possibly multiple response variables as well [51]. Here, the input variables will be process parameters and SBS strength will be used as a quantifiable response variable as an indicator of quality. Using this technique, an appropriate study is designed, the data are collected, an estimation of the relationship between the input variables and response variables is made by fitting a response surface, and optimization strategies are applied to locate the highest level of response [51]. Additionally, the statistical confidence in the optima will be estimated and the optima will be compared.

CCD methodology is a subset of the RSM technique, and they are designed to efficiently produce the quadratic response surface often needed to optimize a response variable [51]. First-order models from 2N designs can manifest some degree of curvature, represented by interaction terms, but this response is limited compared to the response that can be modeled with a second-order model using pure quadratic terms. Figure 25 shows the relative degrees of possible curvature in first-order and second-order models. Consequently, second-order models are more appropriate than first order models to optimize a response variable.

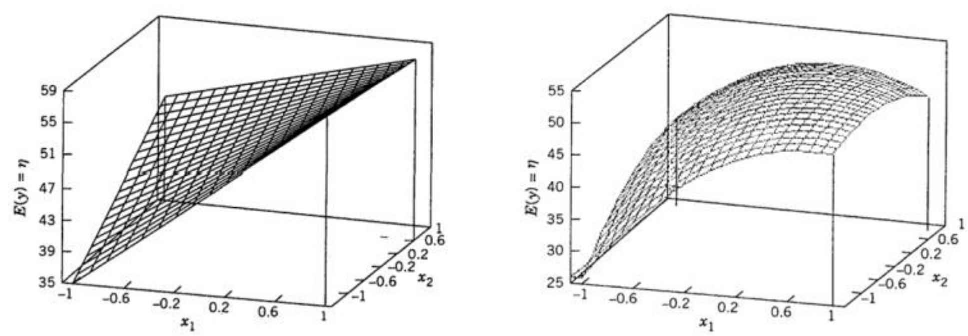

Figure 25: The possible curvature in a first-order model on the left compared to that of a second-order model on the right. E(y) is the response variable and x_1 and x_2 are input variables [51].

CCD techniques, illustrated in Figure 26, consist of a 2N design augmented with axial points, with additional replicated center points [51]. The center points both measure the error variation inherent to the process, and also, along with the axial points, contribute to the curvature that may be needed in the regression model. When five and six input variables are being investigated, the CCD design produces similar results, but requires fewer data points compared to other RSM designs, like Box-Behnken studies, for example. This efficiency was the primary consideration for the choice of the CCD design over the other RSM designs.

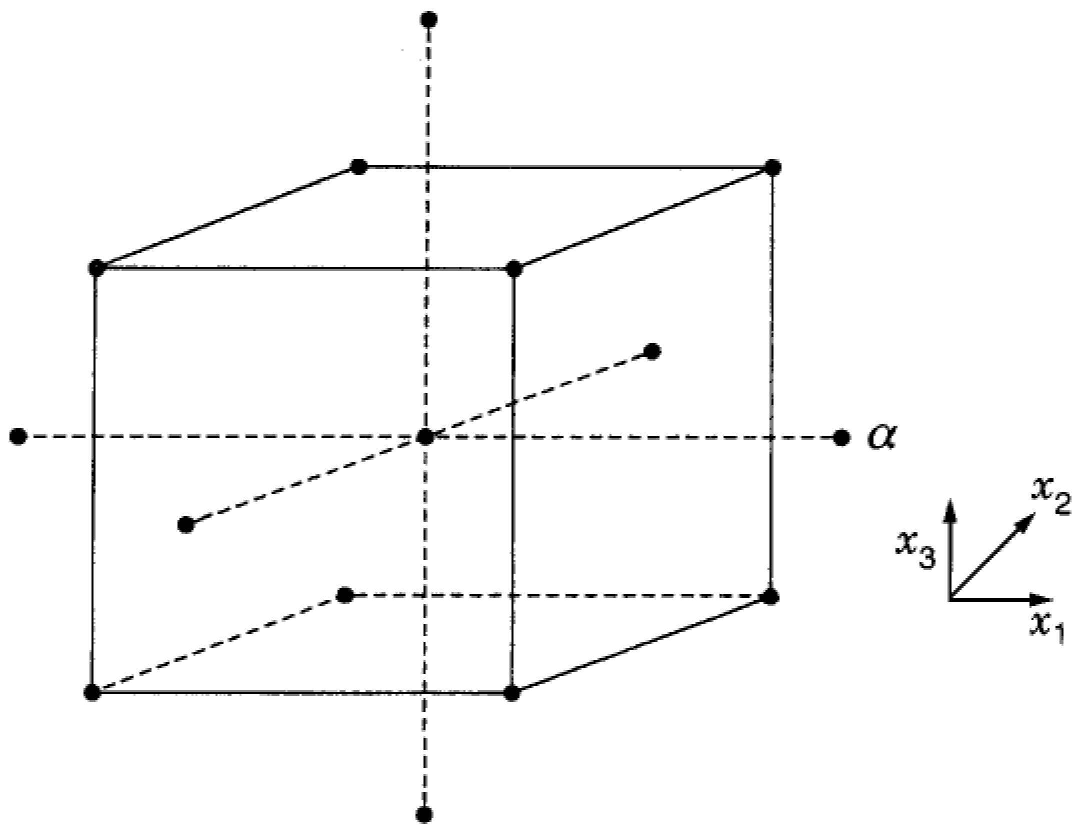

Figure 26: The basic design structure of a CCD study with three input variables. The axial points are measured at α, which represents the variable distance from the center [51].

Optimization studies should be able to model at least second-order response surfaces to capture a maximum response. 3N designs could model these surfaces, but typically require far too many samples to be practical. For example, a 3N study of 4 input variables is conducted with 81 data points. As a result, three-level studies are rare if more than two or three input variables are included in the study [52]. RSM studies are much more efficient when used for optimization experiments with many input variables.

One common method to reduce the sample size is to eliminate variables that will be explored in the study. A 3N study of 3 parameters requires 9 samples, which is much more attractive than a 3N study of

4 parameters that uses 81 samples. These calculations demonstrate why the reduction of a study's size prior to the optimization study can be so useful. Justifications for eliminating the number of specific input variables can be based on prior experience with the process, or by using a screening study.

Compared to relying on intuition formed from experience, using screening studies is a more tenable approach. And, an iterative style of testing with both a screening study and then the main optimization study is generally considered to be 1) ultimately more efficient if it reduces total sample size, and 2) more likely to result in appropriate bounds and parameter levels because response behavior from the screening study can be used to modify the levels used in subsequent studies. However, there are also potential drawbacks to using a screening study.

Firstly, as mentioned, screening studies are typically 2N designs. However, the efficacy of 2N screening designs is questionable [57]. Even if a full factorial study is used to capture significant interaction, it is entirely possible that the two levels will not capture significant variation, and parameters will be erroneously dismissed from the study. This is especially likely if the two levels in the 2N design are good candidates for bounds in an optimization study, showing diminished response at a high and a low level. An unjustified rejection of parameters would be less likely if the two levels chosen only included one bound, and the second chosen level was likely to create a high response. But, by not including both bounds, the evaluation of the bounds is impeded and a large secondary benefit from using a screening study is lost. However, evaluating the significance of a process parameter at three or more levels, as in a CCD study, is more likely to capture variation within the chosen bounds.

Secondly, the reduction in the total sample size may not be as large as expected. RSM designs, for example, can optimize a response variable while varying 5 process parameters, measure the process variation to generate estimates of statistical confidence, identify insignificant process variables for possible elimination, and do so with acceptable aliasing using only 32 samples. By comparison, if a half fraction 2N screening study of five samples was conducted and the process variables were reduced to three, just the screening study alone would already require 16 samples, if comparable aliasing was maintained. The screening study would eliminate variables based on only two levels, which is more likely to eliminate significant terms. If a relatively efficient CCD design was subsequently used, eight of the previous sixteen samples in the screening study could be used in the CCD optimization study because the CCD design is composed of a 2N design, along with additional points. However, 12 additional samples would be needed to complete the CCD study, resulting in a total of 28 required samples using the screening study. And so, in this case, only using one optimization study and no screening study would require four additional samples, but the elimination of any process variables would be based on measuring three levels, instead of two. In realistic scenarios, the non-iterative approach can have significant advantages, relative to the traditional iterative approach. Consequently, this work used a CCD design without a screening study because the CCD design more confidently evaluates the significance of an input variable, and also because a fairly insignificant number of additional samples were needed to use this approach.

To be consistent with the preliminary research nomenclature, the JITA process evaluated in the main study and the associated results and material system will be referred to by the JITA-M designation. The baseline optimization study was conducted first and the JITA-M study followed. The optimum SBS strengths resulting from each of the two studies were compared to one another in order to assess whether the JITA-M system could result in FRP parts of a comparable quality to that of the commercial system. Minitab 16 was used to design both optimization studies and also to perform the statistical analysis of the subsequent results.

4.3.1. Input and Response Variables

The response variable used for both optimization studies was SBS strength. The JITA-M system investigated the effects of six process variables on SBS strength: 1) mandrel temperature, 2) foot temperature, 3) process speed, 4) foot consolidation force, 5) roving tension, and 6) hot end temperature. As the baseline process does not use an extruder to apply the matrix, the baseline study design included only five process variables, which were the same as those used for the JITA-M system, except hot end temperature was not included. A summary of the input variables used as factors in the optimization studies is found in Table 3.

TABLE 3: Summary of the input variables and output variable used in each optimization study.

	JITA-M	Baseline
Input Variables	Mandrel Temperature	Mandrel Temperature
	Foot Temperature	Foot Temperature
	Process Speed	Process Speed
	Foot Consolidation Force	Foot Consolidation Force
	Roving Tension	Roving Tension
	Hot End Temperature	X
Response Variable	SBS Strength	SBS Strength

4.3.2. High and Low Level Bounds

Both optimization studies required that the bounds for the input variables be determined, as they form the corners of the design cube shown in Figure 26. However, methods and strategies for setting the bounds of an optimization study are not well documented. And, the most complete confirmation that the bounds were appropriately selected often occurs only after the study has been conducted. The general recommendation for specifying the bounds is that they define a larger, rather than a smaller interval [58]. Typically, in the case of an optimization study, indications that bounds were appropriately selected include 1) significant variation within the bounded interval, or 2) a drop in the response variable at each end of the interval. Variation within the bounds is evidence that the bounded interval may have been wide enough to capture a global maximum in the response variable, as it is more likely that a response will show less variation as the bounded interval becomes smaller. And, a decrease in response at either end of the bound indicates that a maximum response has been contained by the bound interval.

In order to maintain parity in the comparison of the two processes, the same method was used to determine the bounds in both studies. However, the method to specify the bounds was applied independently in both cases so that the characteristics of one process would not influence the values of the bounds in the other process. Since the midpoint levels are dependent on the values of the bounds, the result is that the study of each process used independently developed parameter levels.

The bounds for each of the two studies were determined by first identifying two processing modes in which the samples were likely to demonstrate poor quality, summarized in Table 4, which illustrates the JITA-M input variable levels.

TABLE 4: A comparison of the JITA-M input variable combinations necessary to produce the two main modes of FRP manufacture expected to result in poor quality.

	Mode #1 Input Variable Level	Mode #2 Input Variable Level
Mandrel Temperature	Low	High
Foot Temperature	Low	High
Processing Speed	High	Low
Foot Consolidation Force	Low	High
Roving Tension	Low	High
Hot End Temperature	Low	High

The first mode (mode 1) was based on the idea that poor quality of FRP parts is often the result of poor consolidation and wetout. The processing characteristics most likely to produce a drop in the response variable due to poor consolidation and wetout are cool temperatures and low consolidation forces, applied for a short amount of time. Therefore, the combination of process variables most likely to cause poor quality in this mode in reference to the JITA-M system are 1) low mandrel temperature, 2) low foot temperature, 3) high processing speed, 4) low foot consolidation force, 5) low roving tension, and 6) low hot end temperature.

The procedure to establish bounds using mode 1 was as follows: First, a sample was made at the midpoint of the anticipated bounds, and it was tested for SBS strength. This established a tentative 'midpoint SBS strength'. Second, a sample was made that was consistent with mode 1 process parameter levels. Third, if the test sample was of too poor quality to be mechanically evaluated, the sample was remade with the temperatures raised, the consolidation forces increased, and/or the process slowed down. On the other hand, if the test sample was of high enough quality to be tested, the mode 1 SBS strength was compared to the midpoint SBS strength. If the mode 1 strength was significantly lower than the midpoint SBS strength, then one bound was considered to be reasonably established for all six of the process variables, because a drop in response at the bounds is the clearest indication that at least a local maximum, and hopefully a global maximum, has been captured. If the mode 1 strength was not significantly lower than the midpoint strength, then the mode 1 features were further exaggerated by decreasing temperatures, reducing consolidation forces, and/or by speeding up the process, if possible, and repeating this strategy until the reduction in response was produced. A typical mode 1 sample is shown in Figure 27.

Figure 27: A typical mode 1 sample.

The second mode (mode 2) that was identified as likely to produce a poor composite was that which would begin to create thermal-oxidative degradation of the composite. The technique used to specify bounds in mode 2 had a similar structure to the mode 1 procedure. The process variable combination most likely to produce this thermal degradation was 1) high mandrel temperature, 2) high foot temperature, 3) low processing speed, 4) high foot consolidation force, 5) high roving tension, and 6) high hot end temperature. Thermal degradation is most likely to occur when the material is held at the highest temperature for the longest amount of time. Of course, high consolidation forces don't directly create thermal degradation, but they do extend processing time. During the fabrication of each sample, the fabrication process continued until 3.43 mm of material had been deposited. But, higher consolidation forces slow the increase in thickness by compressing the laminate as it is being made. Higher foot force, increased roving tension, and slower processing speeds were predicted to increase the time that the FRP material was at a specified temperature, increasing the likelihood of thermal-oxidative degradation.

Employing a method similar to that used with mode 1 levels, the bounds resulting from mode 2 were generated in much the same way. A mode 2 sample was fabricated, and SBS beams were cut from the sample. If the beams were not of sufficient quality, the temperatures were lowered, the consolidation forces were reduced, or the processing speed was increased until beams of sufficient quality were fabricated. If the beams from the sample were of high enough quality, SBS strength was measured and compared to the midpoint SBS strength. If the mode 2 SBS strength was significantly lower than the midpoint SBS strength, then the bounds were considered at a reasonable level. On the other hand, if there was no significant difference between the two strengths, the temperatures were raised, the consolidation forces were increased, or the processing speed was decreased, if possible, until a significant strength difference was achieved. A typical mode 2 sample is shown in Figure 28. Since the processing levels for mode2 were set to be opposite the levels for mode 1 quality degradation, the second bound for each level was then determined upon successfully producing a mode 2 sample. While using the mode 1 and mode 2 strategies, when the opportunity presented itself, all of the intervals were also made as large as possible in order to increase the chance of modeling a global maximum within the experimental study space.

Figure 28: A typical mode 2 sample.

The two mode strategy used here was employed as a compromise between a 2N bounding study that would require more samples and an approach consisting of educated guessing based on prior experience with the process. After the statistical analysis was completed, the main effects plots from both studies showed a diminished response in almost all of the process variables, and so the intermediate approach taken in the course of this work seems to have been successful, and was more efficient than alternative schemes.

4.3.3. Levels

Midpoint levels for each parameter were determined by taking the average of each set of bounds. The CCD structure shown in Figure 26 allows for five levels for each parameter to be specified, these being comprised of the midpoint, two bounds, and two axial levels. The axial values are defined by their distance from the midpoint, and, along with the center points, are the data points which are added to the base 2N structure to generate the possibility of curvature in the response surface necessary for optimization. The location of the axial points on a CCD design cube with three process variables would fall on a vector both normal to, and in the center of each side of the cube, as shown in Figure 26. Typically, the axial points' value are chosen so that they extend beyond the surface of the cube, although the exact distance of the axial points from the midpoint are ultimately left to the discretion of the experiment designer. If the cube point distances from the center are normalized to ± 1, then a typical normalized axial distance is $\sqrt{k}$, with *k* being the number of input variables in the study [51].

Axial points that are extended past the cube surfaces are usually considered ideal because they generate the most statistical confidence over the largest volume of the experimental space [51]. Also, these extended axial points may be able to measure relatively more areas in the design space because they aren't placed at the corners of the cube. However, if the bounds have been aggressively selected such that data points taken outside of their interval are unlikely to be made, it may be better to use smaller axial point lengths. Choosing smaller axial lengths that place axial points on the cube surface generates confidence that all data points will be collected so that the orthogonality of the study will be preserved. Axial points on the cube surface have a normalized distance of ± 1 from the midpoint. The bounds were kept as wide as possible in this study, and so, although 5 levels for each parameter may be used, only 3 levels were used here: +1, 0, and -1. The actual process parameter levels used in the two RSM studies and their corresponding normalized (coded) design levels are shown in Tables 5 and 6.

TABLE 5: Input variable levels for the baseline study and their associated normalized values.

	Low (Code: -1)	Midpoint (Code: 0)	High (Code: +1)
Mandrel Temperature [°C]	130	193	255
Foot Temperature [°C]	200	250	300
Process Speed [rpm]	0.82	2.1	3.3
Foot Consolidation Force [N]	52	72	91
Roving Tension [N]	1.0	9.8	20

TABLE 6: Input variable levels for the JITA-M study and their associated normalized values.

	Low (Code: -1)	Midpoint (Code: 0)	High (Code: +1)
Mandrel Temperature [°C]	190	233	275
Foot Temperature [°C]	250	283	315
Process Speed [rpm]	0.82	1.5	2.1
Foot Consolidation Force [N]	52	75	97
Roving Tension [N]	1.0	9.8	20
Hot End Temperature [°C]	240	266	292

4.3.4. Center Point Replication

In a CCD style study, the variation of the process is only measured at the midpoint of the design cube, unless the entire study is replicated. This variation is extrapolated to other points on the response surface, growing larger as the distance from the midpoint is increased. If additional replications are required at other locations, the entire study is replicated, which doubles the sample size. In this work, only single axial and cube points were measured in both optimization studies, and variation was only measured at the midpoint. The default recommended number of center points was used in each optimization study. Six center point replications were made in the commingled study, and ten central data points were measured in the JITA-M study.

4.3.5. Blocks

The JITA-M study was larger than the commingled study. And, since it also relied on more hardware, used in the matrix extrusion, this study was blocked, while the commingled study was not. The JITA-M study was a larger study because it incorporated six instead of five process variables. With also having additional complexity, it was more likely that something might require a repair or adjustment during the study, which might produce unintended variation in the response variable. Also, being a larger study, more rolls of material were used during the experiment, and so there would be more of an opportunity for unintended effects from material inconsistency during the JITA-M study. However, if it was likely that undesirable variation had been introduced within a block, the block could be retested from the beginning of the block without needing to repeat the entire study. During the analysis of the JITA-M study, variation between blocks could be evaluated and the significance of the variation's effect, if present, could be quantified. The JITA-M study was broken into 3 blocks, the blocks were placed in random order, and the presence of blocks required that one more sample be made, resulting in a total of 54 samples.

4.3.6. Aliasing

In addition to using a screening study, an alternative method to reduce a study's sample size is to eliminate an even distribution of data points throughout the study and interpolate between the data points that have been collected. The result of reducing the sample size in this way, by fractionating the study, is that the effects of some variables or interactions are indistinguishable from the effects of other variables or interactions. This phenomenon is called aliasing, and it is less detrimental if the fractionated study's terms are aliased only with interactions of 3 variables or more. The sparsity of effects principle asserts that it is commonly the lower order terms that have the most significant effects on a response variable [52]. However, as studies are more severely fractionated, the aliasing may be between the lower order terms. Unless it can be assumed otherwise, two-way interactions may very well be significant, as the results of this study will show. And, if they are aliased with the main effects in a highly-fractionated study, it will be uncertain whether anything can be said of those aliased main effects, reducing the utility of the study. Often, highly-fractionated studies are assumed to be free of significant interactions, so that conclusions may be drawn about the main effects. However, this assumption should be justified if a causal relationship between input variables and the response will be relied up to justify the conclusions of the study.

Both the JITA-M study and the commingled study were half fractional CCD studies, and so aliasing was present in both cases. However, using the sparsity of effects principle, the aliasing was not expected to cause significant issues as main effects were only aliased with high order interactions. The aliasing generator for the JITA_M study was I=ABCDEF, which means that main effects are aliased with 5 way interactions and two way interactions were aliased with 4 way interactions, assigning a high degree of confidence to the evaluation of the significance of main effects and 2 way interactions. By comparison, the aliasing generator (I=-ABCDE) for the commingled study was similar, but because fewer variables were studied, it had fewer terms. The practical effects of using this smaller aliasing generator were that main effects were aliased with 4 way interactions and two way interactions were aliased with 3 way interactions. And so, confidence could be high in the evaluation of main effects, but significant 3 way interactions may interfere with the evaluation of 2 way interactions. The complete set of aliased terms in both studies are summarized in Table 7.

TABLE 7: The aliased terms in each optimization study.

Baseline Aliased Terms			JITA-M Aliased Terms		
A	=	-BCDE	A	=	BCDEF
B	=	-ACDE	B	=	ACDEF
C	=	-ABDE	C	=	ABDEF
D	=	-ABCE	D	=	ABCEF
E	=	-ABCD	E	=	ABCDF
AB	=	-CDE	F	=	ABCDE
AC	=	-BDE	AB	=	CDEF
AD	=	-BCE	AC	=	BDEF
AE	=	-BCD	AD	=	BCEF
BC	=	-ADE	AE	=	BCDF
BD	=	-ACE	AF	=	BCDE
BE	=	-ACD	BC	=	ADEF
CD	=	-ABE	BD	=	ACEF
CE	=	-ABD	BE	=	ACDF
DE	=	-ABC	BF	=	ACDE
			CD	=	ABEF
			CE	=	ABDF
			CF	=	ABDE
			DE	=	ABCF
			DF	=	ABCE
			EF	=	ABCD
			ABC	=	DEF
			ABD	=	CEF
			ABE	=	CDF
			ABF	=	CDE
			ACD	=	BEF
			ACE	=	BDF
			ACF	=	BDE
			ADE	=	BCF
			ADF	=	BCE
			AEF	=	BCD

4.3.7. Randomization

Randomization was applied to both studies in order to better detect drift in the manufacturing process or other unanticipated effects on the response variable. Consequently, block order was randomized and sample order within the blocks was also randomized in the JITA-M study. (The JITA-M blocks were randomly assigned the order: 1, 2, 3.) However, the grouping of individual runs is not randomly dispersed among the blocks. For example, block #3 in Table 9 contains all axial points and some center points, while the two other blocks contain a combination of cube points and center points. The commingled study contained no blocking and so the sample order was randomized throughout the entire study.

4.3.8. DOE Summary

During the optimization studies, 86 total samples were made: 32 samples were included in the baseline study and 54 samples were made during the JITA-M study. The baseline study investigated 5 input variables (A-E) and the JITA-M study was comprised of 6 input variables (A-F). Each sample was made with a combination of process parameters at either a high (+1), midpoint (0), or low (-1) level, and then tested for SBS strength. The three coded process parameter levels correlate with the high, intermediate, and low levels of each process parameter shown in Table 5 and Table 6.

Each data point was either an axial point, a corner of the design cube, or a center point, as illustrated in Figure 26. Center points were replicated 6 times in the baseline study and 10 times in the JITA-M study. The JITA-M study incorporated 3 blocks and the baseline study did not use blocking, and so all samples were included in the same block. The order of blocks and the sample order were randomized in both studies. All samples from each optimization study were fabricated before any of the samples were mechanically tested. The complete study design is shown in Tables 8 and 9 for the baseline and JITA-M systems, respectively.

TABLE 8: The baseline CCD structure in randomized order. Data points at the center are in bold.

Blocks	A	B	C	D	E	Type
1	+1	0	0	0	0	Axial
1	-1	-1	-1	+1	-1	Corner
1	**0**	**0**	**0**	**0**	**0**	**Center**
1	+1	-1	-1	-1	-1	Corner
1	+1	-1	+1	+1	-1	Corner
1	+1	+1	+1	+1	+1	Corner
1	**0**	**0**	**0**	**0**	**0**	**Center**
1	0	+1	0	0	0	Axial
1	-1	+1	-1	+1	+1	Corner
1	**0**	**0**	**0**	**0**	**0**	**Center**
1	-1	+1	-1	-1	-1	Corner
1	**0**	**0**	**0**	**0**	**0**	**Center**
1	0	-1	0	0	0	Axial
1	+1	+1	-1	-1	+1	Corner
1	+1	+1	-1	+1	-1	Corner
1	+1	-1	+1	-1	+1	Corner
1	-1	0	0	0	0	Axial
1	-1	+1	+1	-1	+1	Corner
1	-1	-1	+1	-1	-1	Corner
1	0	0	0	+1	0	Axial
1	+1	+1	+1	-1	-1	Corner
1	0	0	+1	0	0	Axial
1	**0**	**0**	**0**	**0**	**0**	**Center**
1	-1	+1	+1	+1	-1	Corner
1	+1	-1	-1	+1	+1	Corner
1	0	0	0	0	-1	Axial
1	-1	-1	-1	-1	+1	Corner
1	0	0	0	-1	0	Axial
1	**0**	**0**	**0**	**0**	**0**	**Center**
1	0	0	-1	0	0	Axial
1	0	0	0	0	+1	Axial
1	-1	-1	+1	+1	+1	Corner

TABLE 9: The JITA-M CCD structure in randomized order. Data points at the center are in bold.

Blocks	A	B	C	D	E	F	Type
1	+1	+1	-1	-1	-1	-1	Corner
1	-1	-1	-1	+1	+1	-1	Corner
1	-1	+1	-1	-1	-1	+1	Corner
1	+1	+1	+1	-1	+1	-1	Corner
1	+1	+1	-1	+1	+1	-1	Corner
1	+1	-1	+1	+1	-1	+1	Corner
1	+1	-1	-1	+1	+1	+1	Corner
1	+1	+1	+1	+1	-1	-1	Corner
1	+1	-1	+1	-1	+1	+1	Corner
1	-1	-1	-1	-1	-1	-1	Corner
1	**0**	**0**	**0**	**0**	**0**	**0**	**Center**
1	-1	-1	+1	-1	+1	-1	Corner
1	+1	-1	-1	-1	-1	+1	Corner
1	**0**	**0**	**0**	**0**	**0**	**0**	**Center**
1	-1	+1	+1	+1	-1	+1	Corner
1	-1	+1	-1	+1	+1	+1	Corner
1	**0**	**0**	**0**	**0**	**0**	**0**	**Center**
1	**0**	**0**	**0**	**0**	**0**	**0**	**Center**
1	-1	+1	+1	-1	+1	+1	Corner
1	-1	-1	+1	+1	-1	-1	Corner
2	+1	-1	+1	-1	-1	-1	Corner
2	**0**	**0**	**0**	**0**	**0**	**0**	**Center**
2	-1	+1	-1	+1	-1	-1	Corner
2	-1	+1	+1	+1	+1	-1	Corner
2	+1	+1	-1	-1	+1	+1	Corner
2	-1	-1	+1	+1	+1	+1	Corner
2	-1	-1	-1	+1	-1	+1	Corner
2	+1	-1	+1	+1	+1	-1	Corner
2	-1	+1	+1	-1	-1	-1	Corner
2	+1	+1	-1	+1	-1	+1	Corner
2	**0**	**0**	**0**	**0**	**0**	**0**	**Center**
2	+1	-1	-1	+1	-1	-1	Corner
2	-1	+1	-1	-1	+1	-1	Corner
2	+1	+1	+1	-1	-1	+1	Corner
2	-1	-1	+1	-1	-1	+1	Corner
2	**0**	**0**	**0**	**0**	**0**	**0**	**Center**
2	+1	+1	+1	+1	+1	+1	Corner
2	+1	-1	-1	-1	+1	-1	Corner
2	**0**	**0**	**0**	**0**	**0**	**0**	**Center**
2	-1	-1	-1	-1	+1	+1	Corner
3	**0**	**0**	**0**	**0**	**0**	**0**	**Center**
3	0	0	+1	0	0	0	Axial
3	0	0	0	0	0	+1	Axial
3	+1	0	0	0	0	0	Axial
3	0	0	0	0	+1	0	Axial
3	-1	0	0	0	0	0	Axial
3	0	-1	0	0	0	0	Axial
3	0	0	-1	0	0	0	Axial
3	0	0	0	-1	0	0	Axial
3	0	+1	0	0	0	0	Axial
3	0	0	0	0	0	-1	Axial
3	0	0	0	+1	0	0	Axial
3	**0**	**0**	**0**	**0**	**0**	**0**	**Center**
3	0	0	0	0	-1	0	Axial

4.4. Regression Models Selection and Error Bars

4.4.1. Generation of Regression Model Candidates

After both optimization studies had been completed and the SBS strengths were measured, two regression models were selected to best represent the correlation between the process parameters and SBS strength when using each of the two manufacturing methods investigated in the main study. The backwards elimination method was used in both studies to generate the regression model candidates, with each candidate containing a different number of terms in the model. First, an alpha value is selected; here it was 0.1, which sets the threshold on how high a p-value for statistical significance may be before it can be eliminated for consideration in the model. Using this method, all main effect, two-way interaction terms, and quadratic terms are initially included. An alpha value of 0.1 was used here. The backwards elimination proceeds by first creating a regression using all of the terms, and then also the p-values for the statistical significance of the effect of each term on the response variable. Next, the term with the least likelihood of being statistically significant, identified by the highest p-value, is removed from the study. Then a new regression model is created, and the new term that is the least likely to have an effect on the SBS strength, based on p-value, is removed. This process repeats until all of the p-values in the model are less than the chosen alpha value, and the process stops. This process necessarily produces models for consideration that include one fewer term each time the process repeats. The generation of each new regression model produces another candidate for being chosen as the model that best describes the continuous relationship between the response variable and the input variables, based on data points that were measured at discrete locations within the design space. The regression model candidates generated by the backwards elimination method for the baseline and JITA-M data sets are shown in Table 10 and Table 11, respectively.

TABLE 10: The baseline regression model candidates generated by the backwards elimination method at alpha=0.1. Each X signifies a present term in a model, and the chosen model is in bold.

		Baseline Model Candidate Number									
		1	2	3	4	5	6	7	8	**9**	10
Included Terms	A	X	X	X	X	X	X	X	X	**X**	X
	B	X	X	X	X	X	X	X	X	**X**	X
	D	X	X	X	X	X	X	X	X	**X**	X
	E	X	X	X	X	X	X	X	X	**X**	X
	F	X	X	X	X	X	X	X	X	**X**	X
	AA	X	X	X	X	X	X	X	X	**X**	X
	AB	X	X	X	X	X	X	X	X	**X**	X
	AD	X	X	X	X	X	X	X	X	**X**	X
	AE	X	X	X	X	X	X	X			
	AF	X	X	X	X	X	X	X	X	**X**	X
	BB	X	X	X	X	X	X	X	X	**X**	X
	BD	X									
	BE	X	X	X	X	X	X	X	X		
	BF	X	X	X	X						
	DD	X	X	X	X	X	X	X	X	**X**	
	DE	X	X	X	X	X	X	X	X	**X**	X
	DF	X	X	X	X	X					
	EE	X	X	X	X	X	X				
	EF	X	X								
	FF	X	X	X							

All considered models preserved the hierarchy of the terms, in this case meaning that all main effects that were included in either significant two-way interactions or in significant quadratic terms were required to be present in the model. Term hierarchy is often preserved, partly because the practical benefit for keeping higher-order terms that include missing lower order terms is dubious since, for example, the experimental control of AB would be unlikely without the independent control of the A variable as well as the B variable. Additionally, the CCD analysis requires term hierarchy in the regression model, and so it was maintained in the regression model candidates.

TABLE 11: The JITA-M regression model candidates generated by the backwards elimination method at alpha=0.1. Each X signifies a present term in a model, and the chosen model is in bold.

		JITA-M Model Candidate Number															
		1	2	3	4	5	6	7	8	9	10	11	12	13	**14**	15	16
Included Terms	A	X	X	X	X	X	X	X	X	X	X	X	X	X	**X**	X	X
	B	X	X	X	X	X	X	X	X	X	X	X	X	X	**X**	X	X
	C	X	X	X	X	X	X	X	X	X	X	X	X	X	**X**	X	X
	D	X	X	X	X	X	X	X	X	X	X	X	X	X	**X**	X	X
	E	X	X	X	X	X	X	X	X	X	X	X	X	X	**X**	X	X
	F	X	X	X	X	X	X	X	X	X	X	X	X	X	**X**	X	X
	AA	X	X	X	X	X	X	X	X	X	X	X	X	X	**X**	X	X
	AB	X	X	X	X	X	X	X	X	X	X	X	X	X	**X**	X	X
	AC	X	X	X	X	X	X	X	X	X	X	X					
	AD	X	X	X	X	X											
	AE	X	X	X	X	X	X	X	X	X	X	X	X	X	**X**	X	
	AF	X	X	X	X	X	X	X	X	X	X	X	X	X	**X**	X	X
	BB	X	X	X	X	X	X	X									
	BC	X	X	X	X	X	X	X	X	X	X	X	X	X	**X**	X	X
	BD	X	X	X	X	X	X	X	X	X	X	X	X	X			
	BE	X	X														
	BF	X	X	X	X	X	X	X	X	X	X	X	X	X	**X**	X	X
	CC	X	X	X	X												
	CD	X	X	X	X	X	X	X	X								
	CE	X	X	X	X	X	X	X	X	X	X						
	CF	X	X	X	X	X	X	X	X	X	X	X	X				
	DD	X	X	X	X	X	X	X	X	X	X	X	X	X	**X**	X	X
	DE	X	X	X													
	DF	X	X	X	X	X	X	X	X	X	X	X	X	X	**X**		
	EE	X	X	X	X	X	X										
	EF	X	X	X	X	X	X	X	X	X							
	FF	X															

There are other methods for generating the regression model candidates. For example, the hierarchical forwards selection technique starts with the main effect terms and chooses from among all other terms the most significant and adds it to the model. However, this method can add terms that are initially statistically significant, but, because it keeps any added terms, the term in question may be present in future regression models even though it is no longer significant. The backwards elimination method avoids this scenario. Also, using the available alternative methods that preserve hierarchy produced no significant differences in the generated model candidates.

4.4.2. Confirmation of Normality

After the regression model candidates were generated, the selection of the best model for each manufacturing process was necessary. Any regression model candidate needed to show that the residuals, the difference in value between the regression model in question and the actual data points, displayed a normal distribution of values. Otherwise, the results from using the regression would be suspect, as this normal distribution is an assumption of the statistically analysis used here. This criterion was used as the principle screening factor as any indications that the regression performed well could be called into question if the assumption of normality was not satisfied. The assumption of a normal distribution was primarily confirmed in both studies by a visual evaluation of the normal probability plots. Additional alternative plots of 1) residual versus observation order, 2) residual versus fitted value, and 3) the residual frequency histogram were also consulted. Generally, the models that best satisfied the normality assumption were also associated with the highest values of metric of fit to the data and also predictive capability.

4.4.3. Predicted R^2 and Additional Model Metrics

Once regression models that showed a non-normal distribution of residuals were eliminated from consideration, the fit of each regression model to the discrete data was evaluated using adjusted R^2. The unmodified R^2 is generally interpreted to be the ratio of variation in the data explained by the model divided by the total variation in the data. And this metric can be used to evaluate how well a regression models the variation seen in measured data points. The explanatory power of the model is, in a way, increased by adding terms in the model until R^2 has been maximized.

However, problems with the model overfitting the data are often seen as a result of using this approach. R^2 is increased each time additional flexibility is given to the model by allowing for a closer fit to the data points. And yet, assuming that there are no other significant extraneous influences, variation in the response behavior can be divided into two types: 1) the variation that results from changing the process parameter levels, and 2) the pure error, the variation that results from the noise inherent to the manufacturing process. If a model acquires enough degrees of freedom that it models not only the former behavior, but also the latter, it diminishes the explanatory power of the model. Concurrently, the model will less accurately predict new, untested data points as it does not solely represent the fundamental relationship between the input variable and the response.

However, using alternative regression metrics can dissuade an analyst from overfitting a model by using either 1) adjusted R^2, or 2) predicted R^2. The former evaluation tool penalizes models for including additional terms without a corresponding large increase in unmodified R^2. The latter tool more directly measures the predictive efficacy of a model containing a certain number of terms. The predicted R^2 value is computed by removing a data point, fitting a regression model to the remaining data, and calculating the residual between the predicted response value and the measured response value at that data point. This process is repeated for all data points, and finally the total amount of error calculated in this process can be compared to the same total error produced when using a different amount of terms. Trends in R^2, adjusted R^2, and predicted R^2 as the regression model candidates change in number of included terms can be seen in Figures 29 and 30.

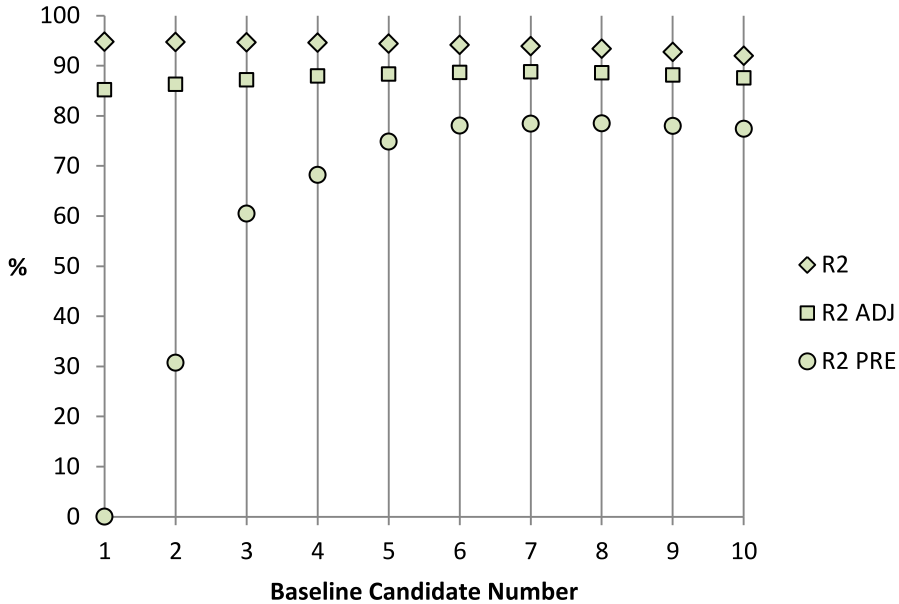

Figure 29: Trends of regression metrics relative to varying numbers of terms in the candidate model. Baseline model candidates are shown here. Model 9 was the chosen model.

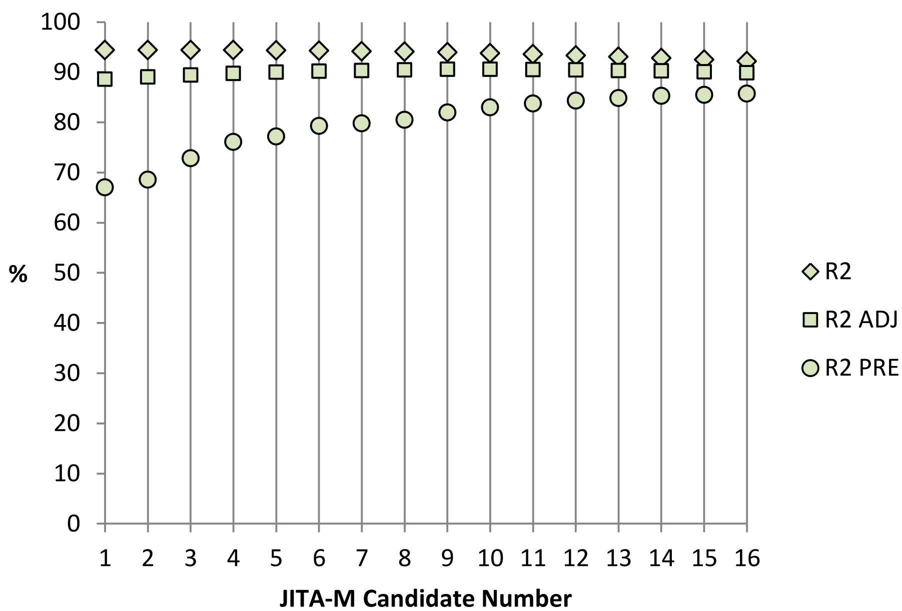

Figure 30: Trends of regression metrics relative to varying numbers of terms in the candidate model. JITA-M model candidates are shown here. Model 14 was the chosen model.

With these inherent safeguards, adjusted R^2 can be maximized while avoiding an overfitted regression model. And, predicted R^2 can directly evaluate a model's capacity for data point prediction, which diminishes when a model has been overfit. However, because the intention of the main studies was to maximize SBS strength, and because the optimized response variable was likely to occur at an untested location within the experimental design, the ultimate goal of the model regressions was to predict SBS strength at a new data point. Consequently, predictive accuracy of the regression model was of primary importance, and predicted R^2 was used as the most important metric to select the best regression model. The size of the confidence and prediction intervals was also noted among the regression model candidates. These interval widths followed the trends in predicted R^2, with both intervals reducing in size as the two predicted R^2 values increased. Consequently, minimizing these intervals leads to the same regression selection as well. Based on the preceding criteria, regression model candidates numbers 14 and 9 were chosen to model the response in the JITA-M and baseline systems, respectively.

4.4.4. Optima and Error Bars

After the regression model for each study was selected, Minitab's optimizer tool was used to identify the point on the response surface of maximum SBS strength, and to also generate the confidence interval surrounding each point. Confidence intervals were selected to be the appropriate error bars used for subsequent inference because they describe the expected variation in the predicted mean of the response at the new point. A 95% confidence level was selected for the confidence intervals. The mean response at a location of max SBS strength is of most interest since the comparison of the two max SBS strengths should be done on the basis of the typical SBS strength one can expect. The variation inherent to both manufacturing responses is important to quantify, and was measured at the midpoints, as previously mentioned. And this error can be predicted at other locations out to the limits of the sampled experimental space. However, fully characterizing the pure error associated with each process was not the primary objective of this study.

Standard deviation (SD) is often reported as the error bars, along with the average value of the measurement being reported. However, relaying the standard deviation and the average does not communicate any measure of the confidence one should have in the average, or in the variation about the mean. Consequently, making confident inferences from the presented data is difficult to justify solely based on those two parameters. Figure 31 illustrates this idea by showing the relationship between sample size, n, and the relative size of a SD interval, and CI. Note that an increase in statistical confidence, which corresponds to the sample size, decreases the CI width, but not the SD width. Generating confidence in statistical inference is useful, both when reporting the SBS strength optima, and when comparing the optima. And so, confidence intervals were used here instead of standard deviation intervals.

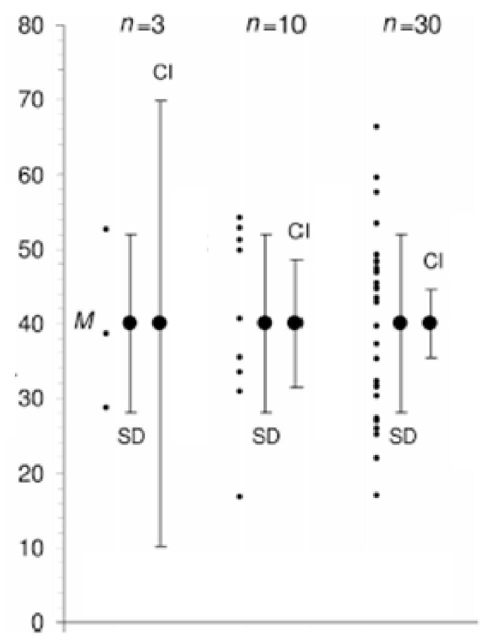

Figure 31: The change in the size of SD and CI as sample size (n) is varied. The sampled data points are shown as dots in each case. The vertical axis shows an arbitrary response variable value [59].

Material Systems

The commingled material used in the optimization of the commercial baseline process was the same as that used in the preliminary research: FGI Twintex commingled E-glass and PETG, 2690 tex. Also, The JITA-M reinforcement was the same E-glass roving as that used in JITA-P: PPG Tufrov 4588, 2200 tex. However, the JITA-M material system was slightly different than the JITA-P system. In the JITA-M study, the PETG matrix was Maker Series 3.00 mm PETG FDM filament, instead of the Form Futura 3.00 mm PETG FDM filament used in the preliminary study. This change was driven by relative availability and cost. In contrast, the reinforcing fibers from each material system used in the preliminary study were the same as those used in the main studies. Consequently, the discrepancy in the glass fiber diameter found in each material system was again present in the optimization studies: The JITA-M glass fiber diameter was approximately 12 microns, while the fiber used in the baseline system was roughly 20 microns in diameter.

4.5. Production Method and Hardware

The manufacturing methods used in both of the optimization studies were the same as those used in the preliminary research. Also, the hardware used in the main study was the same as that in the preliminary research, with one exception. In the preliminary research, forced hot air was used to heat the cantilevered mandrel from the free end. However, in the main study, the hot air gun was replaced by an electrical heating element inserted through the central axis of the mandrel from the free end, extending through the entire length of the open cavity of the mandrel. The length that the replacement heating element extends into the mandrel is indicated in Figure 32.

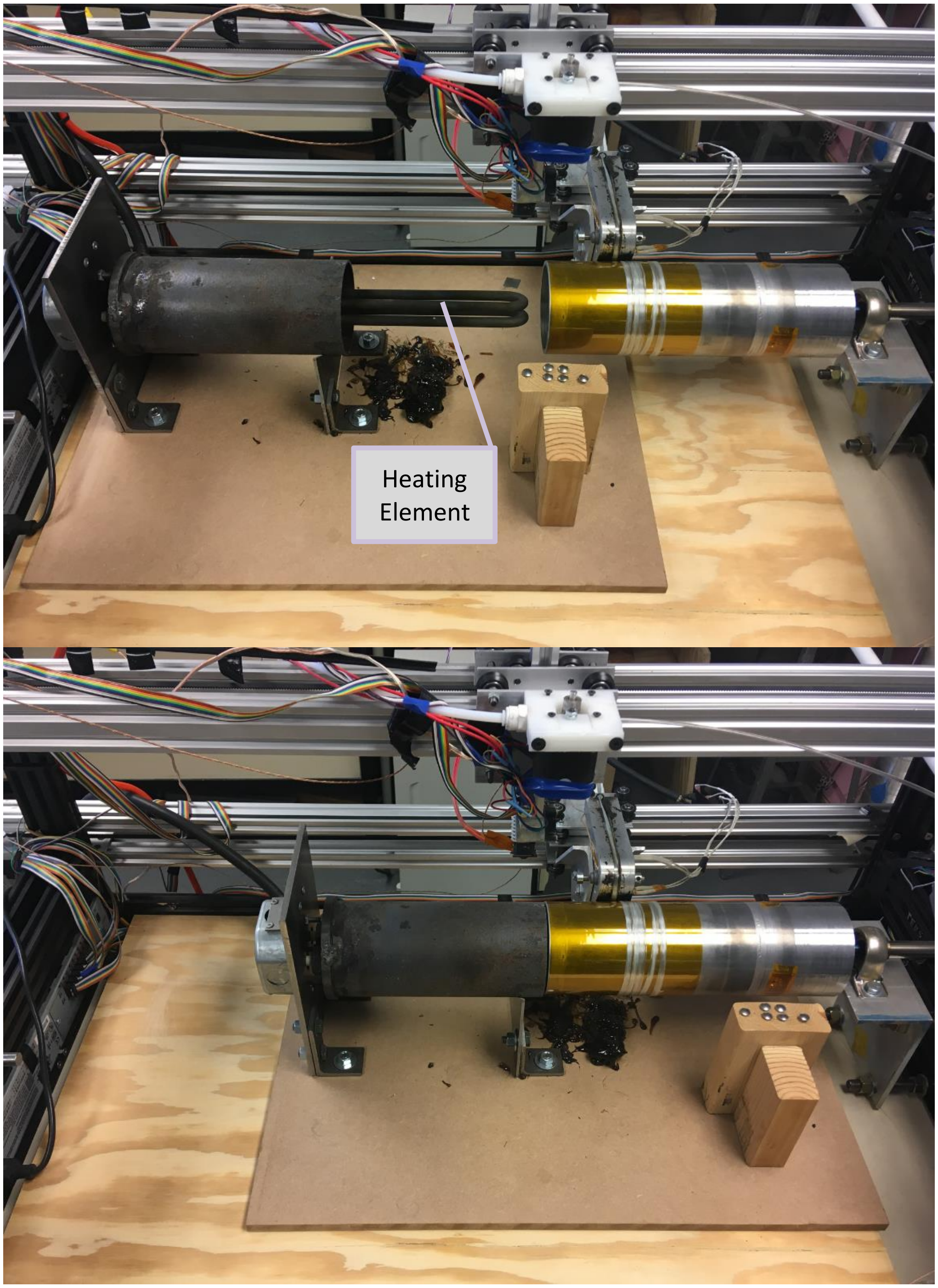

Figure 32: The modified heating system and the extension of the new heating element into the center of the mandrel during sample fabrication.

4.6. Samples

The samples produced in the main study using both processes were the same geometry and fiber orientation as those produced in the preliminary study. Hoop wound FRP material was deposited on the same 102 mm diameter mandrel, until the samples were 3.43 mm thick. As in the preliminary study, the samples contained an anchoring section off to one side, and then a 25.4 mm width of material was created from which to remove material for mechanical testing and other analysis, as shown in Figure 34.

4.7. Response Variable: SBS Strength Testing

As in the preliminary study, SBS strength was used as the primary indicator of quality to compare the maximum possible quality that could be produced using each process. Each of the two optimization studies used SBS strength as the response variable to which a regression model was fitted. The maximum response was determined from the regression model. SBS Testing was conducted in accordance with ASTM D2344 using the same fixtures and processes as those employed in the preliminary study. This testing was conducted in inch-pound units, but is reported here in SI units. The SBS beams were tested with the fibers spanning the 11.4 mm length between steel support pins of 3.18 mm diameter. The steel loading nose was 6.35 mm diameter and was advanced at 0.127 mm/minute. The loading nose was placed on the initially convex side of the beam while the initially concave side of the beam was in contact with the support pins, as recommended by the standard. The orientation of the samples and fixture during SBS testing is shown in Figure 33.

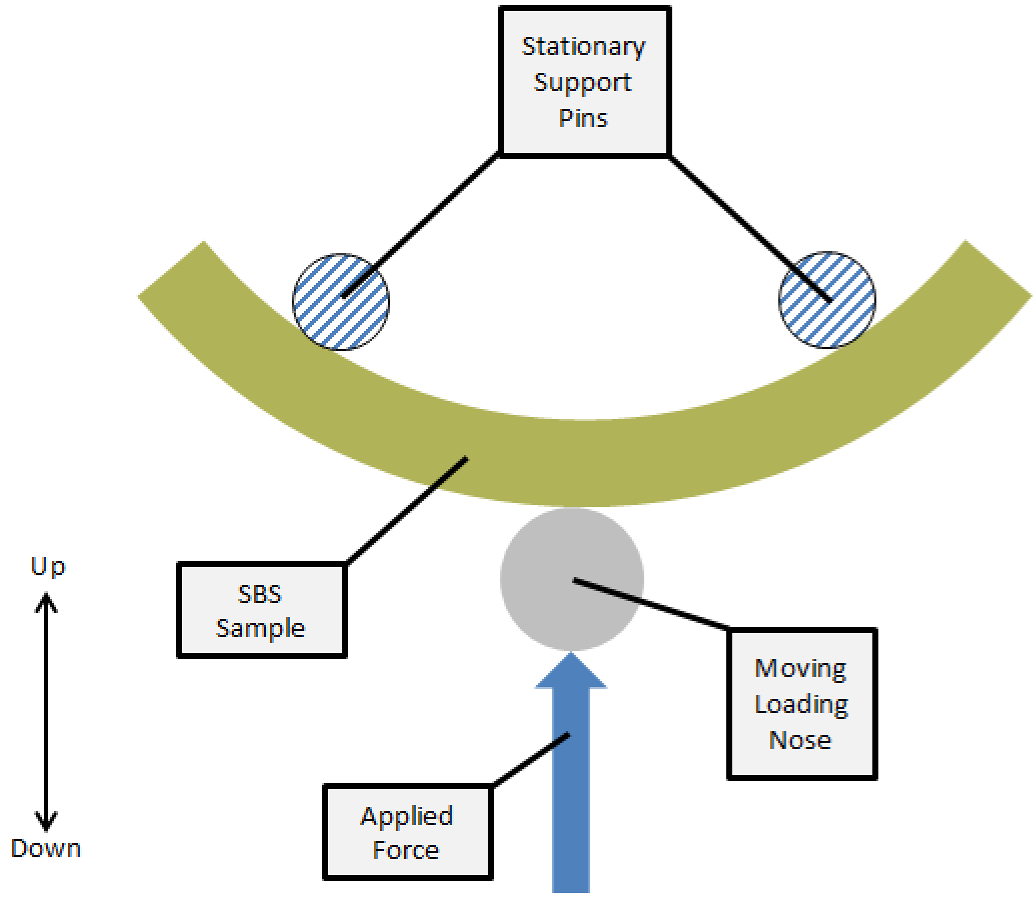

Figure 33: SBS test set up.

Five samples were selected from randomized locations within the 25.4 mm width of testable material from each of the sample tubes for SBS testing. To pick the random locations, the area of testable material in each tube was divided into a grid from which samples could be cut, with one axis across the width and the other axis along the circumference. Two sets of randomized numbers were independently generated. One set determined the location of a sample across the width of the 25.4 mm strip, while the other set specified the location of the test beam along the circumference of the tube. Once the randomized beam locations were generated, the same locations were used for each tube. Figure 34 shows the grid pattern that would be applied to a sample and the locations from which beams might be removed.

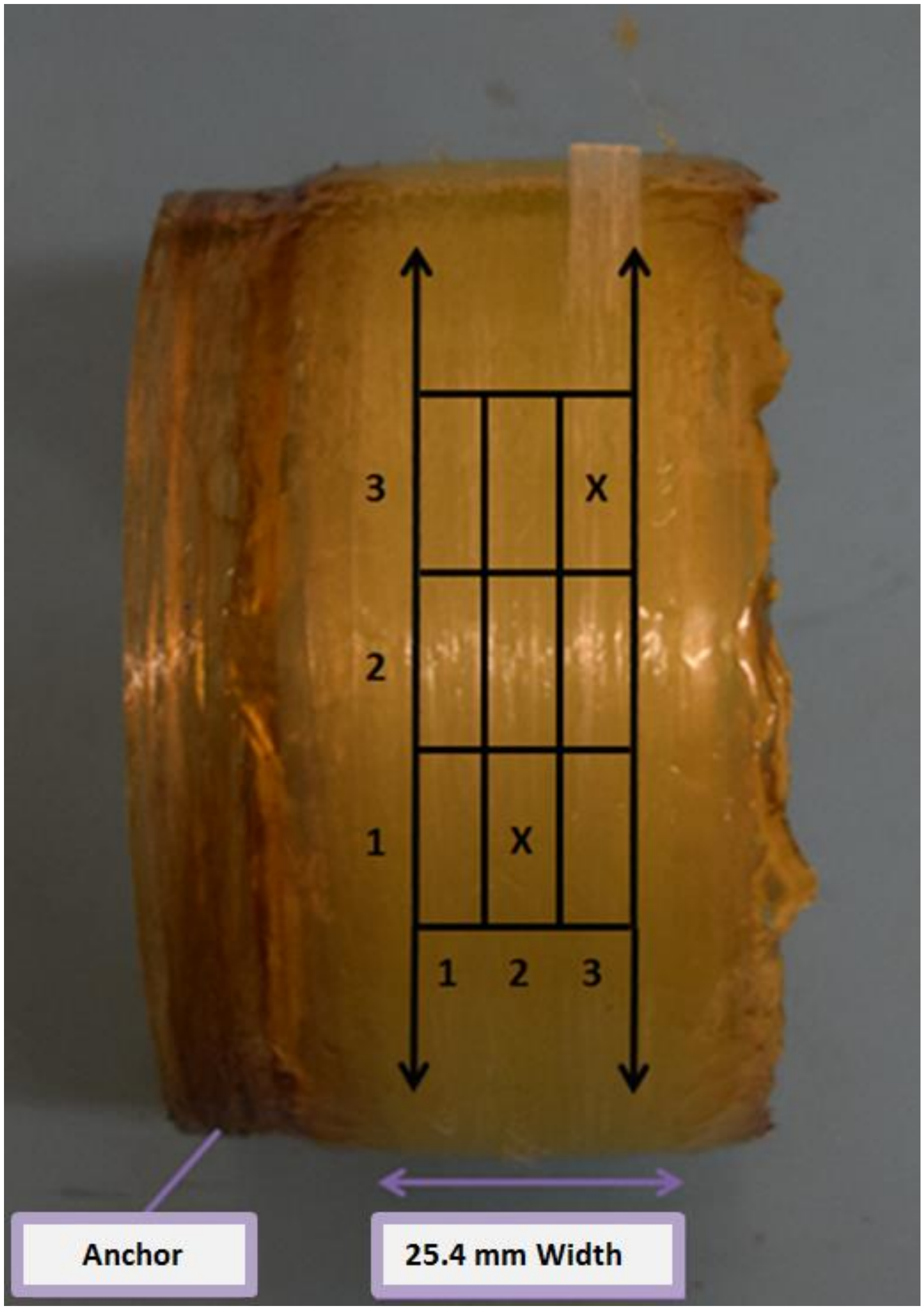

Figure 34: The overlay of the grid used to pick random locations onto the testable area of the sample. Each X indicates the location a test beam might be removed from.

The approximate profile of the SBS test samples was first cut with a diamond blade, and then the beams were ground to their final dimensions. The SBS beam dimensions were 0.572 mm wide, by 2.84 mm thick, with a chord length of 17.1 mm. The beam's radii of curvature were unchanged from their original radius of 50.8 mm as they were prepared for testing. SBS strength values were generated by identifying the first failure on the force/displacement curves under monotonic loading.

4.8. Additional Analysis

4.8.1. Microscopy

Samples were prepared for microscopy by cutting each sample and mounting it in the acrylic mounting resin so that any fiber misalignment in the sample would produce an elliptical cross-section. . The mounted samples were then ground with SiC paper that progressed from 240 grit to 1200 grit abrasive. Finally, samples were polished with 1 micron alumina powder as necessary.

Images were taken with either inverted or upright configuration light microscopes and were captured with a digital camera in each case. Total magnifications of all images ranged from 50X to 500X. The microstructure represented in the images was qualitatively evaluated to discern the dispersion of fibers, the degree of consolidation and the approximate consistency with the V_f results. Voids and defects were identified, and their size, distribution, and location were noted if present.

4.8.2. V_f and Void Content Measurement

The quantitative measurements of V_f percentage and the void content percentage were undertaken using both ASTM D792 and ASTM D3171. Samples were analyzed from random locations within the testable 25.4 mm width created in each sample tube. Samples were stored in a desiccator at all times except when being processed or weighed to avoid mass fluctuations from the variation in ambient relative humidity. Since, at 565°C, the complete combustion of the thermoplastic resin without changing the mass of the glass fiber was reasonable to expect, the masses of resin and fiber were measured using the ASTM D3171 test method 1, subsection G. Complete combustion of the PETG was confirmed prior to testing. Determination of the void content percentage was accomplished by combining a prior weight percentage measurement with ASTM D792, test method A, using distilled water as the buoyancy medium during the Archimedes testing. Water temperature was monitored to track any associated changes in water density.

4.8.3. Thermal Analysis

Thermal analysis techniques were used on test samples to gather information about the three PETG matrices used during the course of the preliminary and main studies. First, thermogravimetric analysis (TGA) was performed to determine the temperatures at which the mass loss from the material becomes significant and so establish an upper bound for differential scanning calorimetry (DSC) analysis. The temperature in the SEIKO TG/DTA 220 was increased during the TGA testing of each material at a rate of 10 °C/min up to 300 °C. It was assumed that a mass loss of less than 1% indicated that significant thermal-oxidative degradation had not yet taken place. Using the information gathered from the TGA, a temperature was established as an upper bound during the DSC testing so that repeated runs could be made without thermal degradation of the material, which, if present, might change the material properties of the PETG. In practice, the DSC tests were programmed so that the temperatures remained well below the maximum temperatures established by the TGA to keep mass loss below 1%. The mass loss of the PETG in each sample during the DSC testing was expected to be below 0.4% in air. Because the DSC tests were conducted in nitrogen gas, the mass loss from thermal degradation of the matrices was anticipated to be somewhat smaller than 0.4% after each test cycle.

Next, T_g was measured using DSC analysis in accordance with ASTM E1356 using a SEIKO DSC 220C. Temperature was increased at 5 °C/min. The midpoint temperature (Tm) was used to report the T_g temperature. Because the T_g of a material actually occurs over a range of temperatures, multiple points can be defined and measured during the transformation of the material, as shown in Figure 35. Several analytical runs were conducted on each specimen to determine the possible effects of changing the thermal history. DSC curves were evaluated to look for any other noteworthy features in addition to T_g.

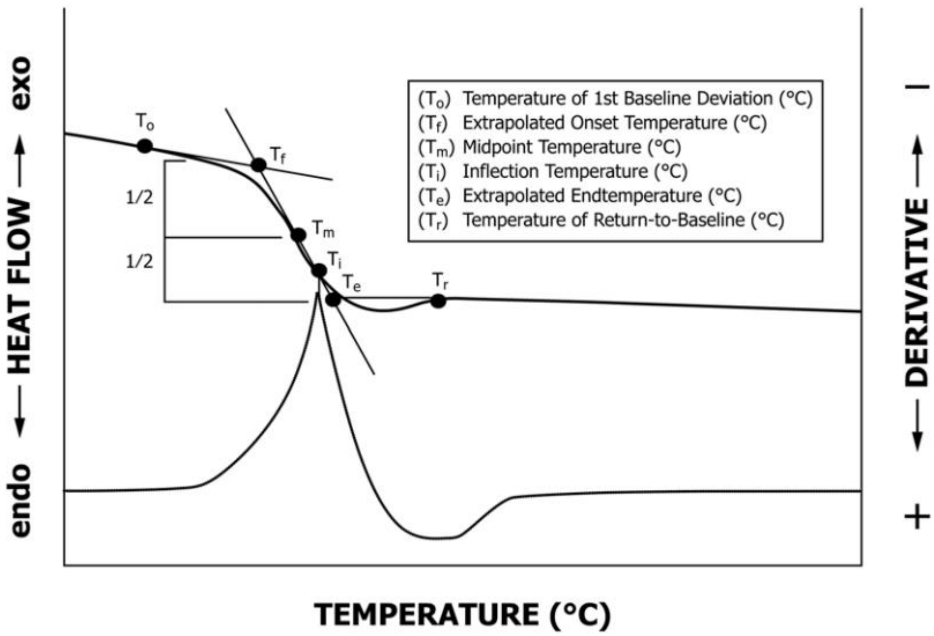

Figure 35: The various defined points on a DSC curve as a material transitions through the T_g [56].

All thermal analysis was conducted on as-received materials. Both the TGA and DSC testing chambers were purged with nitrogen gas before testing commenced. Subsequent nitrogen flow continued at a rate of 50 mL/min while the sample was at elevated temperature. PETG filament samples and the commingled material were contained in aluminum sample pans and lids. The sample size of the commingled material was increased during TGA and DSC testing in order to exaggerate the response signal of the PETG since the mass of the commingled samples contained both the matrix and the glass reinforcement. The glass reinforcement was considered unresponsive at the temperatures used during testing and so the data generated by thermal analysis of the commingled material was assumed to be representative of the PETG matrix only. PETG FDM filament does not initially contain reinforcement before processing and so a sample size of approximately 10 mg was used during the testing of the Maker Series PETG and the Form Futura PETG. The commingled samples had an average total sample mass of 20 mg.

5. MAIN COMPARATIVE STUDY RESULTS

5.1. Background and Motivation of Main Study

The preliminary research indicated that the proposed (JITA) process may be able to make polymer matric continuous fiber reinforced (FRP) parts of comparable quality to those made by a similar process using a commercially-developed material system. However, the preliminary study was brief and insufficient for confidently comparing the two processes on the basis of maximum quality. To remedy this deficiency, the main study in this work consisted of two optimization studies, designed to maximize the quality of both the JITA process and also the baseline process used for comparison. The short beam shear (SBS) strength was again used as the primary indicator of quality and so was assigned to be the response variable in the two studies. Using the results from the two experiments, the two maximum SBS strengths would be determined and compared to discern whether the JITA system produced results that were competitive with the baseline process. A conclusion that the maximum qualities of the two studies are comparable would justify both further use of the process and also the additional effort necessary to extend the investigation and development of the JITA process.

5.2. Main Study Results

The 86 total samples tubes were each sampled 5 times from randomized, disparate locations within the 2.54 width of testable material in each tube. These 5 sample beams were tested for SBS strength, and an average SBS strength for each sample tube was determined. The SBS shear strength results for each tube from both studies are shown in order of descending SBS strength in Tables 12 and 13. Each process parameter in the table is at a high (+1), middle (0), or low (-1) value. The relationship between uncoded and coded process parameter levels for both the JITA and the baseline process can be found Tables 5 and 6. The standard deviation reported applies to the variation in the 5 SBS strength tests conducted on each sample tube. All test beams failed in the inelastic failure mode as in the preliminary study. Minitab 17 was used again, this time to perform the statistical calculations necessary to select regression models, optimize the SBS strength, and to make accurate inferences from the data. A regression model was selected for each of the two manufacturing processes that would best predict a maximum SBS strength, while also satisfying the assumptions of normality. The maximum SBS values were calculated and each optimum was assigned its associated confidence intervals and prediction intervals.

TABLE 12: SBS strengths and coded levels of each sample in the baseline optimization experiment.

Mandrel Temperature	Foot Temperature	Foot Consolidation Force	Roving Tension	Process Speed	SBS Strength [MPa]	Standard Deviation [MPa]
-1	+1	+1	-1	-1	52.8	1.88
-1	+1	-1	+1	-1	49.2	3.10
0	+1	0	0	0	48.5	1.22
0	0	0	0	-1	44.2	2.14
+1	-1	-1	-1	+1	42.1	1.77
-1	+1	-1	-1	+1	39.3	2.93
0	0	0	-1	0	39.2	1.50
-1	+1	+1	1	+1	38.9	2.90
+1	+1	+1	-1	+1	38.6	0.852
+1	-1	+1	1	+1	38.5	1.33
0	0	0	0	0	37.7	0.890
+1	0	0	0	0	37.7	1.43
0	0	+1	0	0	37.5	1.74
+1	+1	-1	+1	+1	37.5	2.02
0	-1	0	0	0	37.2	0.449
0	0	0	0	0	37.0	1.08
0	0	0	0	0	36.9	0.815
0	0	0	0	0	36.7	1.85
0	0	-1	0	0	36.5	1.50
0	0	0	0	0	36.5	0.698
0	0	0	0	0	35.5	1.70
0	0	0	1	0	35.4	1.37
+1	-1	-1	1	-1	34.9	1.03
0	0	0	0	+1	34.6	1.46
+1	-1	+1	-1	-1	34.6	2.57
-1	0	0	0	0	31.8	0.682
+1	+1	-1	-1	-1	31.7	1.77
-1	-1	+1	+1	-1	31.0	1.56
+1	+1	+1	+1	-1	27.0	0.902
-1	-1	-1	-1	-1	25.0	0.945
-1	-1	+1	-1	+1	22.7	1.51
-1	-1	-1	+1	+1	22.0	1.73

TABLE 13: The SBS strengths and coded levels of each sample in the JITA-M optimization experiment.

Mandrel Temperature	Foot Temperature	Foot Consolidation Force	Roving Tension	Process Speed	Hot End Temperature	SBS Strength [MPa]	Standard Deviation [MPa]
0	+1	0	0	0	0	44.9	2.57
0	0	0	0	-1	0	44.9	1.65
0	0	0	0	0	-1	44.6	3.20
0	0	0	+1	0	0	43.5	2.68
0	0	0	0	0	+1	43.0	1.87
0	-1	0	0	0	0	43.0	1.08
0	0	0	0	0	0	42.9	1.00
0	0	0	0	0	0	42.6	1.90
0	0	0	0	0	0	42.4	3.93
0	0	0	0	0	0	41.9	1.23
0	0	-1	0	0	0	41.9	1.72
0	0	0	0	0	0	41.7	1.66
0	0	0	0	+1	0	41.6	2.40
0	0	0	0	0	0	41.4	2.61
0	0	0	-1	0	0	41.4	1.37
-1	+1	+1	+1	-1	+1	41.2	1.14
0	0	0	0	0	0	41.0	2.21
0	0	+1	0	0	0	41.0	2.98
0	0	0	0	0	0	40.6	1.98
0	0	0	0	0	0	40.3	2.33
0	0	0	0	0	0	40.2	0.877
-1	+1	-1	1	-1	-1	39.8	1.54
-1	+1	+1	-1	-1	-1	38.4	3.74
-1	+1	-1	-1	-1	+1	37.9	2.26
+1	-1	-1	-1	+1	-1	37.9	1.97
-1	0	0	0	0	0	37.3	1.61
+1	-1	+1	-1	+1	+1	37.3	1.06
+1	+1	+1	+1	+1	+1	37.2	0.853
-1	-1	+1	+1	-1	-1	37.2	2.33
-1	-1	-1	-1	-1	-1	37.1	0.743
+1	-1	-1	+1	+1	+1	37.1	0.914
-1	-1	-1	+1	-1	+1	36.8	1.53
+1	-1	+1	+1	+1	-1	36.1	1.98
+1	0	0	0	0	0	35.7	1.26
+1	+1	-1	-1	+1	+1	35.6	1.70
-1	-1	+1	-1	-1	+1	34.8	3.76
-1	+1	+1	-1	+1	+1	34.5	1.90
-1	+1	-1	-1	+1	-1	34.2	1.72
+1	+1	+1	-1	+1	-1	34.0	1.10
-1	-1	+1	-1	+1	-1	32.8	2.32
+1	-1	-1	-1	-1	+1	32.6	1.08
-1	-1	-1	+1	1	-1	32.5	0.389
+1	+1	-1	-1	-1	-1	32.4	1.38
+1	-1	1	-1	-1	-1	32.2	1.28
+1	-1	-1	+1	-1	-1	32.0	2.38
-1	+1	-1	+1	+1	+1	31.5	1.51
-1	-1	-1	-1	+1	+1	31.4	1.22
+1	+1	-1	+1	+1	-1	31.2	0.544
+1	+1	-1	+1	-1	+1	30.9	1.99
+1	+1	+1	-1	-1	+1	30.6	1.17
-1	+1	+1	+1	+1	-1	30.4	1.03
-1	-1	+1	+1	+1	+1	29.8	2.32
+1	+1	+1	+1	-1	-1	27.3	1.01
+1	-1	+1	+1	-1	+1	27.1	1.35

5.3. Regression Models

Each input variable was assigned a letter to more efficiently communicate the results of each study, and a variable key is shown in Table 14.

TABLE 14: A key showing the letter assigned to each variable.

Input Variable:	Mandrel Temperature	A
	Foot Temperature	B
	Process Speed	C
	Foot Consolidation Force	D
	Roving Tension	E
	Hot End Temperature	F
Response Variable:	SBS Strength [MPa]	SBS

The regression model chosen for the JITA-M process is based on coded input variables and is shown in Equation 2.

$$\begin{aligned} SBS = 42.7 - 0.90A + 0.13B - 0.24C - 0.33D - 0.39E - 0.020F - 6.62A^2 - 1.65D^2 \\ - 0.90AB + 2.76AC - 0.36AE - 0.46BC + 0.69BF + 0.36CD \end{aligned} \tag{2}$$

The regression model chosen for the baseline process also uses coded input variables and is shown in Equation 3.

$$\begin{aligned} SBS = 38.0 + 0.55A + 4.2B - 0.90C + 0.21D - 0.63E - 4.2A^2 + 3.86B^2 - 1.9D^2 \\ -5.9AB + 3.9AC - 1.1AD - 1.2DE \end{aligned} \tag{3}$$

5.4. Regression Optima

Figure 36 shows the optima from each study and their associated confidence intervals. The JITA-M regression predicts an optimum of 45 MPa while the baseline regression predicts an optimum of 53 MPa. A confidence interval at a confidence level of 95% can be interpreted as the interval in which the mean of samples tested at the optimum combination of input variables is 95% likely to fall.

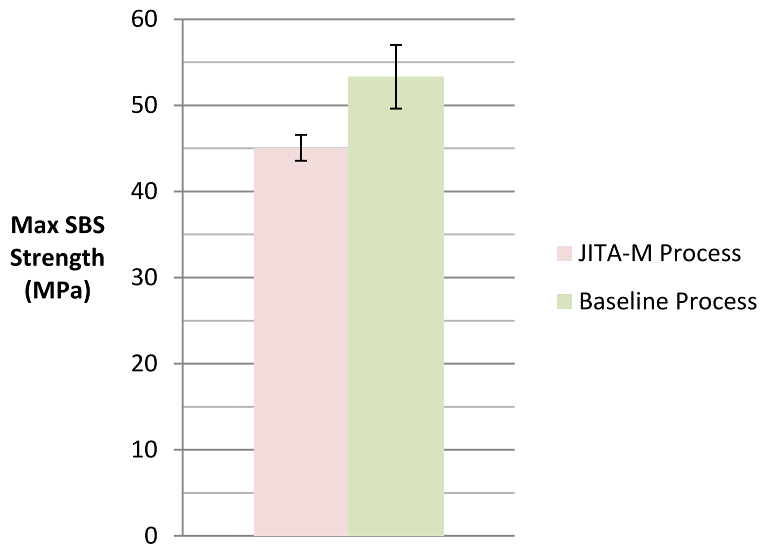

Figure 36: The maximum SBS strengths are shown for the JITA-M process and the baseline process. The error bars are confidence intervals at a 95% confidence level.

The coded input variable levels at which the optima are expected, are shown in Table 15.

TABLE 15: The normalized input variables levels at the optimum levels are shown here, designated by their letter descriptor found in Table 14.

	A	B	C	D	E	F
JITA-M:	-0.31	1.0	-1.0	-0.21	-1.0	1.0
Baseline:	-1.0	1.0	-1.0	0.64	-1.0	X

Each process was tested with replicated measurements at the midpoint level of all values, where the coded level equals zero. Six midpoint replicates were measured in the baseline process and 10 were measured during the JITA-M study. This experimental design feature provides a measurement of the variation inherent to each manufacturing process at the midpoint, which is then extrapolated to estimate the expected error at other points included in the experiment. As seen in Table 16, the coefficient of variation of these measurements of SBS strength was very low in both studies.

TABLE 16: The variation of SBS strength at the midpoint in each study.

	Average [MPa]	SD [MPa]	CV [%]
JITA-M:	42	0.97	2.3
Baseline:	37	0.71	1.9

During the course of the JITA-M study, the two most likely contributors to an inconsistent effect on the response variable were 1) the replacement of a failed hot end temperature controller, and 2) the use of five rolls of JITA-M PETG FDM filament to make the 54 samples. However, the JITA-M study incorporated three blocks into its design. And so, effects from uncontrolled variation could be detected, not only from the residual plots used to confirm normality, but also from the measurement of the statistical significance of an effect from any blocks on the response variable. Nevertheless, all of these statistical tests indicated that there was no significant unintended effect on the response variable either in the JITA-M study or in the baseline test.

5.5. Main Study Results Discussion

5.5.1. Damage and Deformation During Testing

In this study, SBS testing was used as the primarily indicator of quality, upon which a comparison between the JITA and the baseline processes would be made. Although the test uses a 3-point bending fixture, it is intended to produce enough shear stress in a test sample to induce shear failure. This is accomplished by moving the support pins very close to one another. In this manner, a combination of bending stresses and shear stress is applied to the sample, but the shear component overwhelms the bending contribution.

All of the samples in this study failed in an inelastic mode and underwent large deformations during testing. No audible indications of failure were noted during the SBS testing of the beams. Visual indications of damage consisted of lighter regions of material and buckled fibers. These lighter regions developed shortly after yield, while obvious signs of fiber buckling occurred at the end of testing, after significant deformation. Table 17 shows a single typical beam, in this case made from commingled material, which displays these features generated during the physical testing. The black circles represent the points of contact from the support pins and loading nose. Areas contained within a red line or a blue line show features that may not be as readily apparent in the images. Red lines circumscribe regions of lighter material. Areas contained within a blue line contain buckled fibers. Each column shows the same beam from multiple angles during each phase of testing. The 3 views in column A display a beam before testing with relatively consistent coloring and no plastic deformation. Column B shows the same sample just after the initial yielding of the beam. Plastic deformation can be seen in the side view. The lighter, damaged regions have begun to form between each support pin and the loading nose, with more damage occurring on the compression side of the beam (against the foot). A significantly deformed beam with extensive damaged material is shown from 3 angles in column C.

TABLE 17: The damage accumulation and deformation of a single beam during SBS testing. Areas in red show general damage. Areas in blue contain buckled fibers.

Surface Against Foot		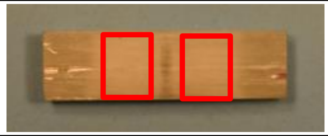	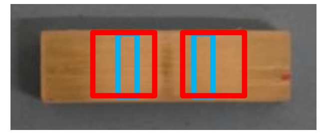
Side View	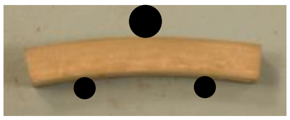	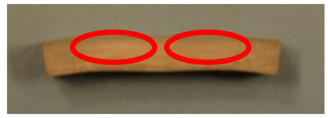	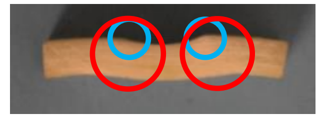
Surface Against Mandrel		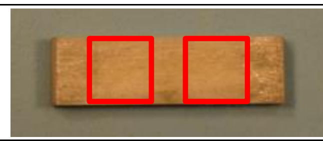	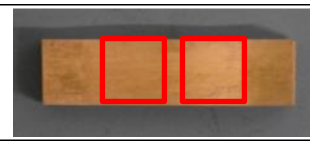
	Column A: Before Testing/Contact with the Loading and Support Pins	Column B: Just After Yield	Column C: Immediately Prior To End of Test

5.5.2. Discussion of Mechanical Response of Samples to SBS-Induced Stress

Researchers Berg, Tirosh, and Israeli have simulated the predicted stress distributions generated during the SBS testing of an FRP beam [63], shown in Figure 37. The response depicted is that of a unidirectional carbon/epoxy composite that has been loaded into the plastic region. FEA analysis using a bi-linear model to represent the elastic and the plastic response was used to generate stress contour plots [63]. The results of this analysis show that the stress state induced by SBS testing is not consistent with that predicted by Euler-Bernoulli beam theory. Primarily due to the complications caused by nearby contact stresses, the maximum shear stress does not occur in the neutral plane of the beam and the bending stresses vary significantly along the length of the beam between the loading nose and the beam support. Due to the differing material systems, the information in Figure 37 should be used in a qualitative manner simply to identify locations of peak shear and compressive stress of the test sample under loading into the plastic region. A red box has been added in Figure 37, A to indicate the portion of the beam to which the contour plots apply. The test fixture in this work used support pins rather than the support plates as shown in Figure 37, A.

<table>
<tr><td>A: Coordinate Sytem and the Region of Interest</td><td>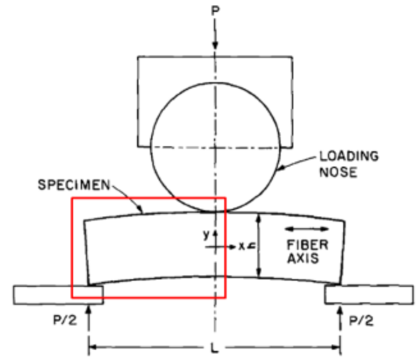
</td></tr>
<tr><td>B: SBS-Induced Shear Stress</td><td>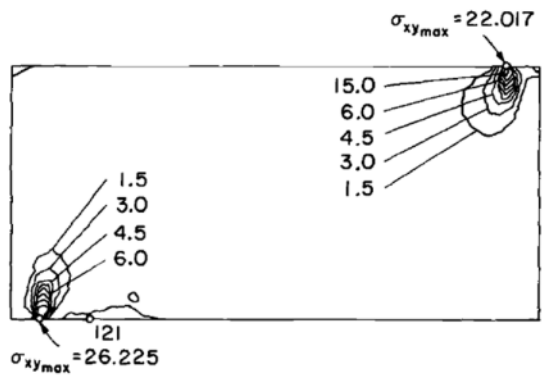
</td></tr>
<tr><td>C: SBS-Induced Compressive Stress in the Fiber Direction</td><td>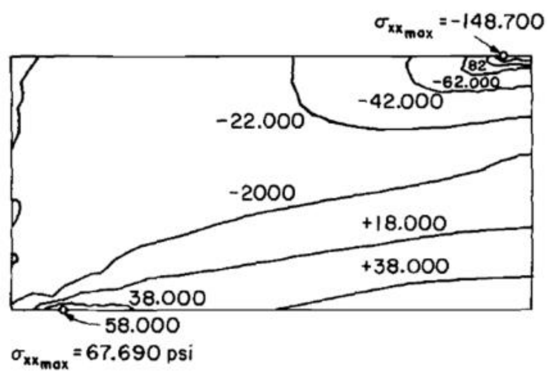
</td></tr>
</table>

Figure 37: Stress contour plots generated as SBS testing proceeds into the plastic region [63].

The E-glass and PETG FRP samples in this study clearly demonstrated damage due to compression along the fiber direction. The side view in Table 17, Column C, showing the sample after it underwent significant deformation, shows fibers buckling away from the foot surface of the beam. Also, Table 17, Column B shows that initial yielding is concentrated on the compression side of the beam. The side view in the column shows lighter material beginning to first appear on either side of the loading nose and biased towards the foot-side of the sample. Also, the foot-side surface of the beam at this loading shows much lighter areas between the support pins and the loading nose compared to those same areas as seen from the mandrel side of the sample. Once again, this indicates that damage is occurring mostly in the compression region of the beam.

The development of compressive failure in these areas corresponds well with the predicted areas of highest compressive stress shown in Figure 37, C. The most obvious signs of compressive damage in the E-glass/PETG samples, the buckled fibers, appear just adjacent to the loading nose on the compression side of the beam just as predicted in the FEA model. However, the predicted compressive stress is significantly diminished away from the loading nose contact point, while the samples tested here show early signs of damage along the entire span between the loading nose and the support pins. This is most likely the result of 1) the significant weakness of the E-Glass/PETG samples in compression, or 2) the result of the added shear stress, or a combination of these two factors.

Fiber reinforced composite materials are generally weaker when loaded along the fiber in compression than when the fibers are loaded in tension, due to the generally poor response of a flexible fiber subjected to compressive stress. This characteristic contributes to the relative insensitivity of tensile testing methods to defects in contrast to ILSS testing or compressive mechanical tests. Tensile tests load the composite samples in a way that would resist the load if no matrix was present at all. In the case of polymer matrix FRPs, it is a relatively weaker and more compliant matrix that supports a stronger, stiffer fiber to impart any resistance to buckling.

In this study, a weak matrix was used to support the glass fibers. Additionally, the studies conducted in this work were intended to optimize the quality of a composite material, necessarily producing a significant amount of samples that were weaker from a lack of consolidation, likely higher void content, and possible thermal-oxidative degradation of the matrix. All of these characteristics would contribute to a matrix that provides diminished support of the fiber, either through 1) a smaller total area of contact with the fiber, 2) a weaker matrix due to defects, or 3) a weaker matrix due to a deleterious change in material properties from being processed at high temperatures for long periods of time. Consequently, while PETG of high quality is more likely to be able to provide some degree of support to the reinforcing fibers, samples with a lower quality PETG matrix will show even poorer performance, and all of these samples are likely to show evidence of compressive failure at low loadings. Compressive failure of an FRP composite loaded along the fiber direction typically results in buckled, broken fibers, along with a 'broomed' appearance, which results from the separation of fibers from one another after the transverse tensile failure of the matrix. These expectations are confirmed by 1) the appearance of large areas of damaged material on the compression side of the beam after small amounts of deformation, shown in Table 17, as well as by 2) the buckled and broomed fibers appearing in the blue circles in the same figure.

The FEA results shown in Figure 37, B also predict the maximum shear stress from SBS testing to occur on the compression side of the beam and adjacent to the area of contact with the loading nose. The SBS testing configuration includes supports that have been moved closely together to decrease the bending stresses while maintaining the now relatively high shear stress. Catastrophic failure at the plane through the centroid of the beam, where Euler-Bernoulli beam theory would predict the shear stress to be the highest, is common in thermoset matrix FRP samples. Due to the use of similar test samples and a test fixture of a standardized geometry, those high shear stresses would also be present during the testing presented in this work. However, because compressive failure was most likely a significant component of the damage produced in the beams, and because the compressive damage was likely to have occurred at low loadings, it is uncertain to what degree the damage in the beams was due to shear stress. Similarly to the compression failure behavior, the low mechanical properties of the PETG matrix in shear would have allowed relatively large deformation of the composite during the elastic response and the ductility of the PETG would have also allowed a large amount of beam deformation before a final failure showing significantly reduced load carrying capacity. One feature of the beam shown in

Figure 37 that is indicative of shear failure is the occurrence of the lighter, damaged material throughout the entire thickness of the beam, seen in the side view of Column C. Because there were no signs of significant tensile damage during the testing, the appearance of damaged material on the tension side of the test sample after a large deformation indicates that some degree of shear damage did occur before the SBS test ended. Lastly, because the failure was graceful to a large extent, rather than catastrophic as would be associated with a buckling failure, it is likely that shear-induced damage was also a significant contributor to the damage of the test beams.

5.5.3. Graceful Failure and the SBS Test

There is general agreement that the SBS test is appropriate to be used for screening studies and for quality comparisons of FRP components, as it is used in this work. However, the graceful failure of a thermoplastic composite can often cause difficulty when attempting to identify the loading at failure of the SBS test specimens. A spectrum of mechanical response was seen during testing, and this interval was bounded by the examples shown in Figure 38. Type 1 behavior is that which clearly displays a maximum loading, labeled F, before the sample is compressed in the fixture and the applied load increases rapidly as the load state becomes dominated by the transverse compression of the sample. Type 2 behavior inhibits the easy identification of a maximum load by monotonically increasing throughout the test before the pinching phenomenon occurs.

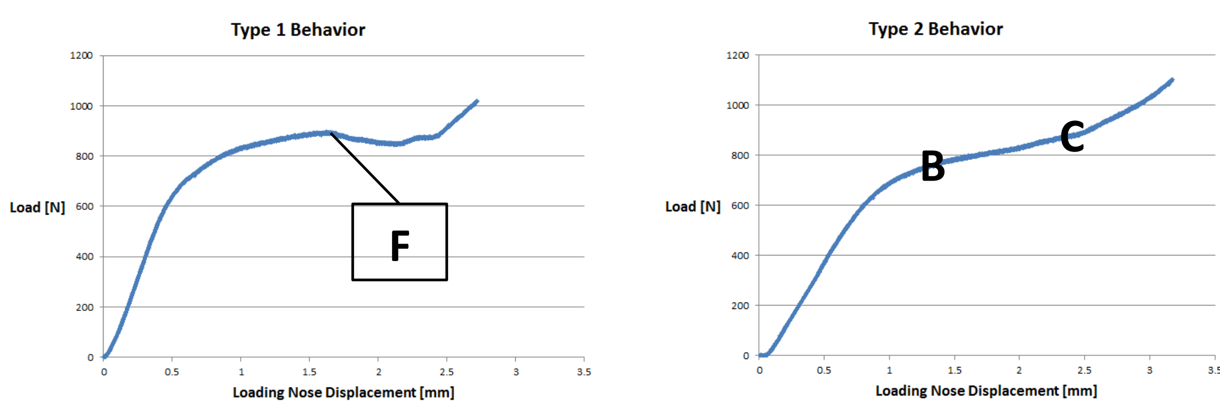

Figure 38: The two types of mechanical response resulting from SBS testing.

The SBS strengths of samples displaying type 1 behavior were calculated based on the loading of the sample at point F. In contrast, the typical morphology of the type 1 response was studied to extract a quantitative approximation of maximum loading in the case of the type 2 response. A simple method of approximation was developed based on the observation that the ultimate strength of the SBS samples, when discernable, appeared between the initial yield of the material and the large deformations that allowed the beam to become pinched in the fixture, labeled in Figure 38 with B and C, respectively. The load at the midpoint between B and C was considered to be a sufficient approximation of the failure load, F. The states of the sample shown in column B and column C in Table 17 give a visual indication of the damage and deformation present at points B and C on the response curve, although the specific sample shown in Table 17 displayed a mechanical response behavior that was neither purely type 1 or type 2.

Both of these mechanical responses are consistent with the inelastic failure illustrated in Table 17 and would not be unexpected when testing an FRP with an amorphous, low T_g thermoplastic matrix such as PETG. The lower modulus and high ductility of the matrix used here would be likely to allow a large amount of deformation before an obvious decrease in load-carrying capacity is observed. Any matrix allowing large strains before failure, such as an elastomeric material, would be likely to show a similar mechanical behavior during an SBS test.

5.5.4. The Midpoint Method of Determining Ultimate Strength

Based on a comparison of 1) the frequency of occurrence of type 2 behavior and 2) the process parameter levels used to make each sample, there appears to be a strong negative correlation between this mechanical response and the processing conditions likely to produce thermal degradation. Although thermal degradation was not directly measured in the course of this work, it is clear that 1) thermal-oxidative degradation of any polymer matrix composite will occur when exposed to sufficiently high temperatures for long durations, and 2) some of the samples produced in the JITA and baseline optimization processes displayed clear signs of this type of damage, as can be seen in Figure28. Creating conditions that caused thermal degradation was necessary to create a drop in the response variable necessary to set the bound levels for the optimization studies.

In the JITA study, the largest effects on the SBS strength were from the mandrel temperature and the processing speed, as can be seen by the regression coefficients in Equation 2. The midpoint method was only necessary for evaluating JITA samples when the mandrel temperatures were at the middle (0) or low (-1) levels. And, among those samples, the processing speed was only at the lowest level (-1) when the mandrel temperature was also at its lowest level (-1). This indicates that the type 2 behavior was seen in samples that were exposed to lower temperatures for shorter durations. Similarly, the foot temperature had the largest effect on the SBS strength of the baseline sample tubes, as can be seen by the relative size of the coefficients of the regression shown in Equation 3. And, the type 2 behavior was almost exclusively observed in samples with the lowest foot temperatures.

Given that the material system here is a thermoplastic matrix composite, it would also be reasonable to suspect that, instead of negatively correlating with thermal degradation, this mechanical response was simply positively correlated with weak samples. Low temperatures used during a short processing time might be likely to produce samples with insufficient consolidation and wetout due to the use of a relatively high viscosity resin, which may not have been allowed sufficient time to completely surround the reinforcing fibers. However, the average SBS strength of a sample showing type 2 behavior was virtually the same as that of all of the samples made for each optimization study, as shown in Table 18. This similarity indicates that the type 2 behavior is not generally associated with either weak or strong samples. Alternatively, the type 2 behavior is associated with a sample that has not been exposed to high temperatures for long periods. Significant thermal degradation would not be expected of the glass at these temperatures, but the ductility of the matrix could be decreased due to detrimental molecular effects such as chain scission.

TABLE 18: The relationship of samples showing a type 2 mechanical response to 1) the average sample made with the same process and 2) the regression model associated with each process.

	Average SBS Strength of All Samples [MPa]	Average SBS Strength of Type 2 Samples [MPa]	Average Residual of Type 2 Samples [MPa]
JITA-M:	37	38	-0.18
Baseline:	37	37	1.4

Although the type 2 mechanical response does appear to have a correlation with certain processing conditions, it is unlikely that the midpoint method led to errors that would have significantly affected the conclusions drawn from the comparison of the optima for the following reasons: First, the midpoint method was used on 115/430 beams subjected to SBS testing. Second, the variation of load within the region between B and C was, at most, roughly 20% of the load in this region. This means that the tolerance on the SBS strength resulting from the midpoint method would be no greater than ±10% since the midpoint of the interval was used as the value for ultimate load at failure. Lastly, the average residuals of the data points that resulted from the midpoint method are relatively small, as seen in Table 18. Consequently, although the shape of the response surfaces could have been altered, the constant in each regression model was not increased or decreased significantly. As a result, the optima from the regression surfaces were also not significantly increased or decreased from data points that resulted from using the midpoint method.

5.6. Comprehensive Conclusions

5.6.1. Statistical Significance

The relationship between the optima and their confidence intervals illustrated in Figure 36 show that there is a statistically significant difference between the maximum SBS strength values that can be produced by each process. And so, on the basis of SBS strength, the maximum quality of the JITA-M process should be considered less than the maximum quality of the baseline process. The statistical significance of this difference can clearly be seen by the distance between the confidence intervals of the two optima. As a practical rule, the statistical significance of a difference between two means can be asserted with at least 95% confidence if there is no overlap of the two confidence intervals [60, 61]. The implication of no overlap is that the associated p-value will be lower than 0.05, and one should reject the null hypothesis that the two optima are the same [61].

5.6.2. Practical Significance

Although there is a statistically significant difference between the maximum SBS strength of the JITA-M process and that of the baseline process, the quality of parts made by the JITA system in general are of comparable quality to those made by the baseline system. This distinction is possible, in part, because of the fact that the establishment of a statistically significant difference between two values does not imply that the difference is practically significant. However, establishing the practical significance of FRP quality is difficult if the process is not intended for a specific part. A particular part will have associated minimum quality standards that will be different from those that are acceptable for a different component. Also, quality is not a function of solely the maximum quality possible from a material deposition process. It is also a function of the part the process will be applied to. A flat part of high quality would be easier to make with a compression molding process compared to using a filament winding technique, for example. As a result, establishing the quality possible when producing one part will not necessarily be relevant when applying the JITA method to a different structure. In addition, choosing a process to make a part involves tradeoffs between resources, risk tolerance, and part requirements, among other things. Quality plays an important role in this decision, but it is not the only factor.

The intent of this study is to discern the feasibility of the JITA process, and to establish whether development and use of the process should continue. And so the standards for evaluating will be different than if the process was fully developed and a final decision was being made whether to use the process for a specific purpose. The JITA-M process is in an early stage of development and, if the predicted optima are compared, it makes parts of only 16% lower maximum quality than the baseline technique. Lastly, even if exact equality of SBS strength is necessary, it is not unreasonable to assume that this small deficiency can be resolved.

5.6.3. Incorporating Preliminary Results

The JITA-M SBS strengths have shown themselves to be lower than those resulting from the baseline process by a statistically significant amount. However, this difference is small, reasonably assumed to be capable of improvement, and it would be rash to dismiss the process at this stage in its development since it also offers significant potential advantages over other manufacturing methods. Nonetheless, although the JITA-M process appears to make parts of lesser quality, the JITA system in general can make parts of at least the same SBS strength as the optimized baseline process. The JITA-P results show that the JITA system can produce parts of competitive SBS strength when the JITA-P matrix is used.

5.6.4. Comparison of Preliminary and Main Study Results

Figure 39 shows the preliminary data points along with the SBS strength optima for the JITA-M and baseline processes. As noted before, the preliminary study was inadequate for optimization purposes. This inadequacy is demonstrated in the case of the baseline process; the preliminary commingled samples are much lower than the maximum value predicted by the baseline optimization study. It is noteworthy that the JITA-P data points are significantly higher that the JITA-M optimum. This result is unexpected since the JITA-M study was intended to maximize SBS strength.

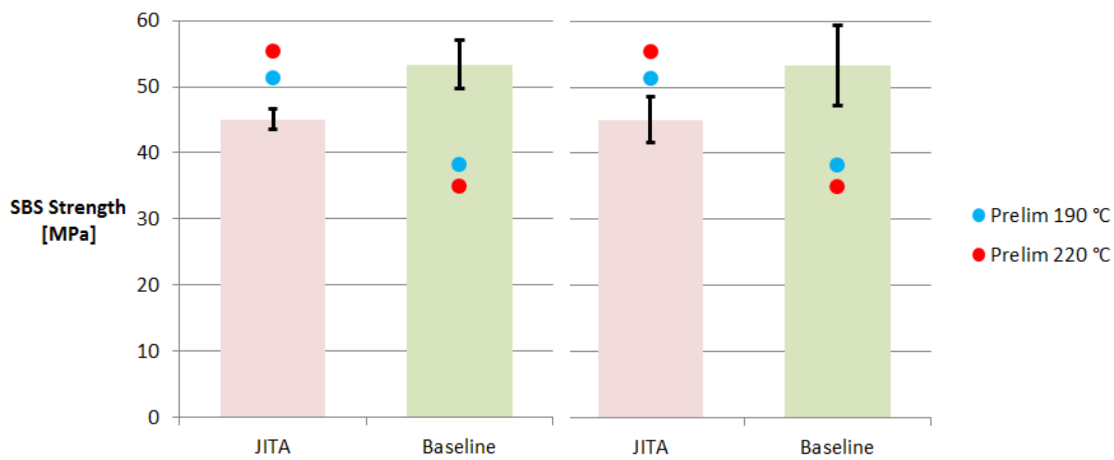

Figure 39: Preliminary data points along with the optima from both processes. The left two columns show optima confidence intervals, while the columns on the right show the larger prediction intervals. All error bars are at a 95% confidence interval.

Confidence intervals are useful for comparing mean values and would be inappropriately applied for comparison to discrete values. In contrast, prediction intervals incorporate the uncertainty in the regression model but also account for the expected variation of individual data points around the mean. Consequently, prediction intervals are more appropriate to compare to the preliminary data points and are used as error bars on the right in Figure 39. As before, one can see that the preliminary baseline samples were not maximized and, as a result, are lower than the prediction interval for those discrete values. And yet, the JITA-P data points, while also not being contained within the JITA-M prediction interval, instead show a *higher* SBS strength than the predicted optimized JITA-M SBS strength.

The JITA-P data has not been maximized by any intentional optimization method. They could very well be maximum JITA-P values, they could be an intermediate value, or they could be low-quality examples of the JITA-P material system. By contrast, the baseline system used for comparison in this work was maximized, and most individual baseline values tested at the optimized process parameter levels can be expected to fall within the prediction intervals for the baseline process shown in Figure 39. The JITA-P values fall well within the baseline prediction interval, and so can easily be considered to have comparable SBS strength values. And so, although the JITA-M system does show a statistically significant difference between its maximized SBS strength and that of the baseline system, the JITA-P system 1) makes samples with a quality that is higher than the JITA-M system, an 2) the JITA-P system can make samples that are at least of comparable quality to the baseline system. Therefore, although the JITA-M system's maximum quality is somewhat less compared to the baseline process, the JITA process can deposit FRP material of comparable quality to that of the baseline process.

5.6.5. Discrepancies Between JITA-P and JITA-M

If the JITA-P data points were simply outliers, but were generally consistent with the JITA-M system, their equivalence to the optimized baseline values would be a coincidence. In this hypothetical scenario, their high SBS strength value could be the result of random error. After all, the JITA-M prediction interval was only assigned a 95% confidence; it is still possible that discrete JITA-M data points could fall outside the interval. However, this interpretation of the data is likely to be inaccurate for multiple reasons.

Firstly, the JITA-P samples were made at temperatures that wouldn't produce viable test samples using the JITA-M system. As shown in Figure 40, the lower bounds of the JITA-M hardware were, on average, set to well above the temperatures used to make the 190 °C JITA-P sample. All other input variables used in the JITA-P process were set to levels that would make the best quality part using low temperatures: the processing speed was slow and the consolidation forces were high. Since the bounds of the JITA-M system were set by looking for a significant *reduction* in the response variable, it is very unlikely that the 190 °C JITA-P could have been made using the JITA-M manufacturing system, and it is even more unlikely that they would have achieved SBS strength values that are so high. Consequently, it would be unreasonable to conclude that the 190 °C JITA-P samples were simply extremely high outliers consistent with the JITA-M process while being manufactured at these relatively low temperatures.

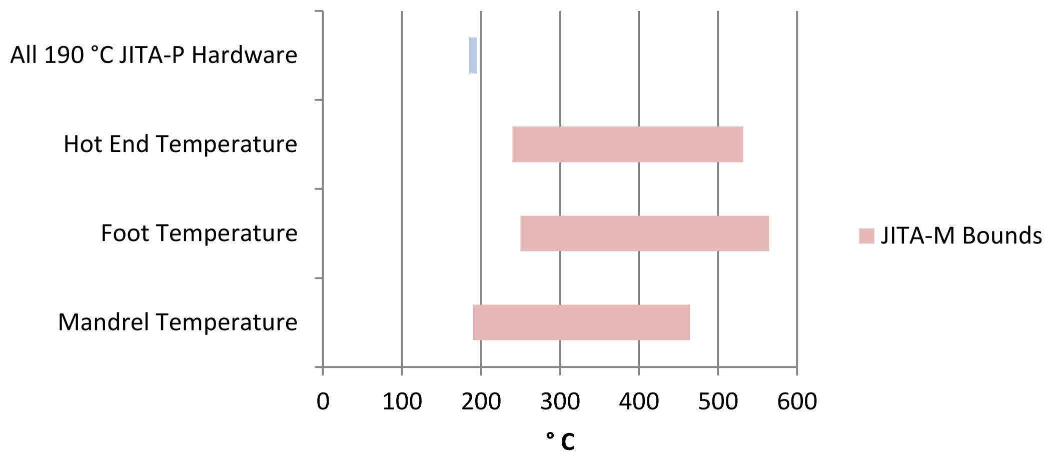

Figure 40: Temperatures used in the JITA-M and 190 °C JITA-P studies.

Secondly, if it is assumed that the preliminary JITA system was essentially the same as the JITA-M system, the likelihood that both of the discrete JITA-P data points would have exceeded the JITA-M prediction intervals is very low. Since the JITA-P samples were made outside of the bounds of the JITA-M study, using the JITA-M response surface to predict a SBS strength value and to generate prediction intervals at those input variable levels would be an inappropriate extension of the model. And so, a direct comparison with a predicted point from the JITA-M regression model wouldn't be meaningful. However, as a conservative test, the likelihood that the measured JITA-P SBS strengths would be generated at the *optimum* JITA-M processing point can be estimated. Any other processing point, by definition, is likely to produce a predicted SBS strength that is lower than at the optimum point, which would make the likelihood of the high SBS strengths associated with the JITA-P samples even less likely. Prediction intervals delineate an interval in which a new test result has a specific likelihood of falling. If higher certainty is required, the prediction interval necessarily widens to offset the need for higher confidence. As can be seen in Figure 39, the JITA-P values lie beyond the 95% confidence level prediction interval around the JITA-M optimum point. Using an iterative process, the confidence level was increased to 99.93%, which widened the interval until it reached the lower of the two JITA-P values, as seen in Figure 41. Therefore, assuming that the JITA-P values were outlying JITA-M values, the likelihood that the next SBS strength value measured at the optimum would exceed the prediction interval is 0.07%. Therefore the likelihood that all samples measured in the JITA-P study would exceed the 99.93% prediction interval is even lower. Since the likelihood is so low that the JITA-M system's SBS strength would reach the SBS strength values measured during the JITA-P test, the assumption that the JITA-M and JITA-P systems are essentially the same should be rejected.

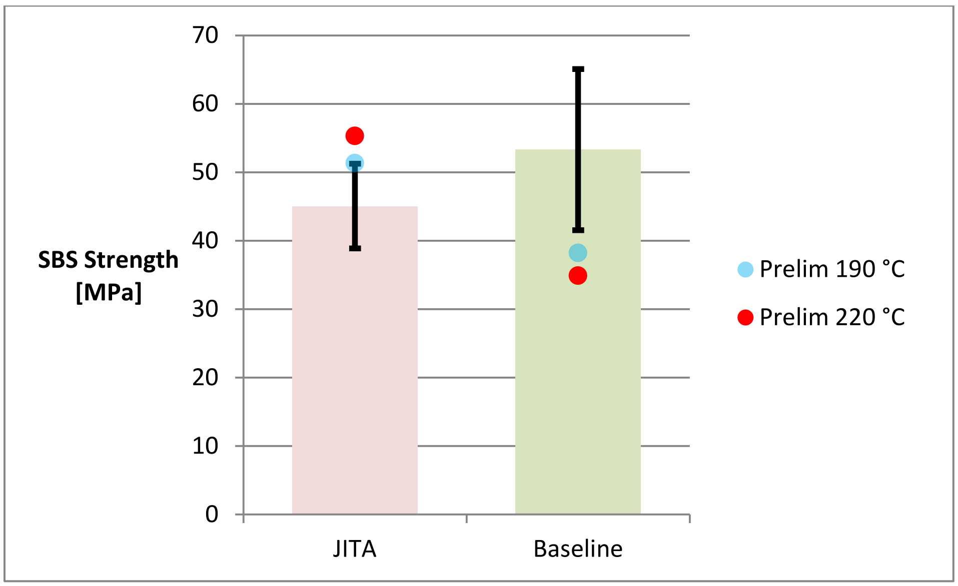

Figure 41: Enlarging the prediction intervals to a confidence level of 99.93%.

For the sake of comparison, one can investigate the accuracy of the baseline regression model in predicting the preliminary baseline points. The bounds of this regression model do include the input variable levels used in the preliminary investigation of the baseline process. So, the difference in SBS strength between the measured baseline process points and the predicted points can be easily calculated and the results of the calculation are shown in Table 19. These differences between the measured and predicted SBS strength values are very small. In contrast, the difference in SBS strength between the predicted maximum value of the JITA-M system compared with the measured JITA-P values averages 15%. Once again, this indicates that the JITA-M and the JITA-P systems are significantly different and that this difference is unlikely to be due to chance.

TABLE 19: A comparison of the measured SBS strengths from the preliminary study of the baseline process with the predicted SBS strength values from the baseline regression model.

	190 °C	220 °C
Measured SBS strength [MPa]:	38.2	35.2
Predicted SBS strength [MPa]:	38.1	35.0
Percent Difference [%]:	0.26	0.57

5.6.6. The Discrepancy Between JITA-P and JITA-M: Possible Causes

Since the high SBS strengths of the JITA-P values are unlikely to have occurred by chance, there is an essential difference between the JITA-P and the JITA-M systems. This difference is most likely the result of a compositional difference in the JITA matrices used in the preliminary and the main study. The JITA-P material system used Form Futura 3.00 mm diameter PETG FDM filament while the JITA-M system used Maker Series 3.00 mm PETG FDM filament. The material change was made due to considerations of availability and cost. However, there were other possible sources of variation that might have influenced the results of the JITA system as well. These should be eliminated from consideration before concluding that changing the brand of PETG FDM filament was responsible for the varying performance of the JITA system.

One possible source of variation was a changing composition of the materials during the course of the studies. The same roll of E-glass reinforcement fiber was used throughout both JITA experiments, and so this is unlikely to be the cause of the varying SBS strengths. Similarly, the commingled material used in the optimization study was from the same doff as that used during the preliminary research. In addition, the possibility of a different composition of the matrix material within each brand should also be considered. The JITA-P test samples were too few to be made from multiple rolls of PETG filament. However, five separate rolls of Maker Series material were used during the JITA-M study. And yet, these rolls of material were ordered so that they would be from the same manufacturing run to increase material consistency. Also, the statistical insignificance of the blocks in the JITA-M study indicates that there was little effect on the response variable from uncontrolled variables during the course of the JITA-M experiment. The small amount of variation in the Maker Series PETG filament is further confirmed by the very small amount of pure error seen at the evaluation of the midpoints, which were randomly tested throughout the course of the JITA-M test and were made from different rolls of PETG filament. And so, it was unlikely that these other forms of material variation significantly contributed to the difference between the JITA-M and JITA-P results.

However, there were significant changes made to hardware both between the JITA-P and JITA-M tests, as well as midway through the JITA-M study. First, the mandrel heating hardware was redesigned between the JITA-P and JITA-M studies. It was discovered that the mandrel temperature control system initially used was inadequate for the consistent control of the high mandrel temperatures required for the JITA-M experiment. In an attempt to maintain consistency, the mandrel surface temperature was fully characterized using thermocouple measurements and thermal imaging before and after changing the heating device from a heat gun to an oven heating element. A thermal image taken during mandrel surface characterization is shown in Figure 42. In this way, the offsets from the nominal mandrel temperature set point to the actual surface temperature of the mandrel were established in both cases, allowing the continued accurate control of true mandrel temperature. These attempts to mitigate the effects from changing the mandrel heating system by maintaining consistent mandrel temperatures appear to have been successful. The baseline regression was able to very accurately predict the preliminary baseline data points, as illustrated in Table 19. The same mandrel and heating system were used for the JITA and the baseline process, so the limited effects of the hardware change on the SBS strength would apply to both processes.

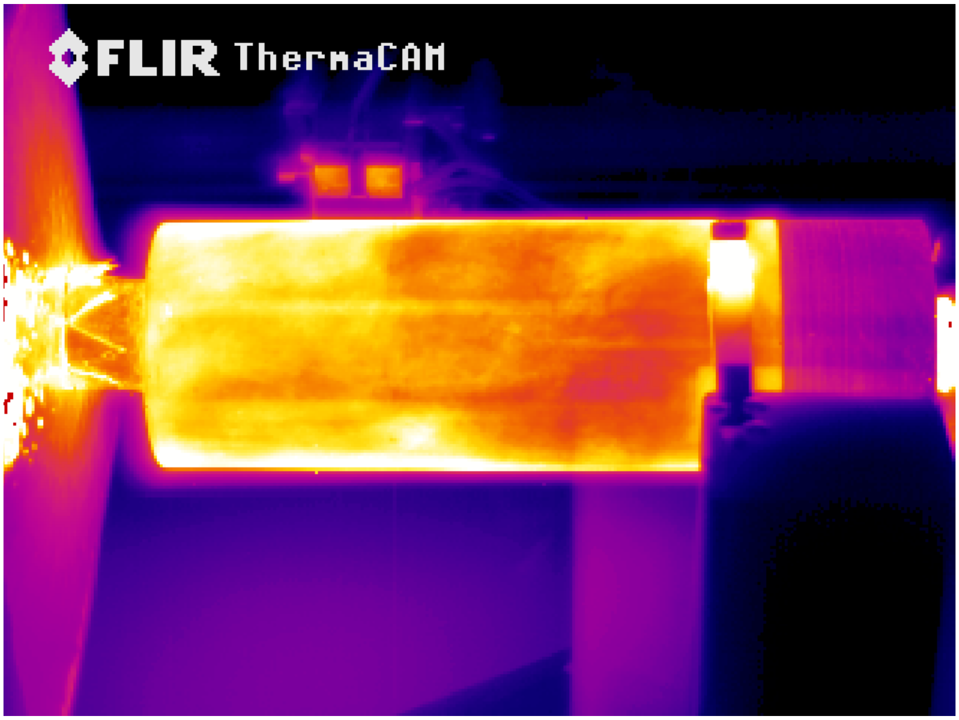

Figure 42: Characterizing the mandrel surface temperature with an infrared camera while using the heat gun to raise the mandrel temperature.

Secondly, the hot end temperature control system was replaced during the testing of the second block of the JITA-M study. To mitigate any unintended variation resulting from this change, the accuracy of the measured hot end temperature was maintained using thermocouple measurements taken both before and after the control system replacement. Also, the existing samples in the second block which used the previous hot end control system were reproduced using the new heating system. As previously mentioned, no indications of unexpected variation between the blocks were seen in the statistical analysis.

Other than those noted above, there were no other notable changes in the JITA or baseline manufacturing hardware. Additionally, when performing the optimization studies, there were also no changes in the processing techniques initially used in the preliminary research. Since it is clear that 1) there was a fundamental change in the JITA-P and JITA-M systems, 2) the matrix brand changed, and 3) that the other possible sources of variation were unlikely to have a significant result, it is most likely that a fundamental change in the JITA *material* system caused the reduction in the SBS strength of the JITA system between the preliminary and the main studies. Instead of being the result of an unintentional change in processing techniques, the difference in JITA-P and JITA-M SBS strengths was due to a difference in the matrices of the two systems. The JITA system can make FRP parts of comparable quality to the baseline system when certain matrix materials are used.

5.7. Material Discrepancies and Possible Effects on SBS Strengths

5.7.1. Fiber Diameter Discrepancies

The reinforcing fibers used in the JITA and the baseline processes were both E-glass, but had significantly different diameters: The dry roving fibers used in the JITA process had a diameter of approximately 12 microns, while the commingled material contained glass fibers with a 20 micron diameter. The discrepancy of fiber diameters is illustrated in Figure 43.

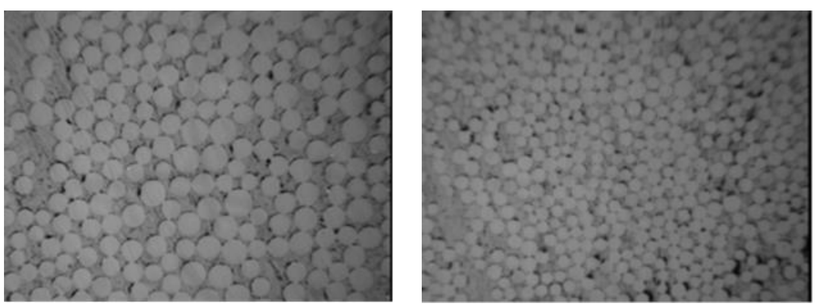

Figure 43: Representative micrographs at 200X of the two material systems used in the main study. The left image shows the commingled tow. The JITA-M material is shown on the right.

All other things being equal, in some loading scenarios, FRP parts with differing fibers sizes would be expected to display a different mechanical response. Since the JITA and baseline material systems did contain fibers with different diameters, it is worthwhile to investigate whether fiber size alone would be likely to create a difference in measured SBS strength. The deformation and damage produced during SBS testing, shown in Table 17, demonstrates that sample failure is most likely due to a combination of shear and compressive stress. Consequently, the load value used to calculate SBS strength will change depending on the response of the specific sample to compressive stress and to shear stress.

Fiber diameter itself should have little effect on the mechanical response of a SBS sample to shear stress. Fibers of constant diameter that are spaced closer or further apart will change the compliance of the composite material. Due to the significantly lower shear modulus of a PETG relative to the glass, glass fibers that are spaced further apart will allow more shear deformation at the same value of shear strain in the polymer. However, this scenario implies a changing V_f as the fibers are moved further apart. If V_f remains the same while the fibers are separated, they necessarily become larger to maintain the ratio of glass to PETG in the sample. And in this case, the ratio of shear deformation to shear strain remains the same. In general, smaller diameter brittle fibers will be stronger as the linear density of voids will decrease. However, there was no evidence that fibers were breaking due to a shear load during testing. Shear stress could distort the beam geometry to the degree that fibers may break due to a changing load character, but this potentiality will not be considered here. As a result, the fact that there are smaller fibers in the JITA samples should not produce a significantly different response under shear loads produced during SBS testing.

In comparison, the compressive stress produced during the SBS strength test should be met with a different response due the difference in reinforcing fiber diameters. The failed samples showed signs of brooming and fiber buckling by the end of mechanical testing. Because the fiber diameters in the JITA are significantly smaller than those in the baseline process, the second moment of area is also much smaller. Consequently, the smaller fibers should display a lower buckling strength, and at an equivalent V_f, the JITA material system should be weaker in compression than the baseline system made from the commingled material. However, this only makes the use of SBS strength to evaluate the JITA process more conservative, and so it should not affect the conclusions drawn from the comparison of the SBS strength data points.

5.7.2. Matrix Discrepancies

It appears as though there was a significant difference between the JITA-M and JITA-P matrices, and that it was this difference that produced a higher quality of JITA-P tube, on the basis of SBS test results. However, there could be multiple properties of the PETG that may contribute to resulting FRP parts of higher quality. In order to identify the likely contributors to the varying levels of SBS strength in the JITA-P, JITA-M, and optimized baseline processes, the best samples from each of the three studies were selected. Comparisons were made between the three samples using V_f and void content measurements, microscopy, and the differential scanning calorimetry (DSC) technique. On the basis of these comparisons, it is likely that the JITA-P matrix displays a lower viscosity at the elevated processing temperatures. And, as a result, the JITA-P matrix creates a higher quality composite than is possible with the JITA-M material system, as illustrated in Figure 39.

5.7.2.1. Sample Selection

The selection of the best JITA-P sample was straight forward; the 220 °C sample was selected because it displayed a higher SBS strength value. The selection of samples from both of the optimization studies was conducted on the basis of the following two criteria: The samples needed to show high values of SBS strength, and they needed to have been produced in a way that was most similar to the significant process parameter levels recommended by the optimization process. First, the individual samples in each optimization study were ordered by SBS strength value. Second, the total weighted difference in process parameter levels between each sample and the predicted optimum was calculated as shown in Equation 4, which was used in the case of the baseline study. This expression shows the relationship between 1) the total difference in parameter levels (PD), 2) the weights (w_1-w_5), and 3) the coded parameter levels for the sample candidate (A_c-E_c) and the predicted optimum (A_p-E_p). The weights were determined by combining the regression coefficients for all of the terms containing each input variable.

$$PD = \sqrt{(w_1 * (A_c - A_p))^2 + (w_2 * (B_c - B_p))^2 + (w_3 * (D_c - D_p))^2 + (w_4 * (E_c - E_p))^2 + (w_5 * (F_c - F_p))^2} \quad \textbf{(4)}$$

The PD expression used to pick a JITA-P sample is similar to Equation 4, except the variable values are different and the process uses more input variables. This expression is shown in Equation 5.

$$PD = \sqrt{(w_1 * (A_c - A_p))^2 + (w_2 * (B_c - B_p))^2 + (w_3 * (C_c - C_p))^2 + (w_4 * (D_c - D_p))^2 + (w_5 * (E_c - E_p))^2 + (w_6 * (F_c - F_p))^2} \quad \textbf{(5)}$$

The sample candidates for both optimization processes were ranked by PD value and sample selection was made by choosing tubes that were the most similar to the maximized SBS value, while concurrently having the lowest PD value. Not surprisingly, both of these metrics selected the same sample candidates. The samples that were made under the most similar, significant fabrication conditions to those of the predicted optimum had the highest SBS strength values. And it was these samples that were used for further investigation.

5.7.2.2. Consolidation

The JITA-P matrix is likely to have a lower viscosity at processing temperatures than the JITA-M matrix. If this were true, one would expect the V_f in the best JITA-P sample to be greater or equal to that in the JITA-M sample. Figure 44 shows that the JITA-P sample does in fact have a higher V_f than the JITA-M sample. V_f was measured using the "burnout" technique described in ASTM D3171.

Figure 44: A comparison of Vf values for each of the three samples.

The higher V_f of the JITA-P sample is also corroborated by the inspection of the micrographs taken of each sample, shown in Figure 45. The micrographs in Figure 45 display the fiber and matrix, and their dispersion throughout the cross-section of each example of the material from the JITA-P, JITA-M, and baseline processes. Dark areas on, but near the edge of the glass fibers are not voids, but result instead from multiple facets on the glass surface produced during the grinding process.

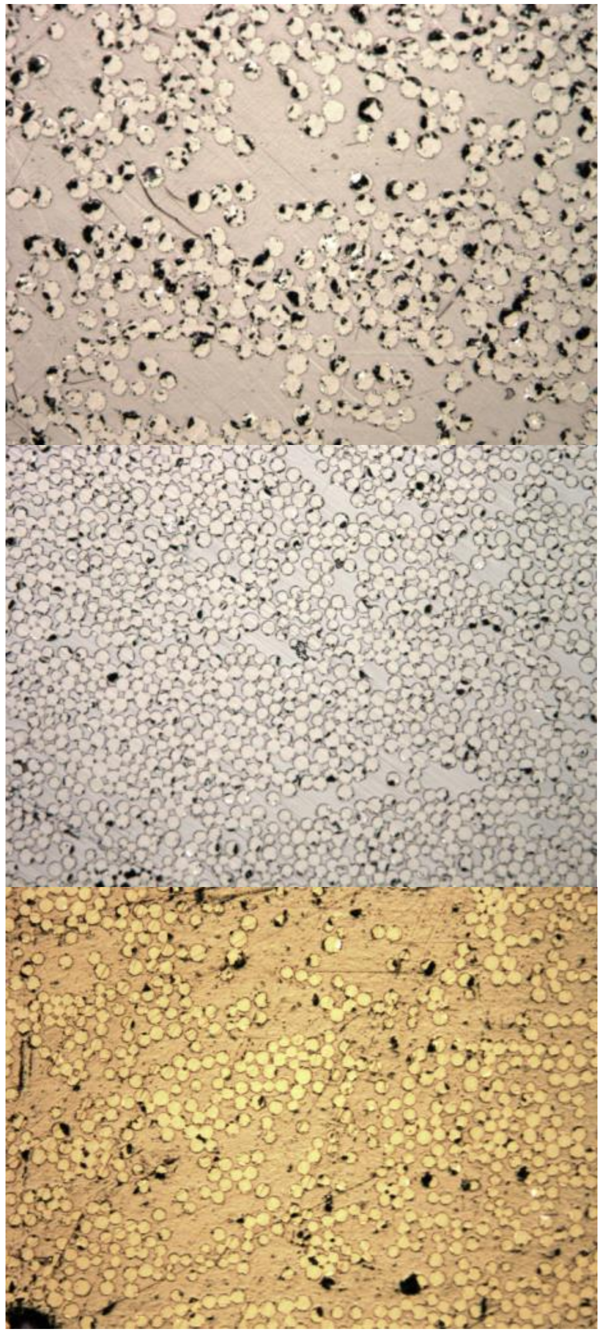

Figure 45: Micrographs of the three samples. The top image is of the baseline sample, the middle image is of the JITA-P sample, and the bottom image is of the JITA-M sample. All images were taken at 100 X.

Higher degrees of consolidation generally produce higher V_f values. With a larger amount of reinforcement material in the JITA-P sample, all other things being equal, the SBS strength would be higher as well. And the JITA-P did indeed have higher SBS strength than the optimized JITA-M material. It should be noted that all of the material has a similar microstructure: the non-laminated, even fiber dispersion seen in Figure 45. Consequently, differing microstructure is unlikely to be the cause for the varying SBS strengths of the JITA-M, JITA-P, and baseline processes.

And yet, the processing conditions that contribute to FRP consolidation are temperature, time, and consolidation force. If the preliminary samples were exposed to higher consolidation forces for a longer amount of time, the higher degrees of consolidation could be the result of these discrepancies, rather than from a difference in the two material systems. However, all of the processing parameter levels used in the preliminary studies, besides the hardware temperatures, were contained within the bounds of the optimization studies. And the lower temperatures of the preliminary work would be *less* likely to produce consolidation, rather than more likely. Consequently, the higher degree of consolidation seen in the JITA-P sample can be attributed to a difference in material system, not a difference in processing conditions. And a likely attribute of a polymer that allows more consolidation at elevated temperatures is a lower viscosity during processing conditions. However, the baseline process also has a similar V_f to that of the JITA-M material, and the former showed SBS strengths significantly higher than the latter. It would be reasonable to ask why, if the consolidation in each sample is the same, the JITA-M and baseline processes do not produce optimized samples with the same SBS strength.

5.7.2.3. Defects

The optimized JITA-M system has a similar V_f compared to the optimized baseline system. And yet, the maximized SBS strength of the baseline system is higher than that of the JITA-M system. This is likely to be the result of a higher void content in the optimized JITA-M parts relative to that found in the optimized baseline parts, shown in Figure 46. Strength values are generally sensitive to defect quantity, and the larger amount of voids in the JITA-M parts made them weaker than the parts made from commingled material.

Figure 46: The void content of each of the three samples.

From Figure 46 we can also see that the void content of the two JITA processes is similar, and so higher void content may be inherent to the JITA process. This is unsurprising since matrix addition occurs so late in the manufacturing process in the JITA system. The baseline process uses commingled roving which contains intermixed reinforcing fibers and PETG fibrils. And so, at the elevated temperatures during processing, the softened matrix of the baseline system only needs to flow short distances to completely surround each fiber and to fill in initial voids that may be present. And so, the commingled material system is likely to require smaller consolidation force at lower temperatures for shorter amounts of time to make a composite of sufficient quality. This relative ease of making a composite is evident in the relative size of the JITA-M and baseline bounds: The commingled material can make a composite of sufficient quality to be tested at a much larger range of temperatures and processing speeds than the JITA-M material system can, as seen in Tables 5 and 6.

However, although the JITA-P system produced samples of higher void content than the baseline system, the SBS strengths were similar. This was most likely the result of the deleterious effects of higher void content being offset by the relatively large V_f of the JITA-P samples. The varying metrics of quality combined into a JITA-P material that was as strong as the optimized baseline material.

5.7.2.4. Glass Transition Temperature

Further evidence of the better rheological properties of the JITA-P matrix can be found when comparing the T_g of each of the three material systems. The as-received PETG matrices of the JITA-P, JITA-M, and baseline processes were evaluated using DSC to measure the T_g in each case. In the case of the two JITA systems, unreinforced PETG material was tested, while the commingled material was tested to discern the T_g of the baseline system's matrix. It was assumed that the glass would exhibit no significant DSC response at the commingled PETG T_g temperature, and that the physical presence of fibers would not significantly affect the measured T_g during DSC testing. The midpoint T_g in each case is presented in Figure 47, which shows the T_g of the commingled material being similar to that of the JITA-M matrix. Both of those materials have a T_g that is approximately 10 °C higher than the T_g of the JITA-P matrix. All other things being equal, a higher T_g can indicate a higher viscosity at a specified temperature [62]. The differences in T_g seen in Figure 47 could be from varying polymer chain structure and composition, differences in molecular weight, discrepancies in the quantities and types of plasticizers and additives. Thermal history can influence a polymer's T_g, but samples were analyzed multiple times to reduce this influence.

Figure 47: The midpoint T_g of the matrices of each material system, as described in ASTM E1356.

5.7.2.5. Available Processing Temperatures

As noted earlier in Section 5.6.5, the processing temperatures that were used in the JITA-P study were outside of the temperature bounds used to make samples with the JITA-M system. That being so, there is evidence that the JITA-M and JITA-P material systems are fundamentally dissimilar. The preliminary studies were conducted at slow speed and with high consolidation forces produced by a large foot force and high roving tension. This combination of these three parameters would be most likely to produce a successful composite at lower temperatures. However, those speeds and consolidation forces were within the bounds of the JITA-M optimization study, and so discrepancies between the speed and consolidation forces in the JITA-P and JITA-M studies is not a reasonable explanation for the differences in the operating temperatures that each study used to make higher quality composites.

However, the temperatures used to make JITA-P samples were not only different from, but were also *lower* than the temperatures needed to make JITA-M samples, as seen in Figure 40. A reasonable explanation for the relative ease with which JITA-P samples could be made into successful FRP components at low temperature is that the JITA-P matrix has a lower viscosity at elevated temperatures than the JITA-M matrix. A possible advantage of having lower viscosity at elevated temperatures is that it may be able to form an FRP part well below temperatures that begin to produce thermal-oxidative degradation. This property would allow full wetout and consolidation at temperatures that would avoid possible weakening of the composite via thermally-induced matrix damage.

5.7.2.6. Matrix Characterization Summary

Although the rheological properties of the JITA PETG matrices at elevated temperature have not been directly measured, there are multiple traits of the samples selected from the JITA-P, JITA-M, and optimized baseline results that support the claim that the JITA-M matrix had a higher viscosity than the JITA-P matrix at processing temps. First, the JITA-P sample appears to have been better consolidated at lower temperatures than the best samples from the JITA-M and baseline systems. This was demonstrated with both V_f measurements and also metallographic evaluation. Second, the relatively low T_g of the JITA-P matrix indicates that it softens at a lower temperature. This behavior may extend to the higher temperatures used during FRP part processing as well. Third, the viable processing temperatures of the JITA-P matrix have a significantly lower minimum than the PETG in the JITA-M material system. The evaluation of the probable relative rheological behavior of the JITA-P matrix at elevated temperature, using these three characteristics indicates that the JITA-P matrix showed relative lower viscosity at elevated temperatures. And this lower viscosity allowed a JITA-P part with higher consolidation and with comparable void content to display higher SBS strengths during mechanical testing, compared to the JITA-M system

6. RECOMMENDATIONS FOR FUTURE RESEARCH

6.1. Process Development

Besides confidently locating an optimum, another significant advantage from using an orthogonal, designed optimization study is that the statistical contribution to the response variable of each process parameter can be independently evaluated. The regression models were used for prediction, and term selection for each model was conducted in order to provide the most accurate predicted optimum. Only correlation between variables is needed to forecast untested data point. Consequently, indications that a term may not be statistically significant, based on a p-value higher than 0.05, are not entirely relevant for these purposes. If a regression model appears to make more accurate predictions with the inclusion of a term, it is a higher performing model and it should be used to make these kinds of predictions. However, to further refine the process, an estimation of the practical significance and interpretation of each term is necessary to justify the possible elimination of process variables considered here. Terms that have a statistically significant, but small effect on the final quality of the composite should be considered for elimination. Also, the sign and magnitude of the term coefficients give more information about how process parameters affect quality and how different parameters interact to produce different qualities of FRP components. The p-value indicating the statistical significance of each term in the regression model chosen to represent the response in each processes is shown in Table 20. Also, the magnitude and sign of each term associated with the p-values is also included. Statistically significant terms in the regression are in bold font.

TABLE 20: Regression term coefficients and associated p-values for significance of each term. An X indicates that a term was not used for the model.

Term	JITA-M: Coeff./P-Value	Baseline: Coeff./P-Value
A (*Mandrel Temp.*)	**-0.90/0.001**	0.55/0.326
B (*Foot Temp.*)	0.13/0.608	**4.2/0.000**
C (*Process Speed*)	-0.24/0.358	-0.90/0.116
D (*Foot Force*)	-0.33/0.212	0.21/0.714
E (*Roving Tension*)	-0.39/0.139	-0.63/0.259
F (*Hot End Temp.*)	-0.020/0.924	X
A^2 (*Mandrel Temp.*Mandrel Temp.*)	**-6.62/0.000**	**-4.2/0.006**
B^2 (*Foot Temp.* Foot Temp.*)	X	3.86/0.011
D^2 (*Foot Force*Foot Force*)	**-1.65/0.041**	-1.9/0.169
AB (*Mandrel Temp.*Foot Temp.*)	**-0.90/0.002**	**-5.9/0.000**
AC (*Mandrel Temp.*Process Speed*)	**2.76/0.000**	**3.9/0.000**
AD (*Mandrel Temp.*Foot Force*)	X	-1.1/0.076
AE (*Mandrel Temp.*Roving Tension*)	-0.36/0.187	X
BC (*Foot Temp.*Process Speed*)	-0.46/0.090	X
BF (*Foot Temp.*Hot End Temp.*)	**0.69/0.011**	X
CD (*Process Speed*Foot Force*)	0.36/0.188	X
DE (*Foot Force*Roving Tension*)	X	**-1.2/0.056**

6.1.1. The Prevalence of Significant Interactions and Quadratic Terms

It should be noted that, in both studies, interactions between the process parameters were often significant, while the linear, main effects of the variables often have a limited effect on SBS strength. Two conclusions can be drawn from this fact: Firstly, a rudimentary screening study would have been likely to eliminate important input variables if it did not capture the curvature that the CCD design can model. Mandrel temperature was much more significant as a quadratic term than a linear term, for example. Secondly, severely fractionated studies used to compare the two processes would have provided limited information about how the process might be functioning. The precise relationships between process parameters, and between the parameters and the response variable would clearly have been uncertain if main effects were aliased with two-way interactions. Erroneous conclusions could have easily been drawn if interactions were simply assumed to be insignificant for the sake of expediency.

6.1.2. Mandrel Temperature

Although the main effects from mandrel temperature are modest, the mandrel temperature appears to be a significant component of both the JITA-M and the baseline process. The linear component of the mandrel temperature term is relatively small compared to the quadratic mandrel temperature term in both studies. The large, negative coefficient of A^2 indicates that the quality of the composite drops significantly when the mandrel temperature is too high or too low. This is consistent with the idea used in the bounding studies that there are two main methods of producing poor quality composite material: poor consolidation and possibly high void content at low temperatures on one hand, and degradation due to excessive temperature on the other.

This large coefficient confirms the sensitivity of the material system to changes in temperature and the large role of the mandrel in determining the actual temperature of the sample during processing. The mandrel has a relatively large contact area with the FRP test sample and it remains in contact with the FRP material system for the largest duration. Because the material system uses a thermoplastic matrix, a sensitivity to temperature is to be expected as temperature is a primary influence on the viscosity of the matrix. Shear thinning of the PETG is likely to also affect the viscosity of the matrix during processing, but there were no significant indications that viscosity decreased as the process speed increased in these results. A reduction in matrix viscosity that is not reliant on elevated temperature could be beneficial by increasing wetout and consolidation while also possibly avoiding thermal degradation. Future studies of the JITA process with higher process speeds and very large consolidation forces could contain the sensitivity necessary to measure this phenomenon.

6.1.3. Foot Temperature

A major discrepancy between the JITA-M study and the baseline process results is the apparently significant role of foot temperature in the baseline process, while its role in the JITA-M process is relatively small. Increasing the foot temperature dramatically increases SBS strength when using commingled material. In the baseline system, the interaction coefficient between mandrel temperature is large and negative; processing the material with both the mandrel temperature and the foot temperature high diminishes quality, again, most likely due to the effects of poor consolidation or thermal-oxidative degradation at either extreme. However, as shown in in Table 15, FRP material made from commingled material with a relatively cool mandrel and a warm pressure foot will have the highest SBS strength.

This discrepancy between the two processes in the case of the significance of foot temperature may be the result of the method of matrix addition inherent to both processes. In the JITA system, the matrix is first added to either the mandrel, or to the existing FRP tube, whose temperature is primarily determined by the mandrel. As a result, although the PETG filament is initially heated by the hot end, the mandrel is a primary influence on the temperature of the PETG immediately prior to the first consolidation cycle as the fiber and matrix pass between the mandrel and the consolidation foot for the first time. In contrast, the baseline process uses commingled material, which passes over the heated pressure foot immediately before deposition. In this case, it is the elevated temperature of the foot that warms the PETG before initial deposition. Later, the temperature of the deposited composite is most likely primarily a function of the mandrel temperature. However, the state of the PETG just prior to the first consolidation cycle may be important: less viscous PETG that will spread over the widened roving as it leaves the foot may display increased wetout that at least partially determines the final wetout of the final part. The practical implications of this hypothesis are that the mandrel could be held at a lower temperature as high quality composite parts are made. This scenario would reduce energy expenditure and possibly avoid thermal degradation and would therefore be another justified area of future investigation.

6.1.4. Processing Speed

As seen in Table 20, of all of the input variables, the processing speed shows the greatest discrepancy between its significance as a main effect and as an interaction. The effect of the parameter on the baseline samples appears relatively large, based on the magnitude of the coefficient of the main effect term. Additionally, the negative coefficient indicates that higher speeds are correlated with lower quality, which may be reasonable given the generally lower temperatures used in the baseline process. The lower temperatures are less likely to produce thermal degradation compared to the JITA-M parameter levels. However, due to the larger error inherent to the baseline regression model, it does not meet the standard criteria necessary to deem it statistically significant.

While the process speed may be insignificant as a linear term, in both processes it is almost certainly significant as an interaction with mandrel temperature. This relationship between the two variables, represented by a large, positive coefficient is consistent with the requirements of a thermoplastic manufacturing process: there needs to be sufficient consolidation pressure, temperature and time to make a high quality part. This interaction addresses the last two of these requirements. If the mandrel temperature is high, the processing speed also needs to be high to avoid matrix degradation. And, if the mandrel temperature is low, the processing speed should be low to provide time for wetout and consolidation to occur.

6.1.5. Foot Force

The foot force was deemed statistically significant as a quadratic term in the JITA-M model, but not in the baseline model in spite of having similarly sized coefficients. This is the result of larger amounts of predicted error in the baseline model; the effects from baseline process variables must be larger than the JITA-M effects to produce a high degree of certainty that the effects are significant. As discussed previously, the foot consolidation force not only affects the degree of consolidation, it also increases the necessary time for a sample to be made. This can increase thermal degradation of the sample, which, if present, will decrease SBS strength. As a result, very high or very low levels of consolidation force from the foot reduced the quality of the resulting samples.

6.1.6. Roving Tension

The tensile force applied to the roving during each processing run was not statistically significant in either process. There is borderline significance as an interaction with foot force. The negative coefficient indicates that if both of the levels are high, or low, quality may be reduced somewhat. This may be consistent with the aforementioned hypotheses of the functions of the process parameters: if both the fiber tension and the foot force determine the consolidation of the FRP samples, then both variables at a high level could create thermal degradation, while both parameters at a low level might produce insufficient consolidation. Additionally, the borderline statistical significance may be the result of a pressure foot being used instead of a consolidation roller. At low levels of roving tension, there will still be tension generated between the drag force occurring from the foot and the turning mandrel. This effect may have decreased the sensitivity of the optimization studies to the effects of low tension. Future work could incorporate a heated roller rather than a heated foot, which would eliminate the tension in the roving produced by drag on the front surface of the foot. Higher levels of maximum roving tension could also be explored.

6.1.7. Hot End Temperature

The effects of hot end temperature were only significant as an interaction with the foot temperature. The positive coefficient implies that the inputs make a positive contribution to quality only when both levels are high or both levels are low. Processing with the temperatures high would contribute to increased quality because this combination would reduce the PETG viscosity and should encourage wetout of the reinforcing fibers. The short duration of contact with the material, once deposited, should limit thermal degradation. In contrast, both pieces of hardware at low temperatures would most likely have the opposite effect, decreasing quality instead. And yet, quality is predicted to increase a small, but significant amount in this case. During the processing of the JITA-M samples, at low levels of hot end temperature, the deposited PETG appeared as though it was not being spread evenly before being compressed by the foot. Consequently, the hot end temperature should not be reduced in the current configuration of hardware while using the PETG/E-glass material system. However, further reducing the low level of the foot temperature below 250 °C may provide more information about the relationship between the foot temperature and the hot end temperature.

6.1.8. Necessary Processing Levels to Produce High-Quality Composites

All of the parameters studied in the JITA-M process and the baseline process were deemed to produce statistically significant effects on SBS strength. However, this statistical significance was partly the result of the very low process variation measured at the midpoints and displayed in Table 16. Although the distances of the other data points from the midpoint, and their associated possible change in variation, are accounted for when predicting their inherent variation, both processes have demonstrated low inherent SBS strength variation. Consequently, a small effect by a variable may be deemed statistically significant. For example, when using the JITA-M process, an increase in the mandrel temperature from the midpoint to the high level is estimated to cause a decrease of the SBS strength by 0.90 MPa from the linear mandrel temperature term. However, this is not a large decrease relative to the average SBS strength values that are produced by the process, shown in Table 18 to be approximately 37 MPa. Consequently, only the largest effects should be carefully controlled when using either the JITA or the baseline process.

The JITA process is apparently most affected by the variation of the mandrel temperature, the processing speed, and perhaps the foot force. Therefore, the foot temperature, the hot end temperature and the roving tension do not appear to require careful control. The practical implications of these relaxed requirements are that less effort is required to carefully control these parameters. For example, perhaps open loop temperature control is sufficient, reducing capital costs. Additionally, the JITA process is more robust than previously thought, and it is now known that, as long as these parameters stay within the bounds used for this study, the resulting quality should not be affected. Lower hardware temperatures may be used, which could reduce power requirements.

Statistical and practical significance associated with the baseline process can be treated similarly, but this approach leads to slightly different conclusions. The baseline process appears to only require precise control of mandrel temperature, foot temperature, and processing speed. Foot force and roving tension do not have large effects on SBS strength. Therefore, similarly to the JITA-M process, the robustness of the process is higher than initially thought, and its efficiency can be increased by simplifying the hardware and reducing the effort necessary for strict control of the roving tension and the foot force. A minimum of roving tension may be needed to allow it to reliably feed into the consolidation foot, but precise control beyond this requirement does not appear to be necessary, for example.

6.1.9. Process Parameters to Investigate

The insensitivity of the SBS strength to roving tension indicates that either this tension does not have a significant effect on quality, or that the drag of the pressure foot independently created roving tension that interfered with tension generated at the roving spool. The effect or roving tension was insignificant in the JITA process and was only close to significant in the baseline process, which shared the same consolidation foot design. The efficacy of a roller rather than a foot as a consolidating device and its effect on FRP quality could be explored. It does not appear that the roller temperature would need to be precisely controlled when performing the JITA process, although this could be confirmed by experiment. Additionally, the surprising relationship between the foot temperature and the hot end temperature suggests that the effects of low consolidation hardware temperature on FRP quality could be investigated further.

While developing the JITA process, alternative parameters were identified as possibly significant, but not included in this study: The PETG was added to the mandrel and reinforcing fiber was placed over it. Alternatively, the degree of wetout may be affected by placing the PETG on the deposited fiber. Additionally, the roving was spread by the pressure foot as it exited the groove in the top of the foot. Spreading the roving further by widening the groove or enlarging the exit of the groove may allow more efficient wetout of the glass fiber. Increasing the distance between the spread fibers could result in the heated thermoplastic to more quickly penetrate the fiber layer and more easily fill in gaps between the fibers. The variation of additional process parameters such as these may allow significant improvement of the JITA process.

6.2. Economic Analysis

Many of the methods of extensively evaluating the economic feasibility of the JITA process rely on contingencies that cannot be predicted at this time such as the specific part to be made and the production volume. Additionally, more exhaustive analyses such as life-cycle cost analysis are outside the scope of this work. However, a significant component of the efficiency of a manufacturing process depends on the cost of its material inputs. The baseline process uses commingled material to make components, while the JITA process uses FDM filament and dry E-glass fiber.

A survey of vendors was conducted to gather the approximate cost of these input materials on a high-volume basis; the obtained material quotes were based on the assumption of an order of roughly a ton or more of each material. The anticipated JITA material input cost was based on the assumption of a composition of 70% glass by weight, the same composition as the commingled material that was quoted. A summary of the results from this survey are presented in Table 21. As conducted in this work, the input materials for the JITA process were 56% less expensive than the equivalent E-glass/PETG commingled material. If a screw extruder is used to deposit PETG in the JITA process, PETG FDM filament is not necessary, and granules or pellets of virgin PETG could be used. This form of PETG is much less expensive that PETG FDM filament and its use would generate a savings of 82% compared to the baseline material system.

TABLE 21: Current and potential input material costs for the JITA and the baseline processes.

	JITA-M (FDM)	JITA-M (Granule)	Baseline
Matrix Cost [$/kg]	11	1.3	N/A
Reinforcement Cost [$/kg]	2.2	2.2	N/A
Total Material System Cost [$/kg]	4.8	1.9	11

Process development that reduces the temperatures required for fabricating quality JITA parts will reduce the necessary electrical energy required by the JITA process. Decreasing the necessary control over process parameter levels could diminish the effort and capital expenditure associated with maintaining control over these parameters. The extent to which these could be reduced could be investigated by testing SBS strength of samples made at temperatures below the lower bounds used in this work. The conclusion that no additional heat to the JITA consolidating hardware is necessary would make the process less expensive.

6.3. Process Flexibility

Based on the results from a comparison with a commercial process using SBS strength, the JITA method has been successfully developed and performs similarly to the baseline process, which uses a material system of commingled roving. The quality of material deposited by the JITA process appears to be sufficient, and the material inputs are significantly less expensive. However, the development of the process incorporated the intention to ultimately produce parts with large degrees of fiber and matrix variation. Consequently, future efforts could explore the ability of the process to maintain quality while demonstrating the anticipated capability of the JITA process to create parts with severely non-geodesic fiber paths. Pressure vessel fabrication appears to be a good candidate for the first component to attempt, since the traditional hardware used to create these parts, primarily consisting of a rotating mandrel and possibly a consolidating device, have already undergone significant development in this work. Fiber path positional fidelity may be explored while possibly attempting to incorporate local structural features.

While the capability to produce non-geodesic fiber paths may significantly improve the mechanical response of an FRP part, little exploration of local matrix variation has been attempted. However, inexpensive FRP equipment currently has the capability to extrude multiple matrix compositions during the construction of a single part. The incorporation of a 'dual head extruder', which can be found on these machines, could efficiently be introduced into the existing JITA process to locally vary matrix composition. The variation of V_f by varying the volume of added matrix to the composite would most likely need active cooling as opposed to relying on the ambient environmental conditions. However, the cooling hardware could be as simple as forced air directed at the initial deposition point.

7. CONCLUSIONS

During the course of this work a new continuous fiber reinforced composite fabrication method was developed and evaluated. By combining automated fiber placement and the use of a matrix that can rapidly stiffen after deposition, the proposed process is consistent with current research efforts intended to expand the capability of continuous fiber reinforced composite manufacturing processes to locally vary the reinforcing fiber angle. Accurate fiber placement occurs in the proposed process using techniques similar to conventional filament winding, which here were used to apply E-glass fiber. The matrix used in the process is a thermoplastic, PETG, which stiffens upon cooling from elevated temperatures.

The proposed process also incorporates an increased independence of the addition of the matrix to the addition of the reinforcing fiber, which results from the matrix being added to the reinforcing fiber just prior to the impregnation and consolidation that occurs between a mandrel and a consolidation foot. This additional independence could allow the local variation of 1) the matrix composition by applying a different matrix to different locations of the part and 2) the fiber volume fraction by adding different amounts of matrix to different locations of the composite.

The viability of the process was evaluated by investigating the quality of test specimens made with the prototypical process using SBS strength measurement. In order to broadly evaluate the potential of the proposed process to make parts of high quality, the SBS strength of test specimens made with the proposed process was optimized relative to the variation of a large number of process parameters: mandrel temperature, foot temperature, process speed, foot consolidation force, roving tension, and hot end temperature. To provide the context needed to understand the significance of the results of the evaluation of the proposed process a second, baseline process was developed. This baseline process uses commercially available PETG/E-glass commingled roving, with E-glass fibers and PETG fibrils premixed, in a manufacturing process very similar to the proposed process, except PETG is not independently added to the reinforcing fiber. The optimized SBS strength of the baseline was found to be higher than the optimized SBS strength of the proposed process by a statistically significant, but not necessarily practically significant amount. However, in the preliminary comparison of the two processes a different PETG matrix was used in the proposed process than was used in the main optimization study comparison, and the SBS strength of these preliminary study samples made with the proposed process matched the optimized SBS strength of the baseline process. Therefore, it has been shown that the proposed process can make samples of comparable quality to those made by the baseline process.

There is evidence that the proposed process is competitive with the baseline process in other respects as well. The variation in SBS strength of the proposed process, measured during the main study with multiple samples at the midpoint, had a coefficient of variation of 2.3% compared to the baseline process midpoint SBS strength coefficient of variation of 1.9%. Also, the prediction interval, measured at the optimum of each process, was smaller in the case of the proposed process compared to the baseline process. Lastly, the input material costs are significantly lower for the proposed process than the baseline process that uses commingled material. These costs are reduced by 56% with the hardware and processes used in this work, and, if a matrix extruder that can accommodate polymer granule feedstock is used, the reduction in material cost could increase to approximately 86%. Therefore, the proposed process is likely to become increasingly cost competitive as production volume is increased.

REFERENCES

[1] D. Gay, *Composite Materials: Design and Application*, Boca Raton: CRC Press, 2015.

[2] E. J. Barbero, *Introduction to Composite Materials Design*, Boca Raton: CRC Press, 2015.

[3] V. Vasilev and E. V. Morozov, *Advanced Mechanics of Composite Materials*, Oxford: Elsevier, 2007.

[4] S. Heimbs and T. Bergmann, "High-Velocity Impact Behaviour of Prestressed Composite Plates under Bird Strike Loading", *International Journal of Aerospace Engineering*, Vol. 2012, Article ID 372167, 2012.

[5] J. Russell, "Composites Affordability Initiative", *CANCOM 2007*, Winnipeg, Manitoba, 2007.

[6] D. De Carvalho, M. Lossie, D. Vandepitte, and H. Van Brussel, "Optimization of filament-wound parts based on non-geodesic winding", *Composites Manufacturing*, Vol. 6, pp. 79-84, 1995.

[7] M. Madhavi, K. R. Swamy, K. V. J. Rao, and K. N. Rao, "Experimental Evaluation of Available Surface Friction Factor on a Hoop Substrate for a Filament-wound Composite Pressure Vessel", *Journal of Thermoplastic Composite Materials*, Vol. 24, pp. 279-297, 2011.

[8] L. Zu, "Stability of fiber trajectories for winding toroidal pressure vessels", *Composite Structure*, Vol. 94, No. 5, pp. 1855-1860, 2012.

[9] S. Koussios and O. K. Bergsma, "Friction Experiments for Filament Winding Applications", *Journal of Thermoplastic Composite Materials*, Vol. 19, No. 1, pp. 5-34.

[10] R. Wang, W. Jiao, W. Liu, F. Yang, and X. He, "Slippage coefficient measurement for non-geodesic filament-winding process", *Composites: Part A*, Vol. 42, pp. 303-309, 2011.

[11] D. Leh, P. Saffre, P. Francescato, and R. Arrieux, "Multi-sequence dome lay-up simulations for hydrogen hyper-bar composite pressure vessels", *Composites: Part A*, Vol. 52, pp. 106-117, 2013.

[12] R. La Magna, F. Waimer, and J. Knippers, "Coreless Winding and Assembled Core-Novel fabrication approaches for FRP based components in building construction", *Construction and Building Materials*, Vol. 127, pp. 1009-1016, 2016.

[13] S. Seereeram and J. T. Wen, "An All-Geodesic Algorithm for Filament Winding of a T-Shaped Form", *IEEE TRANSACTIONS ON INDUSTRIAL ELECTRONICS,* Vol. 38, No. 6, pp. 484-490, December 1991.

[14] K. M. Warlick, "The Effect of Tow Shearing on Reinforcement Positional Fidelity in the Manufacture of a Continuous Fiber Reinforced Thermoplastic Matrix Composite via Pultrusion-Like Processing of Commingled Feedstock", *MS thesis*, Colorado State University, Fort Collins, Colorado, 2017.

[15] M. K. Hagnell and M. Akermo, "A composite cost model for the aeronautical industry: Methodology and case study", *Composites Part B*, Vol. 79, pp. 254-261, 2015.

[16] D. H. J. A. Lukaszewicz, C. Ward, K. D. Potter, "The engineering aspects of automated prepreg layup: History, present and future", *Composites: Part B*, Vol. 43, pp. 997-1009, 2012.

[17] B. C. Kim, K. Potter and P. M. Weaver, "Continuous tow shearing for manufacturing variable angle tow composites", *Composites: Part A*, Vol. 43, pp. 1347-1356, 2012.

[18] K. Croft, L. Lessard, D. Pasini, M. Hojjati, J. Chen and A. Yousefpour, "Experimental study on the effect of automated fiber placement induced defects on performance of composite laminates", *Composites: Part A*, Vol. 42, 484-491, 2011.

[19] C. S. Lopes, Z. Gürdal and P. P. Camanho, "Tailoring for strength of composite steered fiber panels with cutouts", *Composites: Part A*, Vol. 41, pp. 1760-1767, 2010.

[20] K. C. Wu, J. D. Turpin, B. K. Stanford and R. A. Martin, "Structural Performance of Advanced Composite Tow-Steered Shells with Cutouts", *55th AIAA/ASMe/ASCE/AHS/SC Structures, Structural Dynamics, and Materials Conference*, 2014.

[21] X. Tian, T. Liu, C. Yang, Q. Wang, and D. Li, "Interface and performance of 3D printed continuous carbon fiber reinforced PLA composites", *Composites: Part A*, Vol. 88, pp. 198-205.

[22] N. Li, Y. Li, and S. Liu, "Rapid prototyping of continuous carbon fiber reinforced polylactic acid composites by 3D printing", *Journal of Materials Processing Technology*, Vol. 238, pp. 218-225, 2016.

[23] G. W. Melenka, B. K. O. Cheung, J. S. Schofield, M. R. Dawson and J. P. Carey, "Evaluation and prediction of the tensile properties of continuous fiber-reinforced 3D printed structures", *Composite Structures*, Vol. 153, pp. 866-875, 2016.

[24] W. Hao, Y. Liu, H. Zhou, H. Chen and D. Fang, "Preparation and characterization of 3D printed continuous carbon fiber reinforced thermosetting composites", *Polymer Testing*, Vol. 65, pp. 29-34, 2018.

[25] P. Parandoush and D. Lin, "A review on additive manufacturing of polymer-fiber composites", *Composite Structures*, Vol. 182, pp. 36-53, 2017.

[26] Y. Koga, F. van der Klift, A. Todoroki, M. Ueda, Y. Hirano, and R. Matsuzaki, "The Printing Process of 3D printer for Continuous CFRTP", *SAMPE Conference Proceedings,* Long Beach, CA, May 2016.

[27] M. Eichenhofer, J. C. H. Wong and P. Ermanni, "Continuous lattice fabrication of ultra-lightweight composite structures", *Additive Manufacturing*, Vol. 18, pp. 48-57, 2017.

[28] S. Liu, Y. Li, and N. Li, "A novel free-hanging 3D printing method for continuous carbon fiber reinforced thermoplastic lattice truss core structures", *Materials and Design*, Vol. 137, pp. 235-244, 2018.

[29] H. Prüss and T. Vietor, "Design for Fiber-Reinforced Additive Manufacturing", *Journal of Mechanical Design*, Vol. 137, pp. '111409-1'-'111409-7', 2015.

[30] B. T. Astrom and R. B. Pipes, "Thermoplastic Filament Winding with On-Line Impregnation", *Journal of Thermoplastic Composite Materials*, Vol. 3, pp. 314-324, October 1990.

[31] A. G. Gibson, C. Hicks, P. N. H. Wright and A. Fahrer, "Development of glass fibre reinforced polyethylene pipes for pressure applications", *Plastics, Rubber and Composites*, Vol.29, No. 10, pp. 509-519, 2000.

[32] F. Henninger and K. Friedrich, "Thermoplastic filament winding with online-impregnation. Part A: process technology and operating efficiency", *Composites: Part A*, Vol. 33, pp. 1479-1486, 2002.

[33] F. Henninger, J. Hoffmann and K. Friedrich, "Thermoplastic filament winding with online-impregnation. Part B. Experimental study of processing parameters", *Composites: Part A*, Vol. 33, pp. 1677-1688, 2002.

[34] J. Koo, *Fundamentals, Properties, and Applications of Polymer Nanocomposites*, New York: Cambridge University Press, 2016.

[35] F. Rosselli and M. H. Santare, "Comparison of the short beam shear (SBS) and interlaminar shear device (ISD) tests", *Composites Part A*, Vol. 28, No. 6, pp. 587-594, 1997.

[36] K. Schneider, B. Lauke, and W. Beckert, "Compression Shear Test (CST) – A Convenient Apparatus for the Estimation of Apparent Shear Strength of Composite Materials", *Applied Composite Materials*, Vol. 8, pp. 43-62, 2001.

[37] M. Kadlec, L. Novakova, and R. Ruzek, "An Experimental Investigation of Factors Considered for the Short Beam Shear Strength Evaluation of Carbon Fiber-reinforced Thermoplastic Laminates", *Journal of Testing and Evaluation*, Vol. 42, No. 3, May 2014.

[38] D. F. Adams and E. Q. Lewis, "Experimental Assessment of Four Composite Material Shear Test Methods", *Journal of Testing and Evaluation*, JTEVA, Vol. 25, No. 2, pp. 174-181, March 1997.

[39] B. Lauke, W. Beckert and K. Schneider, "Interlaminar Shear Strength Evaluation of Curved Composite Samples", *Applied Composite Materials*, Vol. 1, pp. 267-271, 1994.

[40] L. Di Landro, A. Montalto, P. Bettini, S. Guerra, F. Montagnoli and M. Rigamonti, "Detection of Voids in Carbon/Epoxy Laminates and Their Influence on Mechanical Properties", *Polymers & Polymer Composites,* Vol. 25, No. 5, pp. 371-380, 2017.

[41] Z. Fan, M. H. Santare and S. G. Advani, "Interlaminar shear strength of glass fiber reinforced epoxy composites enhanced with multi-walled carbon nanotubes", *Composites: Part A*, Vol. 39, pp. 540-554, 2008.

[42] L. A. Franco, M. L. A. Graca and F. S. Silva, "Interlaminar Shear Strength and Fractographic Evaluation with Varying Temperature and Moisture Content of Thermoplastic Composites", *Applied Mechanics and Materials,* Vol. 3-4, pp. 179-184, 2005.

[43] K. van Rijswijk, A. A. van Geenen and H. E. N. Bersee, "Textile fiber-reinforced anionic polyamide-6 composites. Part II: Investigation on interfacial bond formation by short beam shear test", *Composites: Part A*, Vol. 40, pp. 1033-1043, 2009.

[44] H. R. Lin and S. G. Advani, "Processing Models and Characterization of Thermoplastic Composite Wound Parts", *Polymer Composites,* Vol. 18, No. 3, pp. 405-411, 1997.

[45] I. Y. Chang and J. K. Lees, "Recent Development in Thermoplastic Composites: A Review of Matrix Systems and Processing Methods", *Journal of THERMOPLASTIC COMPOSITE MATERIALS*, Vol. 1, pp. 277-296, 1988.

[46] J. M. Whitney and C.E. Browning, "On Short-Beam Shear Tests for Composite Materials", *Experimental Mechanics*, Vol. 25, No. 3, pp. 294-300, 1985.

[47] X. Yao, C. Luan, D. Zhang, L. Lan and J. Fu, "Evaluation of carbon fiber-embedded 3D printed structures for strengthening and structural-health monitoring", *Materials and Design*, Vol. 114, pp. 424-432, 2017.

[48] J. Justo, L. Tavara, L. Garcia-Guzman and F. Paris, "Characterization of 3D printed long fibre reinforced composites", *Composite Structures*, Vol. 185, pp. 537-548, 2018.

[49] TenCate, "TenCate Cetex TC940 PET Thermoplastic Composite", *CETEX-TC940_DS_050917* datasheet, Revised 5/2017.

[50] A. Ramanathan and P. K. Mallick, "Consolidation and Microstructure Variation in Compression Molded Commingled E-Glass Fiber/PET Laminates", *20th Technical Conference of the American Society for Composites*, Vol. 1, pp. 158-169, 2005.

[51] R. H. Myers, D. C. Montgomery and C . M. Abderson-Cook, "Response Surface Methodology", Hoboken, New Jersey: John Wiley and Sons, Inc. 2009.

[52] D. C. Montgomery, "Design and Analysis of Experiments", Hoboken, New Jersey: John Wiley and Sons, Inc. 2005.

[53] P. Nyamugure, D. Maposa, C. Sigauke, E. Chiyaka and M. Denwick, "A holistic application of process capability indices", *African Journal of Business Management,* Vol. 5, No. 28, pp. 11413-11424, 2011.

[54] C. Wu, W.L. Pearn and S. Kotz, "An overview of theory and practice on process capability indices for quality assurance", *Int. J. Production Economics*, Vol. 117, pp. 338-359.

[55] R. H. Lochner and J. E. Matar, *Designing for quality: an introduction to the best of Taguchi and western methods of statistical experimental design*, Milwaukee, Wisconsin: ASQC Press, 1990.

[56] ASTM E1356-08 (2014), *Standard Test Method for Assignment of the Glass Transition Temperatures by Differential Scanning Calorimetry*, ASTM International, West Conshohocken, PA, 2014, https://doi.org/10.1520/E1356.

[57] B. Jones and C. J. Nachtsheim, "A Class of Three-Level Designs for Definitive Screening in the Presence of Second-Order Effects", Journal of Quality Technology, Vol. 43, No. 1, pp. 1-15, 2011.

[58] P. Matthews, "Design of Experiments with MINITAB", Milwaukee, Wisconsin: ASQ Quality Press, 2005.

[59] G. Cumming, F. Fidler and D. Vaux, "Error bars in experimental biology", *Journal of Cell Biology*, Vol. 177, No. 1, pp. 7-11, 2007.

[60] N. Schenker and J. F. Gentleman, "On Judging the Significance of Differences by Examining the Overlap Between Confidence Intervals", *The American Statistician*, Vol. 55, Issue No. 3, pp. 182-186.

[61] K. Bower, "Some Misconceptions about Confidence Intervals", *Six Sigma Forum-American Society for Quality*, July 2003.

[62] M. L Williams, R. F. Landel and J. D. Ferry, "The Temperature Dependence of Relaxation Mechanisms in Amorphous Polymers and Other Glass-forming Liquids", *J. Am. Chem. Soc.*, Vol. 77, Issue No. 14, pp. 3701-3707, 1955.

[63] C. A. Berg, J. Tirosh and M. Israeli, "Analysis of Short Beam Bending of Fiber Reinforced Composites", *Composite Materials: Testing and Design*, ASTM STP 497, American Society for Testing and Materials, pp. 206-218, 1972.

[64] R. B. Dupaix and M. C. Boyce, "Finite strain behavior of poly(ethylene terephthalate) (PET) and poly (ethylene terephthalate)-glycol (PETG)", *Polymer*, Vol. 46, pp. 4827-4838, 2005.

[65] J. Jancar, "Structure-property relationships in thermoplastic matrices", *Mineral Fillers in Thermoplastics I,* Berlin: Springer, 1999.

[66] L. M. Nicholson, K. S. Whitley and T. S. Gates, "The role of molecular weight and temperature on the elastic and viscoelastic properties of a glassy thermoplastic polyimide", *International Journal of Fatigue*,Vol. 24, pp. 185-195, 2002.

[67] P. Prentice, "The influence of molecular weight on the fracture of thermoplastic glassy polymers", *Journal of Materials Science*, Vol. 20, pp. 1445-1454, 1985.